The Use of Anatomically Based Models for the Analysis of Imaged Tracer Experiments in Humans

David Robert Fine

A thesis submitted to the Faculty of Engineering, University of the Witwatersrand, Johannesburg, in fulfilment of the requirements for the degree of Doctor of Philosophy.

Johannesburg, November 1994

Declaration

I declare that this thesis is my own, unaided work, except where otherwise acknowledged. The thesis is being submitted for the degree of Doctor of Philosophy at the University of the Witwatersrand, Johannesburg. This thesis has not been submitted before for any degree or examination at any other university.

Signed this 15 day of APRIL 1994

David Fine

David Robert Fine.

Abstract

Organ function is often characterised using imaging techniques. In particular a tracer is often used which does not react with tissue, is low in concentration, follows body fluid flows and is distinguishable from the observed system and thus measurable. These requirements ensure linear characteristics of the tracer. In this thesis, these linear characteristics are used to develop a generalised mathematical theory to determine organ function from imaged tracer experiments. The theory is based on anatomical and physiological information for single and multiple input organs.

Linear tracer characteristics allow one to deconvolve tracer concentration/time curves obtained from an imaged organ and the input/inputs to the organ. The thesis shows that the deconvolution of such data is related to the *residence time* and *internal age* density functions (RTD and IAD) of the imaged organ. This non-parametric deconvolution of experimental data is performed using methods which do not involve *a priori* information, eg., matrix based and Fourier transform methods. However, even with significant data filtering, noise on the deconvolved curves hampers the determination of accurate results and hence the identification of organ physiology. This is further complicated in multiple input systems where it is difficult to associate changes in the deconvolved curve with specific anatomical and physiological changes. As a means to elucidate this information from the deconvolved curves, mathematical models of the flow in the kidney, spleen and liver have been developed. The modelling approach based on probability density functions allows the organ tracer response to be characterised in terms of anatomical structure and physiological blood flow.

Parametric deconvolution eliminates the necessity to remove noise (and perhaps

other information) from the data with strenuous filtering techniques. Parametric deconvolution is performed by simulating a flow model of an organ with the measured input to the organ and comparing the result to the measured organ data. Non-parametric deconvolution is used to provide initial estimates of the model parameters. These parameters are further refined by iterative non-linear least squares estimation techniques which minimise the error between the measured experimental data and that provided by the model.

Negative artifacts are visible in many non-parametric deconvolution studies. Residence time density theory places limits on the behaviour of the deconvolved data. This thesis shows that the deconvolution of tracer concentration/time curves must give rise to a probability density that cannot be negative. It is proposed that uncertainty in identifying a suitable aorta measurement accounts for a significant component of the negative artifacts reported in the literature. An explanation for this phenomenon is provided and a technique for minimising this effect is suggested. This explanation is extended to identify suitable organ backgrounds.

^{99m}Tc-DTPA scintigraphic imaging studies have been used to obtain experimental results to identify organ perfusion. The mathematical theory has been applied to healthy subjects and to those with pathology. Results indicate that the values of some of the calculated parameters correspond to those measured and published in the literature. In particular for twelve healthy kidneys the model of the renal parenchyma identifies the normal renal filtration fraction as 0.217 ± 0.017. The model of the liver applied to eight healthy livers identifies the portal blood flow fraction as 0.752 ± 0.022, the splenic blood flow fraction as 0.180 ± 0.023 and the liver mean transit time as 11.4 ± 1.7 seconds. It thus appears that RTD techniques adequately describe the flow in imaged organs and that parametric identification based on organ RTD models also provides clinically useful anatomical and physiological information which in turn can be used to identify organ pathology. The quantitative values of the parameters available from these studies on individuals could prove useful in characterising organ function. This might enable medical personnel to make useful clinical deductions that were not previously possible, so that suitable corrective action can be taken in the early stages of kidney, spleen and liver pathology.

Acknowledgements

I wish to express my gratitude to my supervisor and mentor, Professor David Glasser. The interest, guidance and encouragement of my other supervisors namely Dr. Diane Hildebrandt and Dr. Nantakumaran Chetty are greatly appreciated.

Many thanks to the Departments of Nuclear Medicine and Medical Physics for their kind assistance. In particular I would like to thank Professor Jan Esser, Dr. David Rubin, Mr. Geoff Candy and Professor Rex Keddy for their support and encouragement.

My appreciation to the staff and postgraduate students of the Department of Chemical Engineering who forced me to question each step of the process in detail.

The assistance of Mr. Roy Lurie from the Department of Electrical Engineering has been invaluable in developing this work. In particular, this work would not have been possible without Roy's contribution to the data filtering and model simulation techniques.

Lastly I would also like to thank my parents, Sharon Fox and Leonard Fine, as well as Amanda Karklin, for all their support.

Preface

The following papers from this thesis have been submitted for publication:

1. FINE, D.R., LURIE, R.E., CANDY, G.P, (1993), An Anatomical and Physiological Model of the Renal Parenchyma :- Model Development and Parametric Identification, *Accepted for publication in Physiological Measurement.*

2. FINE, D.R., LURIE, R.E., GLASSER, D., HILDEBRANDT, D., ESSER, J.D., CHETTY, N., (1993b), Identification of an Aorta Background for Organ Scintigraphic Deconvolution Studies, *Presentation and publication at the IEEE 15th Annual International Conference.*

3. LURIE, R.E, FINE, D.R., (1993), Simulation of the Renal Retention Function for Physiological Model Parameter Identification, *Presentation and publication at the IEEE 15th Annual International Conference.*

4. FINE, D.R., GLASSER, D., HILDEBRANDT, D., ESSER, J.D., LURIE, R.E., CHETTY, N., (1993c), An Anatomical and Physiological Model of the Hepatic Vascular System, *Accepted for publication in the Journal of Applied Physiology.*

Seminars relating to work from this PhD. thesis have been presented at:

1. Albert Einstein College of Medicine, New York.

2. University of Texas Health and Science Center, Houston.

3. William Beaumont Hospital, Royal Oak Michigan.

4. St. Bartholomew Hospital, London.

From a Thorn

An idea, nothing . . .
Time, fancy and a seed divine, divide.
Growth slowly, cautiously,
Buds and branches form from passion semi-formed,
Stubborn hunger spawned, driven.

Hours, minutes, irritations and frustrations,
(Barbs; the inexperienced forewarned)
And in the morn,
When dusk has dwindled to the dawn,
The cards as awesome as to black,
Warn of truth coerced from haste.
Perseverance, patience, mentor, mastered.
All things, all equal,
Raise a blossom from a thorn.

David Fine, 1994.

Contents

List of Figures

List of Tables

List of Symbols and Abbreviations

a	Net flow out the loop of Henle and into the interstitial tissue per unit volume, s^{-1}
A	Cross sectional area, m^2
$\mathbf{A}$	Fractional transfer coefficient matrix
A_1	Constant of integration
$\mathbf{B}$	Matrix of inputs to the w compartmental system
BEIR	National Academy of Sciences Committee on the Biological Effects of Ionising Radiation
Bq	Bequerel, s^{-1}
c	Speed of light in a vacuum
$c_1 \ldots c_p$	Constants of integration obtained from the initial conditions of a compartmental system
$C(x, y, z, t)$	Activity concentration within an organ, MBq/ml
C_{in}	Tracer concentration in a stream flowing into of a system. In this thesis $C_{\text{in}}(t)$ often refers to the concentration of tracer in the aorta
$\bar{C}_{\text{in}}(s)$	Laplace transform of $C_{\text{in}}(t)$

C_{out}	Tracer concentration in a stream flowing out of a system
C''_{out}	Tracer concentration flowing out of the venous sinusoid of the liver
$\tilde{C}_{out}(s)$	Laplace transform of $C_{out}(t)$
$C^a_{measured}$	Experimentally measured aorta activity/time curve, mol.m^{-3}
C^a_{actual}	Tracer within the aorta, mol.m^{-3}
$\int_0^V C(v,t)dv$	Amount of tracer in the system at time t
$\frac{\int_0^V C_{calc}(t,v)dv}{V}$	Calculated organ activity/time curve
$\frac{\int_0^V C_{meas}(t,v)dv}{V}$	Measured organ activity/time curve
CFD	Computational Fluid Dynamics
CO	Cardiac output, $m^{-3}.s^{-1}$
CSTR	Continuous Stirred Tank Reactor or a completely mixed system
C	Curie. 1Ci = 3.70×10^{10} Bequerels
$D(x,y,t)$	Image count density, cps/m^2
$\overline{D(x,y,t)}$	Average image count density, cps/m^2
DFE	Degrees of freedom for the χ^2 goodness-of-fit test = $N - M - 1$
E	Photon energy
E_i	Experimental observation i
f	Filtration fraction
f_{left}	Left kidney filtration fraction, dimensionless

f_{right}	Right kidney filtration fraction, dimensionless
f_{ij}	Mass flow to compartment i from compartment j (GODFREY, 1983)
$f_\gamma(t)$	The gamma density function
$F(t)$	Probability of a tracer particle spending time t or less in the system, $F(t) = \int_0^t h(t)dt$, dimensionless
FFT	Fast Fourier transform (Appendix H.1)
$\mathcal{F}$	Fast fourier transform operator (Appendix H.1)
$g(L)$	Length density function of a capillary system, m^{-1}
GFR	Glomerular filtration rate, $m^{-3}.s^{-1}$
GFR_{left}	Glomerular filtration rate of the left kidney, $m^{-3}.s^{-1}$
$\text{GFR}_{\text{right}}$	Glomerular filtration rate of the right kidney, $m^{-3}.s^{-1}$
GIT	Gastrointestinal tract
$h(t)$	Residence Time Density, s^{-1}
$h(t)dt$	Fraction of particles which spend time between t and $t+dt$ in the system, dimensionless
$\bar{h}(s)$	Laplace Transform of $h(t)$ (Section 3.4.1)
h_{adjusted}	Residence time density (RTD) of the average renal parenchyma accounting for the delay time for blood to flow from the aorta to the the afferent arterioles of the nephron, s^{-1}
$h_{\text{aorta}}(t)$	Residence time density (RTD) of the aorta, s^{-1}
h_{blood}	Residence time density (RTD) associated with blood flow through the kidney, s^{-1}

$h_{\text{combined}}(t)$	Residence time density (RTD) of the average renal parenchyma, s^{-1}
$h_{\substack{\text{capillaries/}\\\text{sinusoid}}}(t)$	Residence time density (RTD) of blood mixing in the venous sinus and venous capillary network of the spleen, s^{-1}
$h_{\text{cv}}(t)$	Residence time density (RTD) of the central vein, length distributed hepatic sinusoids and hepatic venules, s^{-1}
h_{gi}	Gastrointestinal tract residence time density (RTD), s^{-1}
h_{gs}	Residence time density (RTD) of the splenic and gastrointestinal regions (equation 8.3) , s^{-1}
$h_{\text{ha}}(t)$	RTD of the hepatic artery (section 8.3), s^{-1}
$h_{\text{hvs}}(t)$	Residence time density of the hepatic vascular system in Figure 7.1 (hepatic artery, spleen and gastrointestinal tract), s^{-1}
$h_{ms\rightarrow rp}$	Residence time density (RTD) of blood flow through the red pulp of the spleen, s^{-1}
$h_{\text{parenchyma}}(t)$	Residence time density (RTD) of the renal parenchyma with both the cortical and juxtamedullary nephrons, s^{-1}
$h_{\text{spleen}}(t)$	Residence time density (RTD) of the spleen, s^{-1}
h_{tubule}	Renal tubular residence time density (RTD), s^{-1}
$h_{wp\rightarrow rp}$	Residence time density (RTD) of blood flow through the white pulp of the spleen, s^{-1}
$h_{\text{CSTR}}(t)$	Residence time density (RTD) of a CSTR, s^{-1}
h_{LH}	Loop of Henle residence time density (RTD), s^{-1}
$h_{\text{PLUG}}(t)$	Residence time density (RTD) of a plug flow or unmixed system, s^{-1}
h_θ	Scaled residence time density (RTD) (Appendix J.1)
$H(t)$	Impulse Retention Function (IRF), dimensionless

HA	Hepatic Artery
HV	Hepatic vein
$\mathcal{H}(t-a)$	Heaviside function with delay a
$i(t)$	Arbitrary input function
$I(t)$	Internal Age Density, s^{-1}
IAD	Internal Age Density, $I(t)$, s^{-1}
IFFT	Inverse fast fourier transform (Appendix H.1)
IRF	Impulse Retention Function
$I_{\text{aorta}}(t)$	Internal age density (IAD) of the aorta, s^{-1}
$I_{\text{spleen}}(t)$	Internal age density (IAD) of the spleen, s^{-1}
$I_{\text{vess}}(t)$	Internal age density (IAD) of tissue anterior and posterior of the imaged aorta. One can consider the tissue to be an imaged single input system with the aorta as input to this system, s^{-1}
j	Square root of -1
k_{ij}	*Fractional transfer coefficients* (JACQUEZ, 1972) ie., the fraction that has left compartment j
K	Background activity contribution from tissue anterior and posterior of the imaged aorta, mol.m^{-3}
K_1	Scaling factor for the output curve $o(t)$
K_2	Scaling factor for the input curve $i(t)$
$\text{KMTT}_{\text{total}}$	Renal Parenchymal mean transit time with the vascular component, s

$KMTT_{paren}$	Renal parenchyma mean transit time without the vascular component, s
L	Length, m
LMTT	Liver mean transit time, s
LPDF	Liver Probability Density Function (see equation 7.11)
LT	Laplace transform
$\mathcal{L}$	Laplace transform operator
m	Metre
$\vec{m}_1 \ldots \vec{m}_p$	The eigenvectors from the solution of $\lambda \mathbf{I} - \mathbf{A} = 0$
M	Number of unknown parameters in a mathematical model
$MEAN_\gamma$	Mean of the gamma density function
MTT	Mean Transit Time $= \int_0^\infty th(t)dt$
MTT_b	Mean transit time of the blood in the renal parenchyma, s
MTT_{cc}	Collecting duct and inner calyces mean transit time
MTT_{gi}	Mean transit time of the GIT
n	An arbitrary number of parallel plug flow capillaries
$n_y(t)$	Unmeasured experimental noise
N	Number of random samples or observations
NCRP	National Council on Radiation Protection
NRF	Normal renal fraction, dimensionless
$\mathcal{N}$	Length of some arbitrary vector v (Appendix H.1)

$o(t)$	Arbitrary output function
OLS	Ordinary least squares (Appendix I.1)
p	Fraction of portal blood that flows through the spleen as opposed to the gastrointestinal tract, dimensionless
P	Probability
P_i	Predicted value i
P_{ij}	ij element of the covariance matrix (Appendix I.1)
Plug Flow	An unmixed system where material that enters together, stays together and leaves together
PALS	Periarterial lymphatic sheath
PEM	Prediction-error identification method
PLUG	Plug flow system or an unmixed system where material that enters a system together stays together and leaves together
PTTI	Parenchymal transit time index, s
PV	Portal vein
PWP	Peripheral white pulp
q	Fraction of blood that flows through the closed circulation of the spleen
q_i	Fraction of material flowing through plug flow i
Q	Volumetric flowrate, $m^3.s^{-1}$
Q^{Ho}	Initial loop of Henle flowrate, $m^{"3}.s^{-1}$
Q^o	Total blood flow into the liver, $m^3.s{-}1$
$Q'C'_{\text{in}}$	Mass flow into the liver by the portal vein

$Q^*C''_{in}$	Mass flow into the liver by the hepatic artery
Q^oC_{out}	Mass flow out of the liver by the hepatic vein
r	Fraction of blood that flows into the liver through the portal vein, dimensionless
r_{ij}	ij element of the correlation matrix (Appendix I.1)
ROI	Region of Interest (see section 2.2.1)
RTD	Residence Time Density (RTD) which is the same as the Transit Time Spectrum which is discussed in the medical literature
s	Arbitrary complex variable in the laplace domain, or s denotes time in seconds
s^2	Approximate constant variance of measurement errors (Appendix I.1)
SEM	Standard Error of the Mean
SS	Sum of squares (Appendix I.1)
S_o	Gamma camera sensitivity, cps/MBq
t	Time, s
t'	Integration variable
t_{max}	Time at which the maximum in activity/time curve occurs
t_m	Arbitrary constant time (Appendix J.1)
T	Experiment duration
^{99m}Tc-DTPA	^{99m}Technetium-diethylenetriaminepentaacetic acid
TTS	Transit Time Spectrum which is the same as the Residence Time Density

$u(t)$	Arbitrary function which is defined for all $t \geq 0$ and whose integrals in equations 3.22 and 3.23 converge
$\bar{u}(s)$	Laplace transform of $u(t)$
$u_i(t)$	The initial input mass flowrate, f_{i0}
$\vec{v}, \vec{V}$	Arbitrary vector of length $\mathcal{N}$ (Appendix H.1)
V	System Volume, m^3
V_{LH}	Descending loop of Henle volume
V_{sinus}	Volume of the hepatic sinusoid
w	Number of compartments
x_i	Amount of material in compartment i
$\dot{x}$	Derivative of x with respect to time
X_i	Sensitivity vector for parameter i (Appendix I.1)
$X_{jk}(i)$	Sensitivity coefficient for the jth dependent variable in in $f(t, \beta)$, for the kth parameter at the ith time
y	Dummy variable, $y = ln(Q' + \phi v)$
$Y(t)$	Arbitrary density function
z	Skewness of the gamma density
α	Fraction of renal blood which flows to the cortical nephrons and as opposed to the juxtamedullary nephrons $(1 - \alpha)$, dimensionless
β_i	Arbitrary model parameter (Appendix I.1)
χ^2	The χ^2 distribution (CHATFIELD, 1978)
$\delta(t)$	*Dirac* delta function, s^{-1}

Γ	Gamma function, $\Gamma(\alpha) = \int_0^\infty e^{-t} t^{\alpha-1} dt$
κ	Fraction of blood that flows through the white pulp of the open circulation of the spleen
λ	γ radiation wavelength
$\lambda_1 \ldots \lambda_p$	The eigenvalues from the solution of $\lambda \mathrm{I} - \mathrm{A} = 0$
μ	Gamma ray attenuation coefficient, m^{-1}
ν	γ radiation frequency
ω	Largest real pole of the Laplace transform in the complex plane
$\omega_{\mathcal{N}}$	$\mathcal{N}$-th root of unity (Appendix H.1)
ψ	Planck's constant
ϕ	Blood flow per unit volume of the liver sinusoid that enters the liver sinusoid from the hepatic artery
ρ	Fluid Density
σ	Variance of ages of tracer molecules
τ	Mean age, Mean Residence Time or Mean Transit Time (MTT) of tracer molecules
τ_{aLH}	Ascending loop of Henle mean residence time, s
τ_{b}	Renal parenchymal blood time constant, s
τ_{bt}	Mean transit time of the background tissue (Section 1.6)
τ_{c}	Mean confidence time of the aorta measurement, s
τ_{cc}	Mean residence time of tracer in the collecting duct system and inner calyces, s

τ_{cd}	Mean residence time of tracer flowing down the shortest collecting duct, s
τ_{cv}	Time constant of the central vein, length distributed hepatic sinusoids and hepatic venules, s
τ_{d}	Distal tubule mean residence time, s
τ_{delay}	Delay time associated with the flow of blood from the aorta to the afferent arterioles of the kidney
τ_{dLH}	Descending loop of Henle mean residence time, s
τ_{e}	Time constant of the exponential curves appended to $i(t)$ and $o(t)$
τ_{git}	Time constant of gastrointestinal blood flow
τ_{ha}	Transit time of blood travelling down the hepatic artery (section 8.3), s
τ_{hvs}	Residence time density of the hepatic vascular system in Figure 7.1 (hepatic artery, spleen and gastrointestinal tract)
τ_{i}	Transit time associated with plug flow i
τ_{liver}	Volume of the liver divided by the total volumetric flowrate into the liver (V_{liver}/Q^{o}), s
τ_{LH}	Loop of Henle mean transit time
τ_{mr}	Blood transit time through the red pulp of the spleen
τ_{p}	Proximal tubule mean transit time, s
τ_{pv}	Delay time for blood flow up the portal vein
τ_{s}	Time constant associated with blood flow in the venous sinusoids and trabecular veins of the spleen
τ_{sinus}	Mean transit time of the hepatic sinusoid ($\frac{V_{sinus}}{Q^{o}}$), s
τ_{spleen}	Mean transit time of the spleen, s

τ_t	Mean transit time through the shortest nephron and shortest length of collecting duct ie. $\tau_{tc} + \tau_{cd}$, s
τ_{tc}	Cortical nephron tubule transit time, s
τ_{tj}	Juxtamedullary nephron tubule transit time, s
τ_{tn}	Mean residence time of tracer from the point of entry at the glomerulus, to the exit point of a nephron, s
τ_w	Blood transit time through white pulp of the spleen
τ_γ	Parameter associated with the mean of the gamma probability density function
τ_ϕ	$1/\phi = \frac{\tau_t \tau_{tcca}}{1-\tau}$
θ	Normalised time variable t/t_m (Appendix J.1)
ε	error between the measured and approximate activity/time curve
ζ	Fraction of tracer within the aorta that flows through background tissue, dimensionless
$*$	Convolution ie. $a * b = \int_0^t a(t-t')b(t')dt'$
*	Significantly different from normal, $P < 0.05$
$\approx$	Approximately equal to
$\triangleq$	Denotes a definition
∞	Infinity

Chapter 1

Previous Analysis of Imaged Radioactive Tracer Studies

1.1 Introduction

The amount of literature on quantification of organ function from radioactive tracer experiments is very large. The clinical evaluation of these tests has a past which is both subjective and qualitative since there has been limited means of quantifying the contribution of various organ tissues on the measured data. Consequently, imaged radioactive tracer procedures have not had the desired diagnostic precision. Investigators have sought to improve this precision by developing more objective criteria for data interpretation. In general these methods have used a mathematical description of the tracer interaction in the organ under investigation to interpret the data. Most of these mathematical techniques have not gained widespread use because they still do not yield the basic parameters of organ physiology which are of interest to the clinician.

This chapter attempts to review the literature that is specifically related to the mathematical description of tracer interactions within an organ.

1.2 Compartmental Modelling

A large number of published articles in the literature use compartmental modelling in an attempt to explain imaging data. It is for this reason that a detailed explanation of compartmental modelling is provided.

Compartmental systems consist of a finite number of homogeneous, well mixed, lumped subsystems (Termed Continuous Stirred Tank Reactors, CSTR's, in the chemical engineering literature) which exchange with one another (GODFREY, 1983). This means that the time dependent quantity or concentration within each compartment may be described by a first order differential equation. The assumptions made in this analysis are that:

- Each compartment represents a chamber of constant volume, V, with constant flowrates into and out of the compartment.
- There is instantaneous and complete mixing of the input to the compartment.
- The rate limiting step in any process is not mixing dependent. For instance this assumption would probably be a reasonable approximation in the case of the subcutaneous (below the skin) administration of a pharmaceutical and its subsequent concentration as a function of time in the blood. Under these circumstances it would take a long time for the pharmaceutical to diffuse through the various tissues into the blood. The blood and the subcutaneous deposit could then be approximated as perfectly mixed since the concentration within each compartment would be approximately uniform with time.
- The initial impulse into some compartment i must be known. A blood compartment is often defined where the tracer is introduced as an impulse at zero time. The vascular cavity is in practice not well mixed and one expects that the time lags in the vascular compartment would often disqualify such a simplification.

The general form for w compartments is given by:

$$\frac{dx_i}{dt} = f_{i0} + \sum_{\substack{j=1 \\ j\neq i}}^{w} f_{ij} - \sum_{\substack{j=1 \\ j\neq i}}^{w} f_{ji} - f_{0i} \tag{1.1}$$

where

f_{ij} :- Mass flow to compartment i from compartment j (GODFREY, 1983)

x_i :- Amount of material in compartment i

For a closed system $f_{0i} = 0$ $(i = 1, 2, \ldots, w)$. In the case where the flowrates are directly proportional to the quantity in the donor compartment (Donor Compartment must be CSTR), a proportionality rate constant k_{ij} can been defined such that:

$$\frac{dx_i}{dt} = \sum_{\substack{j=1 \\ j\neq i}}^{w} k_{ij}x_j - \sum_{\substack{j=1 \\ j\neq i}}^{w} k_{ji}x_i - k_{0i}x_i + u_i(t) \tag{1.2}$$

where

$u_i(t)$:- The initial input mass flowrate, f_{i0}

k_{ij}, k_{ji} :- *Fractional transfer coefficients* (JACQUEZ, 1972) ie., the fraction that has left the donor compartment

If reaction (or adsorption) occurs then the number of compartments is increased according to the number of possible mechanisms, thus a first order reaction $A \rightarrow B$ would require two compartments, one for A and another for B, with a fractional transfer coefficient equal to the rate constant.

Compartmental modelling problems solve the w systems of equations of equation 1.2 by matrix manipulations. Equation 1.2 can be written in matrix form:

$$\begin{bmatrix} \dot{x}_1 \\ \vdots \\ \dot{x}_w \end{bmatrix} = \begin{bmatrix} a_{11} & \cdots & a_{1w} \\ \vdots & \ddots & \vdots \\ a_{w1} & \cdots & a_{ww} \end{bmatrix} \begin{bmatrix} x_1 \\ \vdots \\ x_w \end{bmatrix} + \begin{bmatrix} b_{11} & \cdots & b_{1w} \\ \vdots & \ddots & \vdots \\ b_{w1} & \cdots & b_{ww} \end{bmatrix} \begin{bmatrix} u_1 \\ \vdots \\ u_w \end{bmatrix} \tag{1.3}$$

or in matrix notation:

$$\dot{\vec{x}} = \mathbf{A}\vec{x} + \mathbf{B}\vec{u} \tag{1.4}$$

where

A :- Fractional transfer coefficient matrix

B :- Matrix of inputs to the w compartmental system

$\dot{x}$:- Derivative of x with respect to time

The general solution of equation 1.4 is given by:

$$\vec{x} = c_1 e^{\lambda_1 t}\vec{m}_1 + c_2 e^{\lambda_2 t}\vec{m}_2 + \ldots + c_p e^{\lambda_p t}\vec{m}_p \tag{1.5}$$

where

$\lambda_1 \ldots \lambda_p$:- The eigenvalues from the solution of $\lambda\mathbf{I} - \mathbf{A} = 0$

$\vec{m}_1 \ldots \vec{m}_p$:- The eigenvectors from the solution of $\lambda\mathbf{I} - \mathbf{A} = 0$

$c_1 \ldots c_p$:- Constants of integration obtained from the initial conditions of a compartmental system

Figure 1.1 shows the effect of mixing on a first order reaction, $A \rightarrow B$, in a constant volume, constant flowrate system. A fixed concentration is fed into the system and the figure shows the output concentration from such a system as a function of residence time within the system. The output concentration is plotted for a completely mixed system or CSTR and for an unmixed system which is often termed a "Plug" flow system. In a plug flow system, material that enters together, stays together and leaves together. It is clear from Figure 1.1 that the effect of mixing can be significant. This in turn implies that compartmental modelling may describe reaction phenomena poorly.

In compartmental modelling a model structure is generally tried and then is changed or *tailored* to the observations (GODFREY, 1983). This is termed **black box** modelling and suffers from the disadvantage that the model parameters often have no physical meaning. The most serious limitation of compartmental modelling is that a system may have areas of complete mixing and others that are unmixed. An example of such a system would be blood flow inside a vessel with lateral diffusion. In such a case, the benefits of compartmental analysis are difficult to define (GODFREY, 1983) and an approach focussing on input output relationships is preferable.

Various approximations have been made to try and use compartmental analysis in unmixed systems. Plug flow is particularly applicable to blood flow in individual

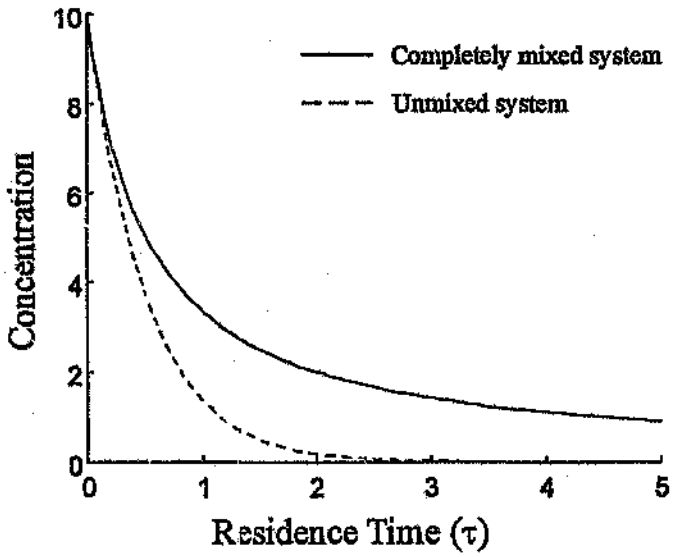

Figure 1.1: The effect of mixing on the reaction $A \rightarrow B$ with first order reaction kinetics in equal volume systems.

capillaries. BURTON (1966) has shown that capillaries act like rigid tubes over a wide range of pressures. PROTHERO AND BURTON (1961) have shown that flow in capillaries is plug flow in nature where the red cells act as moving plugs, and the interstitial plasma is perfectly mixed. This is shown in Figure 1.2. Compartmental approximations for plug flow are based essentially on:

- Infinite number of interacting compartments in series.
- Infinite batch systems with no interaction (Figure 1.2).

Once a model configuration has been chosen, equation 1.5 is then be fitted to the experimental data. In general a sum of exponential terms is sufficiently flexible to fit almost any data, although the solution of the characteristic equation for the eigenvalues is not necessarily straightforward (JACQUEZ, 1972). It is also possible to obtain imaginary eigenvalues which are not physically meaningful although they may fit the data well. Coupled with these problems is the fact that even a large number of CSTR's will never completely approximate a single plug flow system. Ideally one

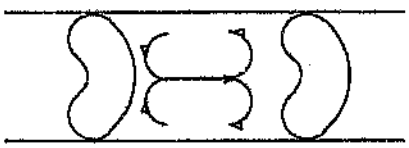

Figure 1.2: Mixing in a Blood Capillary

needs a better modelling theory that is flexible enough to describe mixing and flow in various organs. The theory must:

- Cover a complete spectrum of mixing states from a completely mixed system to an unmixed one.
- Allow reaction and diffusion mechanisms to occur.
- Should allow the development of the model to proceed according to the physical properties of the system.

Compartmental modelling (without making approximations and spurious assumptions) in general fails to provide adequate flexibility as far as these criteria are concerned.

1.3 The Kidney

Models of the kidney have been primarily compartmental in nature (DEGRAZIA *et al.*, 1974; OPPENHEIM AND APPLEDORN, 1978). These models generally have a large parameter space [1]. Recirculation is accounted for by adding an extra compartment which is not effective (see NAOR *et al.*, 1972 for the effect of recirculation on linear flow modelling). The models also fail to address the length distribution of the cortical and juxtamedullary nephrons. The formulation of these models for imaging radioactive tracers has not been sufficiently addressed by these authors (see

[1] DEGRAZIA *et al.*'s (1974) model has eleven parameters and OPPENHEIM'S & APPLEDORN'S (1978) model has even more.

Chapter 3). The compartmental approach has been discussed in section 1.2 and has been found to be deficient for flow modelling.

1.4 The Spleen

There are very few mathematical models of the spleen in the literature. Those models that have been published are primarily compartmental in nature (HEYNS *et al.*, 1980; PETERS *et al.*, 1980). The compartmental models are either oversimplified [2] or complex with a number of compartments and many parameters (SWEETLOVE, 1990). The compartmental modelling approach has been discussed in section 1.2 and has been found to be problematical for physiological modelling.

1.5 The Liver

1.5.1 Computational Fluid Dynamics (CFD)

One approach for analysing tracer flow though the liver is using CFD techniques, where a finite element grid is fitted to the liver anatomy and fluid momentum and continuity equations are then applied to the system (LEE & RUBINSKY, 1990).

The paper by LEE & RUBINSKY (1990) provides an example of how such a technique has been implemented. There are various anatomical constraints that limit the analysis. Often simplifications have to be made. For example LEE & RUBINSKY (1990) neglect the hepatic arterioles which enter all along the venous sinusoid where mixing of high pressure arterial blood and low pressure venous blood occurs through small sphincter like structures (RAPPAPORT & SCHNEIDERMAN, 1976). As a result, the modelling approach fails to describe an important component of blood flow in the liver. Combined with these problems is the large computation time associated with finite element analysis. This limits the clinical application of such techniques.

[2] HEYNS *et al.*'s (1980) model consists of a two compartmental model with one blood compartment and one spleen compartment.

In general to solve such problems one has to have measures of physical properties such as porosity, fluid and tissue density, average length and diameter of venous sinusoid, viscosity and pressures in the various vessels that enter the liver. The effect of variation of these properties between individuals is not accounted for.

An adequate mathematical description of blood flow through the hepatic arterial and portal venous systems is necessary for the *in vivo* application of CFD modelling. Thus while CFD techniques can often be applied to idealised *in vitro* conditions, they are impractical for routine clinical application.

1.5.2 Distributed and Convective Dispersion Models (CDM)

These models fall within the scope of residence time density (RTD) modelling (LEVENSPIEL (1972) provides a detailed review of RTD modelling). There are essentially three models that are discussed in the literature, the **undistributed sinusoidal perfusion** model, **distributed sinusoidal perfusion** model and the **convective-dispersion** model. A review of these models is given in a paper by BASS *et al.* (1987). These models have primarily been applied to data from reactive tracers which are injected into the hepatic artery of isolated livers. The models assume that there is unidirectional flow through independent tubes.

In the **undistributed sinusoidal** model each liver sinusoid has a common arterial input with an initial concentration of substrate. The concentration of substrate is depleted along the tube as it flows with the blood to the venous end of the sinusoid. Each tube is modelled as a plug flow system. The outputs in the undistributed system are all the same for any sinusoid.

In the **distributed sinusoidal** model there are differences in the sinusoidal outputs because of the length distribution of the venous sinusoids. The outputs of all the sinusoids are then averaged in an appropriate manner to represent the mixing of all the individual sinusoidal outputs. The mixing is achieved by taking the flow weighted mean of the outputs. Sinusoidal perfusion models do not allow intermixing between sinusoids and no account is taken of the portal venous blood.

Convective dispersion models introduce a dispersion coefficient to allow intermixing between parallel sinusoids to occur. The interpretation of the dispersion coefficient becomes difficult from a physiological standpoint and it is difficult to describe how the dispersion coefficient changes with hepatic blood flow. Again no account is made of the interaction of portal venous and hepatic arterial blood. BASS *et al.* (1987) tried to relate the convective dispersion model to the sinusoidal perfusion model in an attempt to characterise the dispersion coefficient. These authors approximated the dispersion model by putting a number of distributed sinusoidal systems in series. While this may give rise to the same residence time density, the approximation is not valid if the model is being used to describe systems in which reactions with non-linear reaction kinetics occur (ZWIETERING, 1959). The only way that the distributed sinusoidal model can approximate the axial dispersion model is if there is cross mixing between all possible plug flows so that material of different ages can move forward or backward in residence time. The cross mixing scenario is shown in Figure 1.3 and it is clear from this figure that the derivation of an analytical expression for such a system is problematical. This in turn means that an interpretation of the dispersion coefficient from a physiological perspective will in all likelihood remain obscure. While the convective dispersion models do allow mixing between the different sinusoids, there is some question as to whether this analysis characterises the length distribution of sinusoids sufficiently.

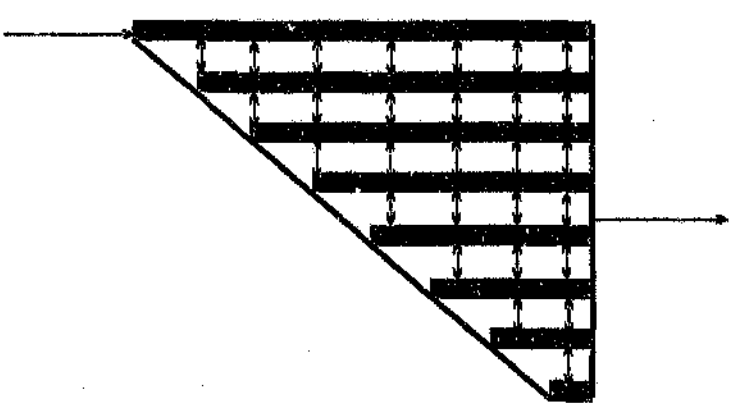

Figure 1.3: True distributed sinusoidal model approximation of the axial dispersion model.

1.6 Length Distributed Vessel Beds

Many theoretical formulations have been used to explain the shape of peripheral indicator dilution curves (WARNER, 1962; THOMPSON *et al.*, 1964; EVANS, 1959). In such experiments a tracer is injected into the right atrium of the heart or the pulmonary artery and the peripheral arterial blood is continuously sampled and the tracer concentration measured. THOMPSON *et al.* (1964) applied the gamma density function to the results of a large number of subjects and showed statistically that this density could be used to represented tracer flow from the heart to the peripheral circulation. The gamma density function is given by equation 1.6 where z affects the skewness of the density and τ_γ is related to the mean of the density by equation 1.7.

$$f_\gamma(t) = \frac{1}{\tau_\gamma^z \Gamma(z)} t^(z-1) e^{-t/\tau_\gamma} \tag{1.6}$$

where

Γ :- Gamma function, $\Gamma(\alpha) = \int_0^\infty e^{-t} t^{\alpha-1} dt$

$$\text{MEAN}_\gamma = \int_0^\infty t \, \frac{1}{\tau_\gamma^z \Gamma(z)} t^(z-1) e^{-t/\tau_\gamma} dt = z\tau_\gamma \tag{1.7}$$

One might expect that the length distribution of vessels between the heart and the periphery is greater than the length distribution of vessels within most organs. It is thus likely that the gamma density would characterise the behaviour of a tracer within an organ which contains a length distributed vascular system. It is for this reason that the Gamma density has been used in this thesis to model vascular flow in tissue. Based on THOMPSON *et al.*'s (1964) results, the value of z should be less than four and greater than one. In this thesis a value of $z = 2$ has been chosen for systems which are assumed to have relatively small length distributions and $z = 3$ for larger length distributions. $z = 1$ is not generally useful as this implies that the fraction of vessels of zero length is a maximum. The relationship between a length distributed system and a probability density such as the gamma density is derived in Appendix C.1.

Chapter 2

General Experimental Procedure

2.1 ^{99m}Technetium-diethylenetriaminepentaacetic acid :- A Suitable Radioactive Tracer

To measure plasma and urine flow a radioactive tracer is often used which does not react with tissue (has no physiological interaction), is low in concentration, follows the plasma and urine flow and is distinguishable from the observed system and thus measurable.

2.1.1 The Kidney

The choice of radioactive tracer to determine renal function depends on whether one wants to investigate tubular function or glomerular filtration, transit times and renal blood flow. In this thesis the latter was investigated. ^{99m}Tc-DTPA has been used as a tracer as it follows plasma and urine flow and is filtered in the glomerulus in the same way inulin with only minimal cortical retention (McAfee *et al.*, 1981). ^{99m}Tc-DTPA is not reabsorbed in the tubular system of the kidney and flows with urine to the bladder. This also means that ^{99m}Tc-DTPA has a short biological half life because it is actively excreted from the body. Another advantage of ^{99m}Tc-DTPA is that is forms very few complexes with plasma proteins which is a problem associated with other tracers like ^{99m}Tc-GHA, ^{99m}Tc-AC, ^{99m}Tc-DMSA, ^{99m}Tc-MDP, ^{99m}Tc-HEDP, ^{99m}Tc-PPi (McAfee *et al.*, 1981). Renal extraction

of ^{99m}Tc-DTPA is also higher than any of the other technetium agents (McAfee *et al.*, 1981). Thus the radioactive tracer ^{99m}Tc-DTPA has been used for all the renal investigations presented in this thesis.

2.1.2 The Liver and Spleen

The choice of radioactive tracer for the determination of spleen and liver function is somewhat easier than that for the kidney. The criteria for an ideal tracer included:

- No reaction with hepatic or splenic tissue.
- Short biological half life.
- Low radiation dose.
- Rapid bolus injection (approximation of a Dirac $\delta(t)$ function) possible.

The first criterion eliminates the extractable radiolabeled colloid materials which interact with the spleen and liver tissue (Wraight *et al.*, 1982). The last criterion excludes labelled red blood cells because rapid injections damage these cells which then adhere and react with the spleen and liver parenchyma. Pertechnetate (^{99m}Tc O_4^-) was first shown to be a suitable non-interacting tracer for hepatic and splenic procedures by Sarper *et al.* (1981). Later ^{99m}Tc-DTPA was also shown to be a suitable non-interacting tracer (Gianpaolo *et al.*, 1989). ^{99m}Tc-DTPA has a biological residence time that is about seven times less than that of Pertechnetate (Roedler, 1981). It is for these reasons that the radioactive tracer ^{99m}Tc-DTPA has been used for the splenic and hepatic studies presented in this thesis.

2.1.3 Effects of Low Level Radiation

A large body of literature has found no evidence of increase in human malignancy or other harmful effects, as a consequence of ionising radiation, even at cumulative exposures comparable to those of natural background or even ten-times higher (Yalow, 1981). The National Academy of Sciences Committee on the Biological

Effects of Ionising Radiation (BEIR) provides an average natural background radiation level (USA) as 184mrem per year (BEIR, 1980). ROEDLER (1981) has shown that a 5mCi ^{99m}Tc-DTPA experiment contributes 150mrem to a patient. Thus a 10mCi intravenous ^{99m}Tc-DTPA experiment contributes 300mrem. If the average yearly background and experimental dose are added together, then the total yearly dose is increased to 484mrem. The National Council on Radiation Protection and measurements (NCRP) provide guidelines for radiation protection. The maximal safe radiation dose per year is given as 5000mrem (WRENN *et al.*, 1982). It is clear that typical natural background counts combined with the amount administered in a 10mCi intravenous ^{99m}Tc-DTPA injection falls well below this value.

2.2 Theory of Dynamic Scintigraphy

The energy and wavelength of γ photons is given by:

$$E = \psi\nu = \frac{\psi c}{\lambda} \tag{2.1}$$

where

E :- Photon energy

ψ :- Planck's constant

ν :- γ radiation frequency

c :- Speed of light in a vacuum

λ :- γ radiation wavelength

γ-radiation has sufficient energy to penetrate the body tissue and be measured. γ-radiation can be measured using a scintillation camera which consists of essentially four components:

Collimator: The purpose of this device is to ensure that photons which pass through the collimator are all parallel. Thus radioactivity that passes through a particular part of the collimator is from tissue directly beneath it. The collimator in essence consists of a lead plate with small holes drilled through it. The thickness and hole density are chosen to maximise resolution or sensitivity. The

collimator used in this thesis was a low energy, medium resolution Elscint™ COL APC-3S (Haifa, Israel) collimator. This collimator provides sufficient image resolution while maintaining reasonable radioactive count rates.

Sodium-Iodide Crystal ($NaI(Tl)$): Converts the γ-ray into visible light photons by the scintillation process. The crystal which has a Thalium impurity is transparent and the flashes of light can be measured. The intensity of light is directly related to the γ-photon energy.

Photomultipliers: Light emitted from the NaI-crystal is amplified and converted to an electrical pulse. The intensity of the electrical pulse is proportional to the light intensity.

Threshold Counter: A threshold is used to determine whether a pulse lies in the correct energy range. Multiple events and background isotopes are thus excluded. The energy window for ^{99m}Tc was set at $\pm 10\%$ of the 140keV maximum γ photon energy associated with the decay of ^{99m}Tc.

2.2.1 Activity/time curves from a Region of Interest (ROI)

Data that is collected using a scintillation camera is generally displayed as a number of images on a computer screen. Each image represents the number of radioactive counts over the imaged area within a time interval. Typical images detailing the flow of a radioactive tracer through the body are shown in Figure 2.1. Image processing techniques can be used to enhance these images and thus visualise the physical location of various structural components of the body. Once these structural components have been located, the image processor allows one to draw a region on the computer screen, and then to count the radioactivity within that region as a function of time. These regions are termed Regions of Interest (ROI's). The data from this procedure is normalised with respect to the time interval between frames and the ROI area. A plot of this normalised data against time has a dependent variable (Y-axis) with units of Counts.pixel^{-1}.s^{-1} and an independent variable (X-axis) with units of seconds. If the concentration of radioactive tracer is low enough (in this thesis this is always the case), then such a graph is analogous to the average

concentration within the ROI as a function of time. The choice of a suitable ROI for a particular organ is addressed below.

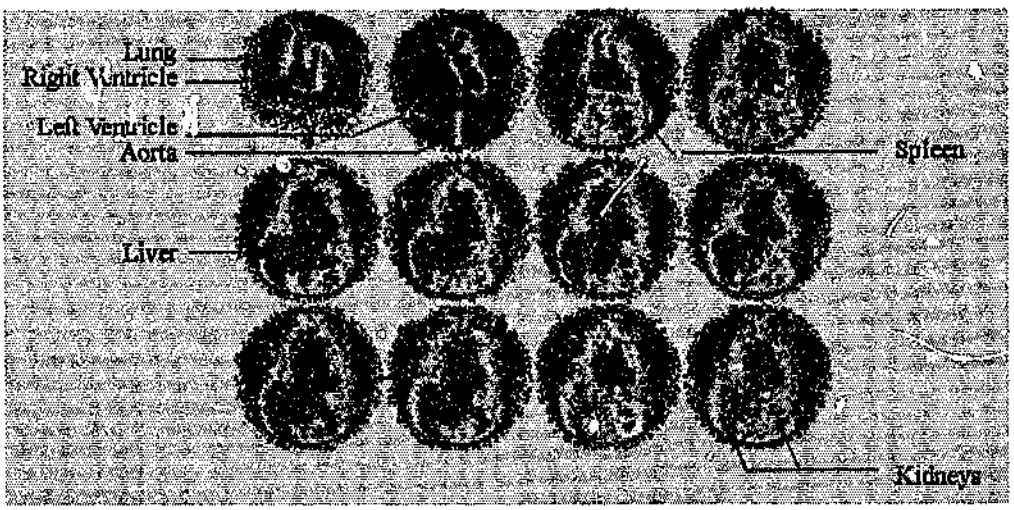

Figure 2.1: ^{99m}Tc-DTPA Tracer study :- 128 × 128 pixels grouped in 10 second intervals.

2.2.1.1 Aorta

The input to the various organs under investigation in this thesis was taken from a rectangular Region of Interest (ROI) drawn on the descending aorta which was clearly observed in the first 15 seconds.

2.2.1.2 Kidney

Tissue anterior and posterior to the kidney accounts for significant background photon counts. Several organs superimpose in the regions of interest of the kidney and contribute to renal background. These organs include: the liver, the spleen, the adrenals in the upper poles of the kidneys, the large vessels and the duodenum at the medial border, the gut at the lateral border, the skin, muscle and fat layers and other tissues anterior and posterior of the kidney (FLEMING, 1988). In attempts to obtain representative background ROI's, proposed backgrounds have included: the liver, a one pixel width perirenal area (PIEPSZ *et al.*, 1977), the inter-renal

area (FLEMING, 1988), a ROI round the external border of the kidney (BLAUFOX, 1989;ROSENTHALL *et al.*, 1981), and a subrenal area (GATES, 1983). None of these ROI's appeared to adequately account for the background radiation contribution. In order to work within the constraints of the available experimental information, a semi-theoretical approximation of renal background was determined. This approximation uses the activity/time curve obtained from a region of interest inferior to the lower pole of the kidney. The determination of this renal background is discussed in section 5.4.1.

The selection of regions of interest of the renal parenchyma have been a major source of error in renal studies (FLEMING 1988; PIEPSZ *et al.*, 1990). In this thesis, the most satisfactory parenchymal ROI was found to be the lateral subrenal ROI described by BLAUFOX (1989).

2.2.1.3 Spleen and Liver

The liver and spleen ROI's were drawn so as to exclude contribution from the lower poles of the lungs, the kidneys and the descending aorta.

The extreme lateral situation of the spleen and the large transaxial cross section of the liver within the abdomen, precludes the necessity to account for anterior or posterior tissue which would otherwise account for significant background tissue radiation.

2.3 Experimental Protocol

2.3.1 General

Normal volunteers were selected for organ imaging according to the criteria accepted by the Committee for Research on Human Subjects (medical) of the University of the Witwatersrand [1]. Informed consent was obtained in all cases. Patients were

[1]Protocol Ref:14/49, Ref:02/8/92

selected on the basis that:

- There was no prior history of chronic renal, hepatic, splenic or cardiopulmonary disease.
- The volunteers had not undergone any major surgery in the cardiothoracic or abdominal regions.

2.3.1.1 Kidney

The twelve normal kidneys selected for the study were obtained from a data base of renal donor subjects admitted for renal function evaluation at the Department of Nuclear Medicine, University of the Witwatersrand. Approval from the Committee for Research on Human Subjects (medical) of the University of the Witwatersrand was obtained to use the data from these studies. The procedure for all subjects was identical. The subjects were placed in the supine position and an intravenous dose of (10mCi (370MBq)) was injected into the right antecubital vein as a bolus. All the subjects were hydrated by oral administration of 300ml of water half an hour before the study, and venous administration of 1ml/min of saline during the study (COSGRIFF ET AL., 1992). Image acquisition was performed using an Elscint™ Apex 409M (Haifa, Israel) scintillation camera. Data was collected posteriorly using a 128 x 128 pixel matrix at 1 second per frame for the first 120 seconds followed by 10 seconds per frame for the remaining 1680 seconds. The total scanning time was 30 minutes.

Two additional patients with suspected renal arterial stenosis were selected to determine whether the parametric deconvolution technique could identify the pathology.

2.3.1.2 Spleen and Liver

The experimental procedures were performed at 7:30am. The volunteers were required to abstain from all fluids and solid foods from 11:00pm the previous evening. This was to ensure fasting blood perfusion of the spleen and liver. The volunteers

were placed in the supine position and an injection of 10mCi of ^{99m}Tc-DTPA was administered as a bolus into the antecubital vein. Image acquisition was performed using an Elscint™ Apex 409M (Haifa, Israel) scintillation camera. Anterior scintigraphic images were acquired on a 128 x 128 pixel matrix at a rate of 2 frames per second for the first minute, and a rate of one frame per second for another five minutes. This was to allow enough time to ensure complete perfusion of the spleen, gastrointestinal tract and liver.

Experimental data for two portal hypertensive patients was chosen from a database of subjects referred to the Department of Nuclear Medicine, University of the Witwatersrand.

2.3.2 Data Analysis

It is known that tracer count rates are subject to random errors associated with detection of events from radioactive sources. This noise can be characterised by Poisson statistics. The non-linear data-bounding technique proposed by DIFFY & CORFIELD (1976) assumes a Poisson noise distribution. According to DIFFY & CORFIELD (1976), the data bounding approach may be regarded as a non-linear, non-stationary operator which effectively filters the high frequency components present in the data. This technique proved to be more useful than conventional linear filtering methods, although the gamma camera renogram has counts that are moderately large and the error distribution could be regarded as essentially gaussian in nature.

In this thesis, all **non-parametric** deconvolution was performed using the fast Fourier transform (FFT) method (NIMMON *et al.*, 1981; Appendix H.1) with data bounding (DIFFY & CORFIELD, 1976) and filtering (FLEMING, 1988). The aorta, kidney, spleen and liver data for **parametric** deconvolution was not altered. The experimental data for the renal, splenic and hepatic studies appears in Appendix S.1.

All data analysis was performed on a 486 IBM compatible computer using Matlab™, (MOLER *et al.*, 1987), with the associated signal processing and optimisation toolboxes.

2.3.3 Statistics

2.3.3.1 Model Parameters

All model parameters obtained by analysing the data from normal subjects in Chapters 5, 6 and 8 were assumed to be normally distributed (CHATFIELD, 1978) [2]. A parameter value from an organ pathology was significantly different from the normal value if that value fell outside two standard deviations from the normal subject mean, or in other words, within the 95% confidence interval ($P < 0.05$).

2.3.3.2 χ^2 Goodness-of-Fit Test

The χ^2 goodness-of-fit test was used in this thesis to determine whether the mathematical models derived in Chapters 5, 6 and 8 represented the distribution function of the experimental data (CHATFIELD, 1978). χ^2 is determined by:

$$\chi^2 = \sum_{i=1}^{N} \frac{(E_i - P_i)^2}{P_i} \tag{2.2}$$

where

N :- Number of observations

E_i :- Experimental observation i

P_i :- Predicted value i

The degrees of freedom (DFE) are determined by taking the number of observations minus the number of unknown model parameters, M, minus one. In this thesis $P < 0.05$ was chosen as the χ^2 test statistic. All the model curves displayed in Appendices Q.1 and R.1 were found to represent the distribution function of the experimental data ($P < 0.05$).

[2] As $N \rightarrow 10$, one generally tends to the normal distribution in biological systems where N is the number of random samples.

Chapter 3

Deconvolution and Imaged Single Input Organs

3.1 Introduction

In this chapter, the theory of residence time and internal age densities is reviewed and the results are then applied to experimental data obtained by imaging single input organs in a time-invariant, recirculating system. General results are presented which relate the deconvolved data to the internal age density. Bounds are placed on the deconvolved curves. In developing the concepts of mixing we consider steady flow (time-invariant) systems with constant density fluids.

3.2 Theory of Residence Time and Internal Age Densities

Each particle in the outflow from a system possesses a previous history. The residence time or transit time of the particle within the system can be defined in statistical terms. Each distribution of residence times can be associated with a function $F(t)$ where this function represents the fraction of particles possessing a residence time of t or less in the system (ZWIETERING, 1959). $F(t)$ is a nondecreasing function of t with a value of zero at $t = 0$ and which tends asymptotically to

one as $t \rightarrow \infty$. $F(t)$ can also be interpreted in statistical terms as the probability of a single particle staying in the system for time t or less (NAOR AND SHINNAR, 1963). The density function associated with this probability function is termed the Residence Time Density (RTD), $h(t)$, and is the derivative of $F(t)$:

$$h(t) = \frac{d\,F(t)}{dt} \tag{3.1}$$

$h(t)dt$ represents the fraction of particles which spend time between t and $t + dt$ in the system, or the probability of a residence time being found between t and $t+dt$ in the system. $h(t)$ is often termed the Transit Time Spectrum (TTS) in the medical literature. This terminology does not however reflect the statistical properties of the function and consequently this terminology is not used in this thesis.

3.2.1 Residence Time Density, $h(t)$

Using the above definitions it is possible to define the mean residence time or mean transit time (MTT), τ, and variance of ages, σ, of the molecules by:

$$MTT = \tau = \int_0^\infty t h(t) dt \tag{3.2}$$

$$\sigma^2 = \int_0^\infty (t-\tau)^2 h(t) dt \tag{3.3}$$

How does one relate the mean age of the molecules to volumes and flowrates of a physical system? Consider an experiment where a perfect tracer is injected as an impulse (Mathematically called a Dirac Delta (δ)) into a steady state system and the output concentration is measured. The exit concentration will vary according to the flowrate and the degree of mixing in the system. LEVENSPIEL (1972) has shown by conservation of mass for a steady state system, that $h(t)$, is related to the exit concentration, $C_{out}(t)$, by:

$$h(t) = \frac{C_o(t)}{\int_0^\infty C_o(t) dt} \geq 0 \tag{3.4}$$

Now for a system where all the material that entered the system must eventually leave:

$$\int_0^\infty h(t) dt = 1 \tag{3.5}$$

Equation 3.5 is consistent with the definition of $h(t)$ as probability density function. The *mean transit time*, τ, of a system described by $h(t)$ can be related to the total volume of the system, V, and the volumetric flowrate, Q by (ZWIETERING, 1959):

$$\tau = \frac{V}{Q} \tag{3.6}$$

The *variance*, σ^2, of $h(t)$ can be used to provide information about the degree of mixing in a system.

3.2.2 Internal Age Density (IAD), $I(t)$

The probability density of ages of molecules within a system, $I(t)$, can be related to $F(t)$ and $h(t)$. For a small time interval, dt, and a given fluid density, ρ , a mass $Q\rho dt$ enters the system, while a fraction, $F(t)$ leaves. The amount of remaining molecules is therefore $Q\rho(1 - F(t))dt$. The total mass of molecules present in the system is $V\rho$ and thus the fraction of molecules with age between t and $t+dt$, $I(t)dt$, is given by:

$$I(t)dt = \frac{Q}{V}(1 - F(t))dt \tag{3.7}$$

$I(t)$ is thus found to be:

$$I(t) = \frac{1 - F(t)}{\tau} = \frac{1 - \int_0^t h(t)dt}{\tau} \tag{3.8}$$

It is easily shown that (Appendix A.1):

- $$I(t) \geq 0 \tag{3.9}$$

- $$\int_0^\infty I(t)dt = 1 \tag{3.10}$$

- $$I(0) = \frac{1}{\tau} \tag{3.11}$$

  τ is the mean residence time of the system as a whole and is the sum of residence times for systems in series and a weighted sum of residence times for systems in parallel.

- $I(t)$ must be a monotonically *decreasing* (NIMMON *et al.*, 1981) function from $I(0) = 1/\tau$ to $I(\infty) = 0$.
- An ideal $I(t)$ need not be smooth, nor continuous which for instance is demonstrated by $I(t)$ of a plug flow system (pure delay) in Figure 3.4.

3.2.3 Conservation of Mass and Convolution in Recirculating Systems

Tracer [1] experiments in time-invariant, recirculating systems have been shown to be linear in concentration (NAOR *et al.*, 1972; LEVENSPIEL, 1972). The relationship between some arbitrary tracer concentration of a stream flowing into a system, C_{in}, and the measured concentration of a stream flowing out of the system, C_{out}, is given by (LEVENSPIEL, 1972):

$$C_{\text{out}}(t) = \int_0^t C_{\text{in}}(t - t')h(t')dt' = C_{\text{in}} * h(t) \tag{3.12}$$

where

$*$:- Convolution ie. $a * b = \int_0^t a(t - t')b(t')dt'$

t' :- Integration variable

Equation 3.12 is in general only valid for a time invariant system. Although the assumption of time invariance is often violated (due to physiological variances eg. pelvo-uretic contractions) these effects are likely to have a small influence on the tracer measurements. This is supported by the fact that deconvolution studies on many normal organs yield similar results. A frequency-time plot of typical scintigraphic data in Figure 3.1 shows that the frequency components of the data are constant with time. This is further evidence that the assumption of time invariance is acceptable. As a result, the organs under investigation can be approximated as time-invariant with an small error that manifests itself as experimental noise. In this thesis, this assumption of time-invariance is made for all the organs studied.

[1] A tracer does not chemically interact with the body, is low in concentration, follows plasma and urine flow (bulk or diffusional), does not saturate transport mechanisms and is distinguishable from the body and thus measurable.

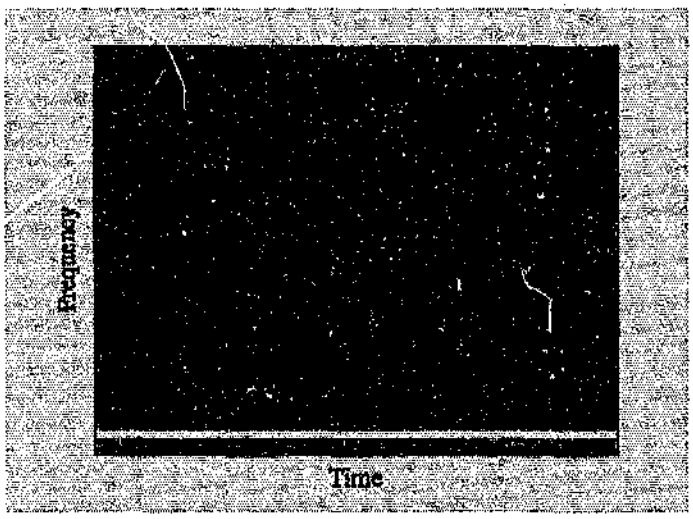

Figure 3.1: Frequency time plot of typical scintigraphic experimental data

NAOR *et al.* (1972) have extended the convolution arguments to recirculating systems, where the input to the system is not independent of the output. If C_{in} and C_{out} are measured at two different points in a recirculating system (vascular system), then equation 3.12 still applies.

3.2.4 Dynamic Imaging and $I(t)$

To relate $h(t)$ and $I(t)$ to data obtained from dynamic imaging equipment we examine a single input organ, where a perfect tracer is injected into the input of the organ in an arbitrary manner. We assume that the organ lies within a recirculating system. A diagram of such a system is shown in Figure 3.2. At any time, conservation of mass holds and thus:

$$\text{Mass In of Tracer} - \text{Mass Out of Tracer} = \text{Accumulated Mass of Tracer} \quad (3.13)$$

Thus in some small time interval:

$$QC_{in}.dt - QC_{out}.dt = \int_0^V C(v, t+dt)dv - \int_0^V C(v,t)dv \quad (3.14)$$

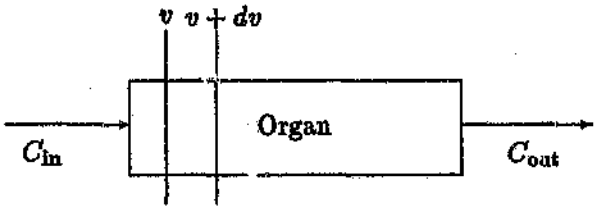

Figure 3.2: A single input organ in a recirculating system.

where

dv :- Volume element

$\int_0^V C(v,t)dv$:- Amount of tracer in the system at time t

Dividing by dt and taking limits as $dt \to 0$ gives:

$$QC_{in} - QC_{out} = \frac{d}{dt}\left\{\int_0^V C(t,v)dv\right\} \tag{3.15}$$

Time-invariance implies that Q and V are time independent (section 3.2.3) and substituting equations 3.6, 3.8 and 3.12 into equation 3.15 and simplifying (Appendix A.1) we get:

$$C_{in} * I(t) = \frac{\int_0^V C(t,v)dv}{V} \tag{3.16}$$

This equation says that the convolution of the transient input to the system with the internal age density of the system gives the volume averaged concentration in the system. The volume averaged concentration is analogous to the area normalised histogram obtained from dynamic imaging (Appendix B.1). For example if this analysis was applied to the kidney then the deconvolution of the renal curve with the aorta data would give the renal internal age density. The above result is only derived from conservation of mass for constant density, time-invariant systems and is thus devoid of other *a priori* information.

3.2.5 RTD Modelling of Mixed and Unmixed Systems

A physiological and thus functional interpretation of the deconvolved data (equation 3.16) may be enhanced by the development of theoretical models of the internal

age density. The RTD and thus IAD (equation 3.8) can be determined by solving the dynamic mass balance for a tracer in a system with a carrier flowrate, Q, equal to that of the bulk fluid flowrate and the system volume, V. $h(t)$ for a Continuous Stirred Tank Reactor [2] (CSTR) and a plug flow or unmixed system is given by (LEVENSPIEL, 1972):

$$h_{\text{CSTR}}(t) = \frac{1}{\tau} e^{\frac{-t}{\tau}} \tag{3.17}$$

$$h_{\text{PLUG}}(t) = \delta(t - \tau) \tag{3.18}$$

where

$h_{\text{CSTR}}(t)$:- Residence time density (RTD) of a CSTR, s^{-1}

$h_{\text{PLUG}}(t)$:- Residence time density (RTD) of a plug flow or unmixed system, s^{-1}

Equations 3.17 and 3.18 are shown graphically in Figure 3.3. The IAD's corresponding to equations 3.17 and 3.18 are shown in Figure 3.4. Flow in individual

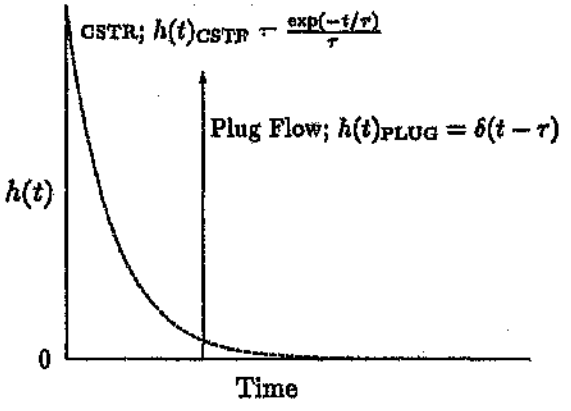

Figure 3.3: Plug Flow and CSTR residence time density functions

capillaries is closely approximated by plug flow (BURTON, 1966).

[2] Sometimes termed a compartment

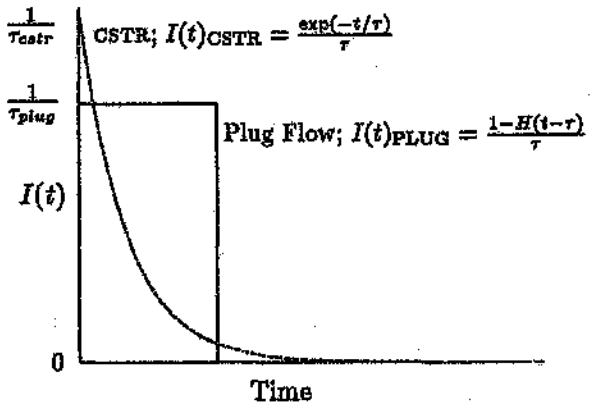

Figure 3.4: Plug Flow and CSTR internal age density functions

3.3 Impulse Response Functions and RTD Theory

The resultant curves from deconvolution studies in the medical literature are typically termed Impulse Response Functions. This terminology is misleading, as it can be applied to both the deconvolution of input–output measurements, as well as the deconvolution of input–content measurements obtained using imaging technology. The deconvolution of input–output data in the medical literature has been described as the Transit Time Spectrum (TTS). As discussed section 3.2, the TTS is the same as the Residence Time Density, $h(t)$. The deconvolution of input–content data in the medical literature is often termed the Impulse Retention Function. In the past, the term Impulse Retention Function (IRF) has been used to describe both types of deconvolution (NIMMON *et al.*, 1981; BRITTON & NIMMON, 1989).

Typically, non-parametric deconvolution techniques need not distinguish between input–output and input–content measurements, even though the resultant curves have very different properties and units. However, in order to perform parametric deconvolution the relationships between $h(t)$, $I(t)$ and the IRF need to be carefully analysed. Defining $H(t)$ as Impulse Retention Function:

$$H(t) \triangleq 1 - \int_0^t h(t) \tag{3.19}$$

$$I(t) \triangleq \frac{H(t)}{\tau} = \frac{1 - \int_0^t h(t)dt}{\tau} \tag{3.20}$$

where

$\triangleq$:- Denotes a definition

Thus from Equation 3.16,

$$C_{\text{in}} * \frac{H(t)}{\tau} = \frac{\int_0^V C(t,v)dv}{V} \tag{3.21}$$

It is important to note that the units in equation 3.21 are consistent. In the literature, τ is left out of equation 3.21 and the units are then inconsistent (FLEMING AND GODDARD, 1974; NIMMON *et al.*, 1981; VAN HUFFEL *et al.*, 1987; BRITTON AND NIMMON, 1989).

The properties of $h(t)$, $H(t)$ and $I(t)$ appear in Table 3.1 below, and are properties of the conservation of mass constraints.

Table 3.1: Properties of $h(t)$, $H(t)$ and $I(t)$

Name	*Residence Time Density*	*Impulse Retention Function*	*Internal Age Density*
Abbrev.	RTD/TTD	IRF (ambiguous)	IAD
Symbol	$h(t)$	$H(t) = 1 - F(t)$	$I(t)$
Distribution	probability density	probability	probability density
Units	sec^{-1}	dimensionless	sec^{-1}
Constraints:	$h(t) \geq 0$	$H(t) \geq 0$	$I(t) \geq 0$
	$h(0) = 0$	$H(0) = 1$	$I(0) = 1/\tau$
	$h(\infty) = 0$	$H(\infty) = 0$	$I(\infty) = 0$
	$\int_0^\infty h(t)dt = 1$	$\int_0^\infty H(t)dt = \tau$	$\int_0^\infty I(t)dt = 1$
Shape	any positive value	monotonically decreasing	monotonically decreasing

$I(t)$ is a probability density and thus once deconvolution is performed, the resultant curve has to be normalised with respect to the area under the curve. The effect of uniform attenuation, or changes in the dose of radioactive tracer (provided the

concentration is kept low enough) are removed by this normalisation. Furthermore, $I(t = 0)$ corresponds to the total mean transit time of tracer through the organ, τ. τ can thus be determined without knowing the system volume or volumetric flowrate.

3.4 Deconvolution and Experimental Noise

The above analysis showed that the deconvolution of experimental data obtained by dynamic imaging gives rise to the IAD (equation 3.16). It thus appears from Figure 3.4 that in principle we can find all the information on the mixing of a tracer in a system by examining the plateaus and decays in the IAD. This is often impractical because of noise in the experimental data and the noise generating nature of deconvolution. Filtering of noise is often employed to reduce these effects (FLEMING, 1988) and Figure 3.5 shows the effect of filtering on the deconvolution of measured splenic activity/time data with aorta activity/time data. Figure 3.5 (a) shows the noise generating nature of deconvolution. In Figure 3.5 (b), there may be plateau like regions although the identification of such regions is subjective. Figure 3.5 (c) shows the effect of over filtering. The plateaus have been removed along with most of the important mixing characteristics inherent in the data. The constraints on $I(t)$ in Table 3.1 are clearly violated in Figures 3.5 (a,b,c).

It might thus be preferable to develop mathematical models and to fit these models to the experimental data. By minimising the sum of squares between the model and experimental data, in an objective manner, we can obtain model parameter values with a statistical confidence interval. Obviously such models should have the following desirable characteristics:

- They should approximate the real behaviour of the system. The specific objective in this thesis has been to develop models based on the structural anatomy and mechanistic physiology. This constrains the choice of possible models and should in principle (if the anatomy and physiologies are adequately described) yield the actual mixing behaviour observed using independent experiments.
- The variation in the model parameters between normal individuals should be

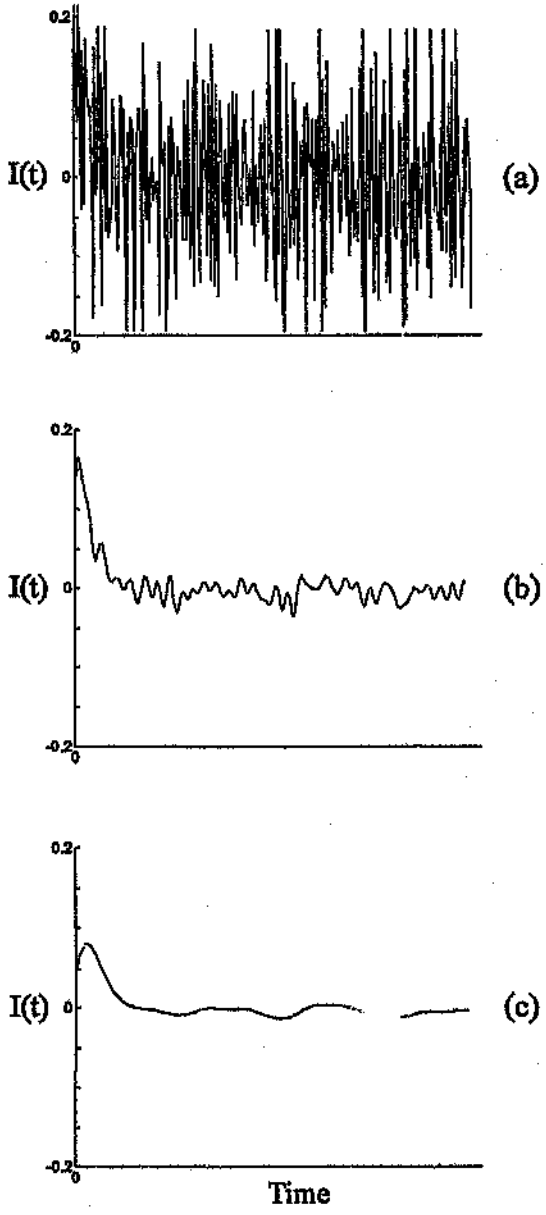

Figure 3.5: Deconvolution of splenic activity/time curves with aorta activity time curves obtained by dynamic imaging of ^{99m}Tc-DTPA (equation 3.16). (a) No filtering (b) Filtering according to FLEMING (1988) (c) Overfiltered

small.

- The number of model parameters should be kept to a minimum.
- The model parameters should be physically meaningful. In this thesis an attempt has been made to relate model parameters to physiological mechanisms and anatomical structure. If successful, defects in either anatomy or physiology should be illuminated by the parameters in the mathematical model.
- The models should be based on RTD theory because deconvolution of scintigraphic data from imaging radioactive tracers should give rise to curves which have properties related to RTD theory.

Such a model can be fitted to the experimental data in two ways:

Deconvolution: The deconvoluted organ data can be compared to the model RTD representation. The disadvantage with this method is that one has to strenuously filter the experimental data in order to determine the deconvoluted curve. In the case of a single input system in a time-invariant, recirculating system, the deconvolution of experimental data gives the IAD of the organ. We recall that an IAD must be a monotonically decreasing, non-negative function. A noisy deconvolved curve is not necessarily monotonically decreasing and thus may violate the conditions of the IAD. The strenuous filtering techniques may also remove important information on the mixing in the particular organ.

Simulation: An alternative method is to simulate the model with the measured experimental input to the organ, and to compare the result with the measured organ data. For example one would convolute the aorta with the renal model IAD and compare the output from this to the measured renal parenchymal activity/time curve. It is not necessary to filter either the aorta nor the renal data. This latter approach has been chosen on the basis that the less processing of the experimental data required, the better. Using this technique the useful information is retained.

3.4.1 Modelling the Input Curve for Non-Parametric Deconvolution

One of the deconvolution techniques discussed in the literature is that of the Laplace Transform (LT) technique of FLEMING AND GODDARD (1974). In order to discuss this technique we define the Laplace transform, $\mathcal{L}\{u(t)\}$, and inverse Laplace transform, $\mathcal{L}^{-1}\{\bar{u}(s)\}$ of function u as:

$$\mathcal{L}\{u(t)\} = \bar{u}(s) = \int_0^\infty u(t)e^{-st}dt \tag{3.22}$$

$$\mathcal{L}^{-1}\{\bar{u}(s)\} = u(t) = \frac{1}{2\pi j}\int_{\omega-j\infty}^{\omega+j\infty} \bar{u}(s)e^{st}ds \tag{3.23}$$

where

$u(t)$:- Arbitrary function which is defined for all $t \geq 0$ and whose integrals in equations 3.22 and 3.23 converge

$\bar{u}(s)$:- Laplace transform of $u(t)$

s :- Arbitrary complex variable

ω :- Largest real pole of the Laplace transform in the complex plane

j :- Square root of -1

Taking the Laplace transform of equation 3.16 and rearranging gives:

$$\bar{I}(s) = \frac{\int_0^V \bar{C}(s,v)dv}{V}/\bar{C}_{\text{in}}(s) \tag{3.24}$$

FLEMING AND GODDARD (1974) and VAN STEKELENBURG (1978) applied a compartmental model approximation to the measured input curve, $\bar{C}_{\text{in}}(s)$ and then expressed $I(t)$ as integrals and derivatives of the measured organ activity/time curve, $\int_0^V \bar{C}(s,v)dv/V$. After the input curve is modelled the measured data is discarded.

Renal deconvoluted curves using this Laplace transform technique have no negative component which is a feature of both the FFT and Matrix deconvolution methods (FLEMING AND GODDARD, 1974; VAN STEKELENBURG, 1978). The removal of this negative component probably arises from the fact that the compartmental model of the input curve contains certain constraints and *a priori* information which has not

been addressed by the authors. A thorough analysis of this negative component of deconvolved curves is discussed in Chapter 4.

3.4.2 The Method of Appending Curves for Non-Parametric Deconvolution

JUNI *et al.* (1988) appended a smooth exponential curve to the measured aorta and organ activity/time curves. They then performed the deconvolution of these curves and the resultant curve was then truncated to the original sample time. To analyse the validity of this technique, we consider an input function, $i(t)$ and an output function, $o(t)$ which are related by some arbitrary probability density function, $Y(t)$, by the convolution integral, ie.

$$o(t) = \int_0^t i(t-\hat{t})Y(\hat{t})d\hat{t} \tag{3.25}$$

If we append exponential curves to the data for some experimental time, T, then equation 3.25 becomes :

$$\begin{pmatrix} (1-\mathcal{H}(t-T))o(t) \\ + \\ \mathcal{H}(t-T)K_1 exp(-t/\tau_e) \end{pmatrix} = \int_0^t \begin{pmatrix} (1-\mathcal{H}(\hat{t}-T))i(\hat{t}) \\ + \\ \mathcal{H}(\hat{t}-T)K_2 exp(-\hat{t}/\tau_e) \end{pmatrix} Y(t-\hat{t})d\hat{t} \tag{3.26}$$

where

$\mathcal{H}(t-a)$:- Heaviside function with delay a

K_1 :- Scaling factor for the output curve $o(t)$

K_2 :- Scaling factor for the input curve $i(t)$

τ_e :- Time constant of the exponential curves appended to $i(t)$ and $o(t)$

By taking the Laplace transform and simplifying for $\bar{Y}(s)$,

$$\bar{Y} = \frac{\bar{o}}{\bar{i}} + \left(\frac{\tau_e}{\tau_e s+1}\right)\left(\frac{exp(-Ts)}{1-exp(-TS)}\right)\left(\frac{K_1 - K_2\bar{Y}}{\bar{i}}\right) \tag{3.27}$$

In order for appended, deconvolved curves to approximate the unappended deconvolved curves, the second term on the right hand side of equation 3.27 must be

small. The second term tends to zero only when $\tau_e \to 0$, $T \to \infty$ (infinite experimental time), if $K_2 \approx K_1 Y(t)$ which depends on *a priori* information, or if $Y(t)$ is a constant. If $Y(t)$ is constant in the case of a single input organ then the organ is completely obstructed. It is important to note that convolution implies that any point in the output curve depends in some way on every point in the input curve. It is thus clear that appending a curve to the input and output curves is very problematic except under very specific conditions. Furthermore, a tracer's concentration in a circulating system will tend to a non-zero concentration (NAOR *et al.*, 1972). Thus although the technique of appending curves might appear to reduce the noise associated with the Gibbs phenomena in the FFT, this technique is based on dubious mathematical and physical principles which may give limited confidence in the deconvolved curve.

3.4.3 Simulation for Performing Parametric Deconvolution

RTD models are typically non-linear in their parameters, and it is almost impossible to find an analytic solution for each parameter. Numerical algorithms have to be used to iteratively search for the best parameters.

The approach chosen for the parametric deconvolution was that of the the *prediction-error identification method* (PEM), (LJUNG 1987). Figure 3.6 shows the prediction-

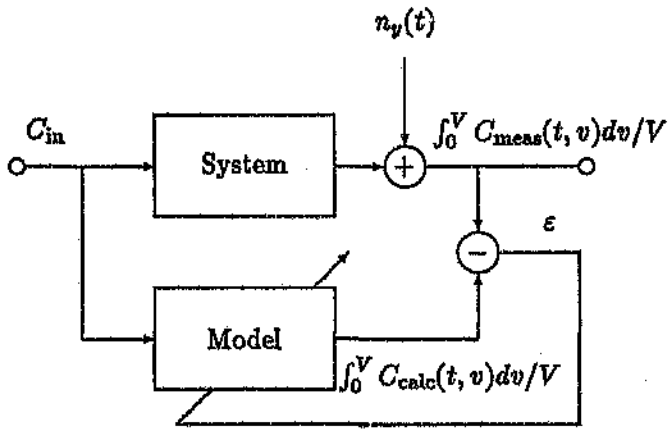

Figure 3.6: Prediction-error approach to parametric deconvolution

error configuration. In general, the input C_{in} excites the system and produces the measured organ activity/time curve $\int_0^V C_{\text{meas}}(t,v)dv/V$. This response may be corrupted by unmeasured noise $n_y(t)$. The measured iuput C_{in} is passed through a parametric model of the system to produce a calculated organ activity/time curve $\int_0^V C_{\text{calc}}(t,v)dv/V$. The error between the measured and approximate activity/time curve, ε, determines how well the model approximates the system. The model parameters are then adjusted to minimise ε.

Typically parametric deconvolution of single input organs comprises four parts. The experimental aorta activity/time data is modified to account for the background tissue radioactive contribution (Chapter 4). Vascular background is then removed from the measured organ activity curve. The modified aorta data, C_{in}, is then convolved with the organ IAD (Equations 3.8, 3.16) to produce an estimate of the content of the organ, $\int_0^V C_{\text{calc}}(t,v)dv/V$ where the simulated curve has been scaled so that the measured and simulated curves have identical area, i.e.

$$\int_0^\infty \frac{\int_0^V C_{\text{calc}}(t,v)dv}{V}dt \approx \int_0^\infty \frac{\int_0^V C_{\text{meas}}(t,v)dv}{V}dt \tag{3.28}$$

The error between the system and the model can be calculated by the conventional least square criterion,

$$\varepsilon = \int_0^T \left(\frac{\int_0^V C_{\text{meas}}(t,v)dv}{V} - \frac{\int_0^V C_{\text{calc}}(t,v)dv}{V} \right)^2 dt \tag{3.29}$$

In this thesis the optimum model parameters were found by using the Levenberg-Marquard (MOLER *et al.*, 1987) technique to minimise ε. This method was chosen as it converges rapidly to the minimum. The programs for the various organs discussed in this thesis are presented in Appendices L.1, M.1 and N.1.

3.5 Conclusion

Equation 3.16 is general for any imaging experiment of a single input organ and provides a framework for researchers to include other models of organ perfusion. Any parametric model of an organ must implicitly embody all the constraints associated

with $h(t)$, $I(t)$ and $H(t)$ and this in turn places limits on the deconvolution behaviour according to a model of tracer transport.

The method of modelling the measured input curve to facilitate deconvolution (section 3.4.1) has not been implemented because of the assumptions and constraints that are associated with the technique. The negative component seen in many deconvolution studies is absent in the deconvolved curves which use this technique. The absence of the negative component is probably a result of the assumptions and *a priori* information inherent in the model of the input curve (section 3.4.1). An alternative way to handle the negative component associated with the deconvolution of imaging data is addressed in Chapter 4

The noise generating nature of deconvolution has been shown to be a major problem and the Prediction Error Identification Method (PEM) has rather been chosen to compare the experimental data with data predicted by mathematical models. The predicted data is obtained by simulating the model with the measured input to the organ. This data can then be compared to the measured organ data. This method is affected by noise to a far lesser extent than non-parametric deconvolution.

Chapter 4

Identification of an Aorta Background for Organ Scintigraphic Studies

The previous chapter showed that the deconvolution of dynamic imaging curves of the aorta and any single-input organ was related to the organ *internal age density* (IAD). Conservation of mass and *residence time density* (RTD) theory was used to place limits on the behaviour of the organ IAD and thus the deconvolved experimental data.

In particular it was shown that:

- $I(t) \geq 0, \quad \int_0^\infty I(t)dt = 1, \quad I(0) = \frac{1}{\tau}$.
- $I(t)$ must be continuous (not necessarily smooth), monotonically *decreasing* and bounded from $I(0) = 1/\tau$ to $I(\infty) = 0$.

A number of renal deconvolution studies exhibit a negative component in the IAD. This is typically attributed to noisy data (JUNI *et al.*, 1988; VAN HUFFEL, 1992). The purpose of this chapter is to investigate this issue more carefully.

4.1 Aorta Background

To address the negative component in deconvolved curves one has to analyse the implicit assumptions that have been made with respect to radiation and photon

counts from tissue background and the removal of this background contribution from experimental results of organ imaging. Background tissue radiation or photon count correction assumes that:

- One can find a region which has tissue similar to that found anterior and posterior of the imaged aorta. Tissue background can then be measured and subtracted from the aorta data.
- There is no venous blood supply above or below the imaged aorta.
- Blood flow in the aorta behaves in a "plug flow" manner with zero transit time ($I_{\text{aorta}}(t) = 1$, or $h_{\text{aorta}}(t) = \delta(t)$). Thus from equation 3.16, C_{in} equals the aorta activity/time data. In general the fluid velocity profile in large vessels is parabolic in nature. The dispersive effects in these vessels is however likely to be small relative to that in other organs and thus the effect of this velocity profile on the aorta measurement is not addressed in this thesis.

Using equation 3.21 we can define the aorta background by:

$$C^a_{\text{measured}} = C^a_{\text{actual}} + \zeta C^a_{\text{actual}} * I_{\text{vess}}(t) \tag{4.1}$$

where

C^a_{measured} :- Experimentally measured aorta activity/time curve, $\text{mol}.m^{-3}$

C^a_{actual} :- Tracer within the aorta, $\text{mol}.m^{-3}$

ζ :- Fraction of tracer within the aorta that flows through background tissue, dimensionless

$I_{\text{vess}}(t)$:- Internal age density (IAD) of tissue anterior and posterior of the imaged aorta. One can consider the tissue to be an imaged single input system with the aorta as input to this system, s^{-1}

In principle given ζ and $I_{\text{vess}}(t)$ we could use equation 4.1 and perform deconvolution to determine C^a_{actual}. This turns out to be numerically difficult because of the

discontinuities in C^a_{measured} and $I_{\text{vess}}(t)$ and the noise generating nature of deconvolution. The rest of this chapter is devoted to determining functional forms of ζ and $I_{\text{vess}}(t)$ and the use of these functions to approximate C^a_{actual}.

In order to simplify the discussions in the next two subsections, consider Figure 4.1 which represents a transaxial section through the abdomen. In this figure, a radioactive tracer is initially introduced into the aorta in the cardio-thoracic region and shortly afterward the tracer can be observed within the aorta in the abdomen. As time progresses, the tracer can also be observed in other arterioles within the abdominal cavity. At even later times, tracer can be observed in the aorta, arterioles and venules of the abdominal cavity and in vessels outside the abdominal cavity. From Figure 4.1 it is clear that a camera imaging the aorta would observe the tracer in the aorta as well as tracer in the background tissue. The measurements would show more material in the aorta than is actually present in the aorta.

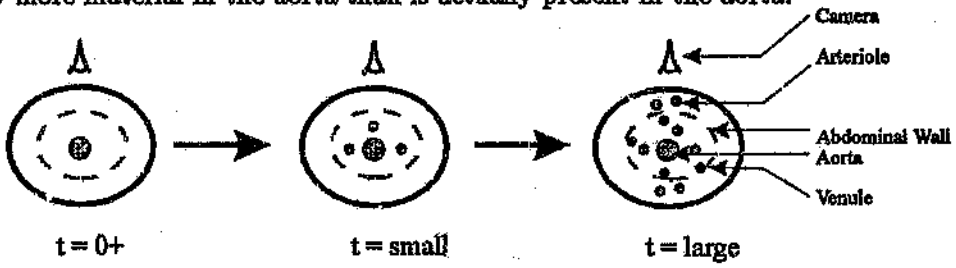

Figure 4.1: A tracer experiment where tracer is introduced into the aorta in the cadio-thoracic cavity and then monitored at a transaxial section through the abdominal cavity. The camera images all the tracer below it.

4.1.1 A Proposed Model of Background Tissue

Background tissue activity/time curves typically rises rapidly in the same manner as the aorta activity as shown in Figure 4.2. This is expected since any background tissue region has an arterial supply. As discussed above, shortly after the radioactive tracer leaves the left ventricle of the heart, the tracer may be found primarily within the aorta. Thus the tissue background contribution in the aorta is likely to be small at the beginning of the experiment. As the experiment progresses, tracer material

moves into tissue anterior and posterior of the aorta and the tissue background contribution to the measured aorta increases. It is in principle very difficult to measure a true tissue background activity/time curve because any background tissue chosen near the aorta contains large arterioles which have similar characteristics to the aorta. One might then postulate a suitable, aorta background curve of equation 4.1 as:

$$C^a_{\text{measured}} = C^a_{\text{actual}} + K * (1 - exp(\frac{-t}{\tau_c})) \tag{4.2}$$

where

K :- Background activity contribution from tissue anterior and posterior of the imaged aorta, mol.m^{-3}

τ_c :- Mean confidence time of the aorta measurement, s

Equation 4.2 represents a small tissue background contribution to the aorta measurement at early times which then increases to an asymptote as time progresses. The above model is probably the simplest one that has these characteristics. The values of τ_c and K can be determined according to the procedure outlined below in section 4.2. The effects of this adjustment on a typical deconvolved curve is shown

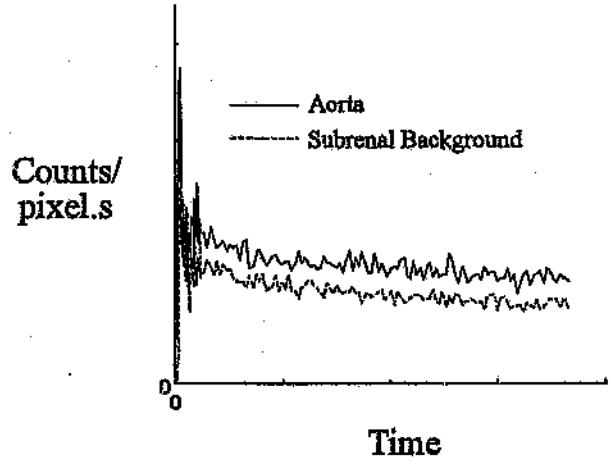

Figure 4.2: A comparison of measured aorta and tissue background activity/time curves

in Figure 4.3.

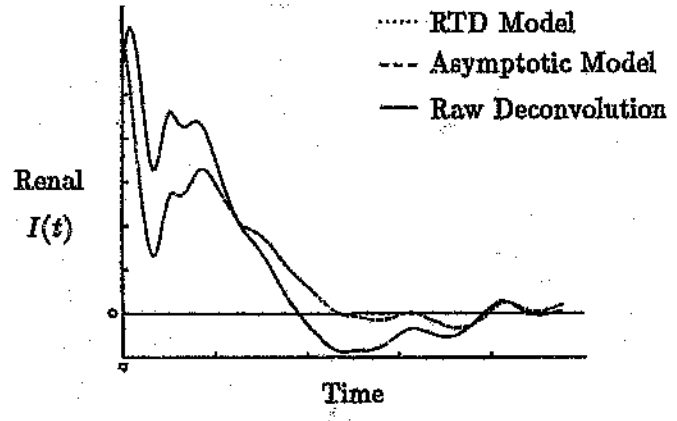

Figure 4.3: The effect of three methods of aorta correction on a typical renal deconvolution study. $\int_0^\infty I(t)dt = 1$ for all curves. An Internal Age Density must be a monotonically decreasing function. The large initial dip in the internal age density of Figure 4.2 violates this constraint and is a result of vascular background in the organ concentration/time curve. This issue is addressed in Chapter 6.

4.1.2 A RTD Model of Tissue Background

We could also attempt to model the background tissue taking into account the anatomy. Consider Figure 4.1 where a tracer is introduced as a perfect *dirac* δ into the aorta in the cardio-thoracic region. If we were to plot the fraction of tracer that came through the cross section in the abdomen as a function of time, then we would probably see the curve shown in Figure 4.4. In a radioactive imaging experiment of the aorta, we observe all the tracer in Figure 4.4 as the aorta. This is however erroneous since only tracer within the aorta enters an organ. The measurements show more tracer in the aorta than is in the vessel. One way to deal with this phenomena is to propose a RTD for the blood vessels anterior and posterior of the aorta. We can then convolute C^a_{actual} with this RTD using equation 4.1. In this way we generate an aorta background representation. We choose a gamma density for $I_{\text{vess}}(t)$ (see section 1.6). Thus $I_{\text{vess}}(t)$ is given by:

$$I_{\text{vess}}(t) = \frac{1 - \int_0^t \frac{t^{n-1}}{\tau_{\text{bt}}^n} \frac{e^{-t/\tau_{\text{bt}}}}{(n-1)!} dt}{\tau_{\text{bt}}} \tag{4.3}$$

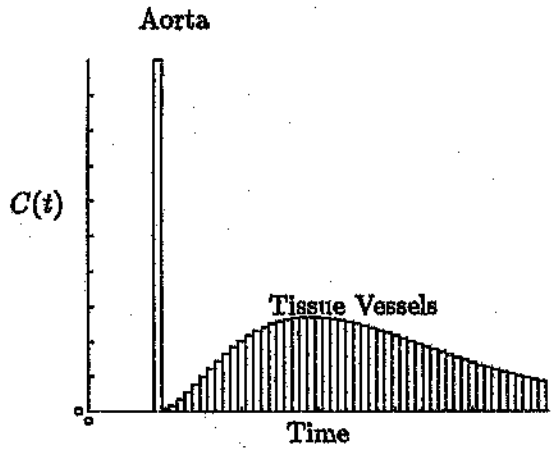

Figure 4.4: Venous Return Histogram

where

n :- The skewness of the density and is chosen as $n = 3$ because there is likely to be a large length distribution of blood vessels (Section 1.6)

τ_{bt} :- Mean transit time of the background tissue (Section 1.6)

I_{vess} is valid for a recirculating system (Chapter 5). To perform the calculation we recall that the aorta measurement should be accurate at the beginning of the experiment ie. $C^a_{measured} \approx C^a_{actual}$ for small t. If τ is large, then:

$$C^a_{actual} * I_{vess}(t) \approx C^a_{measured} * I_{vess}(t) \tag{4.4}$$

We now substitute equations 4.4 and 4.3 into equation 4.1 to determine C_{actual}. The values of τ_{bt} and ζ are determined according to the procedure outlined below in section 4.2. This has been done with renal activity/time data and the result is shown in Figure 4.3. Tissue background determined by this method is illustrated in Figure 4.5.

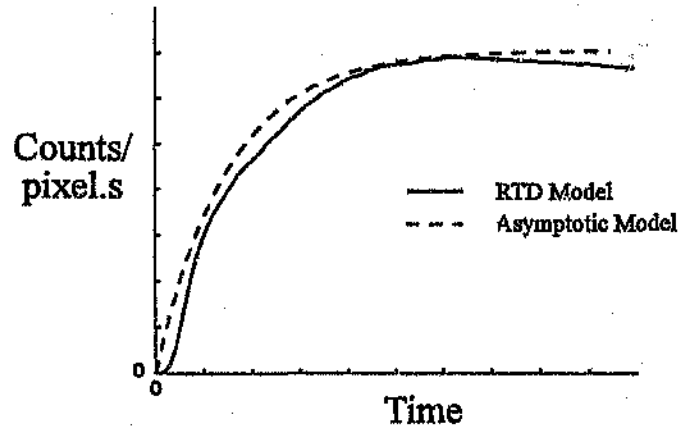

Figure 4.5: A comparison of aorta backgrounds

4.2 Determination of Background Tissue Model Parameters

The parameter values associated with the functional forms of ζ and $I_{vess}(t)$ above are determined in this thesis by:

1. Deconvolving the observed activity/time data of an organ under investigation with the measured aorta activity/time data.
2. Adjusting the functional forms of ζ and $I_{vess}(t)$ to minimise negative component of the deconvolved curve.

In the liver and spleen experiments this technique is applied to the spleen and C^a_{actual} is then used for both the spleen and the liver. In the kidney, the healthiest kidney is chosen for this procedure and C^a_{actual} is then applied to both kidneys. The programs to perform the aorta adjustment appear in Appendix P.1.

4.3 Conclusion

The negative artifact seen in organ deconvolution studies seems to be due to inaccuracies in the aorta measurement. In particular, due to background tissue activity,

more material is measured in the aorta than is actually present. This is compounded by the fact that no background region can be chosen that represents the tissue anterior and posterior of the imaged aorta since any background tissue is vascular in nature and thus contains small arteries which have similar characteristics to the aorta. The unthinking subtraction of such background data from the aorta can remove accurate information from the beginning of the aorta curve while removing an insufficient background contribution which is present in the latter part of the curve. Two different methods for handling this problem have thus been presented that take account of the negative artifact and both effectively arrive at the same result. The second method suggests that the choice of the gamma density for flow in capillary and vessel beds is a valid choice which supports the results of THOMPSON *et al.* (1964). The programs to perform the aorta adjustment appear in Appendix P.1.

Chapter 5

An Anatomical and Physiological Model of the Kidney

5.1 Introduction

Renal radioactive tracer studies have been used as non-invasive means of identifying renal pathologies. Renal function is then characterised by the activity/time curves obtained from dynamic imaging of the aorta and kidney. Typically, the tracer ^{99m}Tc- diethylenetriaminepentaacetic acid (^{99m}Tc-DTPA) has been used to identify glomerular function abnormalities. This substance behaves as an ideal tracer: does not chemically interact with the body, low in concentration, follows plasma and urine flow (bulk or diffusional) and is distinguishable from the body and thus measurable.

As shown in Chapter 3, the deconvolution of measured aorta and kidney activity/time curves produces an impulse response termed the internal age density. This internal age density can then be used to calculate transit times which indicate organ function (FLEMING, 1988, BRITTON & NIMMON, 1989).

Several non-parametric, renal deconvolution techniques reported in the literature contain assumptions and drawbacks which have prevented their routine clinical use as reported by JUNI, *et al.* (1988). The matrix method has the disadvantage in that errors in the early data points are reflected throughout the entire curve (JUNI *et*

al., 1988). The uncertainty in the calculation of transit times can only be reduced if random noise is filtered out (FLEMING, 1988). Fitting of an arbitrary function to the deconvolved curves, requires a prior knowledge of the expected result (JUNI *et al.*, 1988). JUNI *et al.* (1988) extended the input and response curves by appending a smooth curve with a gradual taper to zero. This produced smoother deconvolution results however this technique is theoretically questionable (section 3.4.2). In initial attempts to obtain kidney parenchymal transit times, the methods of BRITTON AND NIMMON (1989) were used. However, random noise appeared to be a major problem and even with data bounding (DIFFY AND CORFIELD, 1976) and filtering (FLEMING, 1988) there was limited confidence in the minimum transit time (MinTT) estimation. D ivative methods could not be used to determine the time of the end of the plateau of the renal retention function (BLAUFOX, 1989), as the noise present caused significant fluctuations in the gradient evaluations.

In this chapter a physiological and anatomical flow model of the kidney is developed to investigate parametric deconvolution. The parametric approach is adopted in an attempt to reduce the noise magnification effects that appear to be inherent in most non-parametric deconvolution techniques (JUNI *et al.*, 1988) which in turn obscure physiological information. The model provides the basis for the identification of physiological and anatomical parameters from experimental data. The model provides transit time, reabsorption rate and the filtration fraction information for an individual kidney.

5.2 Development of Parametric Model

We wish to model the renal internal age density from a physiological and anatomical perspective using the tracer ^{99m}Tc-DTPA . This should allow us to identify the specific physiological flow mechanisms within a typical nephron. We begin by examining the anatomical representation of a nephron with collecting ducts as shown in Figure 5.1. Blood with tracer enters the kidney through the renal artery which then splits into the various renal arterioles. The concentration at each split point is the same and if we assume that the lengths of the arterioles are approximately equal,

and the flow velocity is relatively high, then the concentration of the tracer : a function of time for every afferent arteriole will be roughly the same. If the lengths differed substantially and the flowrate was small, then each glomerulus would have an input that differed from the next by some delay time.

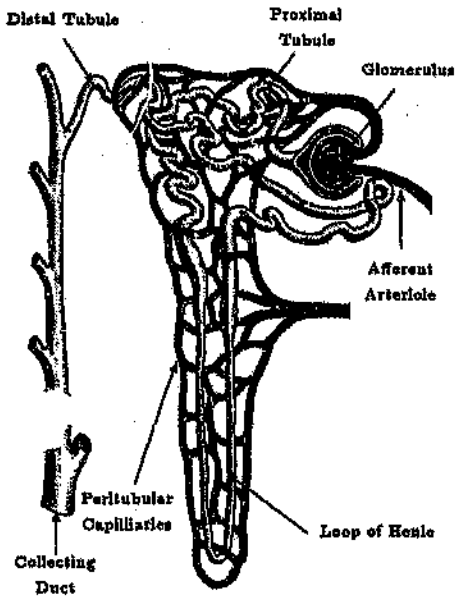

Figure 5.1: Anatomical Structure of the Nephron (Redrawn from Smith: The Kidney: Structure and Function in Health and Disease., Oxford University Press, 1951)

The blood in the afferent arteriole enters the glomerulus and a fraction of the plasma, f [1], is filtered. The rest of the blood flows through the efferent arteriole and into the peritubular capillaries. The peritubular capillaries have a broad length distribution and the blood mixes in a "segregated" manner (also called macromixing). Segregated mixing implies that elements of tracer of different ages meet at a common point (ZWIETERING, 1959; GLASSER AND JACKSON, 1984). Appendix C.1 shows that the RTD associated with this mixing is a result of the length distribution of capillaries, $g(L)$. If we assume that the length distribution of these vessels is not large then we can approximate the length distribution by the gamma density for the reasons discussed in section 1.6. A value of $z = 2$ has been chosen for this density with time

[1]Typically called the "filtration fraction", ±19% (GUYTON, 1986, PP 398)

constant, τ_b [2] (see equation 1.6). The renal blood flow RTD is thus given by:

$$h_{\text{blood}}(t) = \frac{t}{\tau_b^2} e^{-t/\tau_b} \tag{5.1}$$

$$\text{MTT}_b = \int_0^\infty t \frac{te^{-t/\tau_b}}{\tau_b^2} dt = 2\tau_b \tag{5.2}$$

where

h_{blood} :- Residence time density (RTD) associated with blood flow through the kidney, s^{-1}

MTT_b :- Mean transit time of the blood in the renal parenchyma, s

Let us examine the tracer inside the glomerulus as it moves down the proximal tubule. The tracer, ^{99m}Tc-DTPA , does not move out of the tubule in any substantial quantity and is thus carried by the flowrate of water/urine inside the tube. It can be shown that if the net water flow is always out of the tubules, then this system can be modelled as a series combination of plug flow systems (LEVENSPIEL, 1972) given by:

$$h_{\text{tubule}}(t) = \delta(t - \tau_p) * \delta(t - \tau_{\text{dLH}}) * \delta(t - \tau_{\text{aLH}}) * \delta(t - \tau_d) \tag{5.3}$$

where

h_{tubule} :- Renal tubular residence time density (RTD), s^{-1}

τ_p :- Proximal tubule mean transit time, s

τ_{dLH} :- Descending loop of Henle mean residence time, s

τ_{aLH} :- Ascending loop of Henle mean residence time, s

τ_d :- Distal tubule mean residence time, s

$*$:- Convolution

Combining the above residence times into a single parameter, τ_{tn}, gives:

$$h_{\text{tubule}}(t) = \delta(t - \tau_{tn}) \tag{5.4}$$

The parameter, τ_{tn}, represents the mean residence time of tracer from the point of entry at the glomerulus, to the exit point of a nephron. We note that the flowrate in the descending loop of Henle changes because of the reabsorption of water into

[2] A physically measured distribution could be substituted if available

the peritubular capillaries. From Appendix D.1, $\tau_{dLH} = \frac{1}{a} ln[\frac{Q^{Ho}}{Q^{Ho} - aV_{dLH}}]$ where Q^{Ho} is the initial loop of Henle flowrate, V_{LH} is the descending loop of Henle volume and a is the net flow out the loop of Henle and into the interstitial space per unit volume. Thus in principle, the model includes a parameter, a, which could be used to determine whether this reabsorption mechanism functions properly. We also note that a similar analysis to that in Appendix D.1 could be used to identify the residence time density of a tracer which is actively secreted by the proximal tubular system. This however falls outside the scope of this thesis.

Segregated mixing occurs at the points where the distal tubules meet the collecting duct and where the urine meets in the inner calyces. In addition, there is a length distributions of the two nephrons of the kidney (cortical and juxtamedullary nephrons). It is assumed that the gamma density with $z = 2$ in equation 1.6 should characterise the behaviour of this system. The time constant associated with this gamma density is represented by τ_{cc} [3]. The collecting duct and inner calyces mean transit time associated with τ_{cc} can be determined from equation 1.7 and is given by:

$$\mathrm{MTT}_{cc} = 2\tau_{cc} \tag{5.5}$$

There is also a small delay time associated with flow down the shortest collecting duct, τ_{cd}. Combining these terms, the model of the parenchymal RTD is given by equation 5.6. A flow representation of equation 5.6 is shown in Figure 5.2. In deriving equation 5.6, the approximation has been made that mixing in the peritubular capillaries and collecting ducts/inner calyces are similar for both types of nephrons. The filtration fraction, f, is also assumed to be the same for both nephrons as it is related to blood pressure.

$$\begin{aligned} h_{\text{parenchyma}}(t) = \; & \alpha f \delta(t - (\tau_{tc} + \tau_{cd})) * \frac{te^{-t/\tau_{cc}}}{\tau_{cc}^2} + \alpha(1-f)\frac{te^{-t/\tau_b}}{\tau_b^2} + \\ & (1-\alpha) f \delta(t - (\tau_{tj} + \tau_{cd})) * \frac{te^{-t/\tau_{cc}}}{\tau_{cc}^2} + (1-\alpha)(1-f)\frac{te^{-t/\tau_b}}{\tau_b^2} \end{aligned} \tag{5.6}$$

[3] A physically measured density could be substituted

where

$h_{\text{parenchyma}}(t)$:- Residence time density (RTD) of the renal parenchyma with both the cortical and juxtamedullary nephrons, s^{-1}

α :- Fraction of renal blood which flows to the cortical nephrons and as opposed to the juxtamedullary nephrons $(1-\alpha)$, dimensionless

τ_{tc} :- Cortical nephron tubule transit time, s

τ_{tj} :- Juxtamedullary nephron tubule transit time, s

The combination of nephrons with collecting ducts and inner calyces is termed the renal parenchyma. We note that in deriving equation 5.6 we have made a large num-

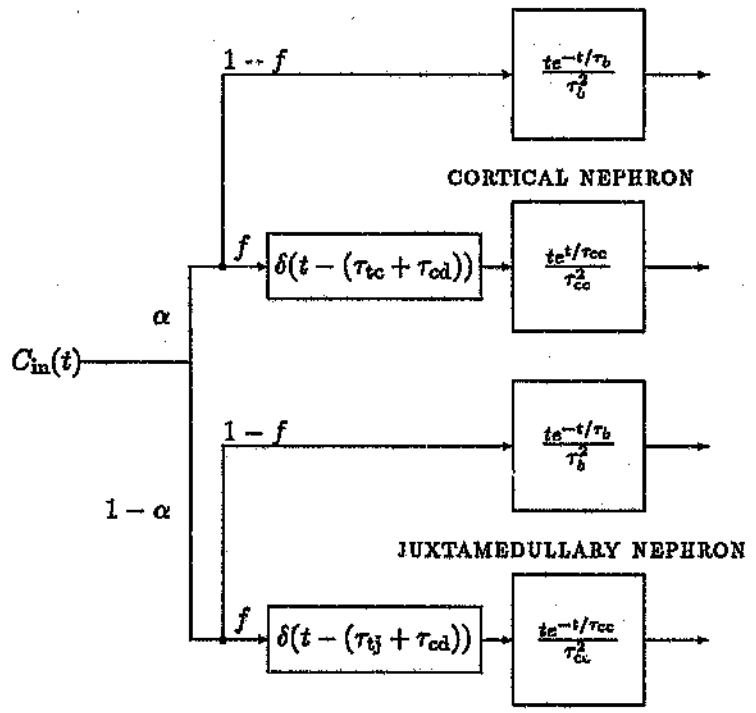

Figure 5.2: A flow representation of equation 5.6.

ber of assumptions about the flow in various sub-systems. Some of these assumptions have not really been tested, but if not made the number of model parameters would become excessive. One could of course have made other assumptions and the approach that has been taken allows other researchers to try other alternatives. In the end though it is not reasonable to try and extract too many parameters from the

measurements. Even this equation probably has too many parameters as it stands.

We can now use equation 3.8 to determine the shape of the parenchymal internal age density. The IAD for the parenchyma is shown in Figure 5.3 with the associated parameters and is related to the renal impulse retention function discussed in the medical literature using equation 3.20 (NIMMON *et al.*, 1981; BRITTON & NIMMON, 1989). The minimum transit time through the renal tubular system, $\tau_{tc}+\tau_{cd}$, is primarily affected by the cortical nephron. Generally the noise in scintigraphic experimental data obscures the juxtamedullary minimum transit time, $\tau_{tj}+\tau_{cd}$ (Figure 5.7). The clinical significance of this part of the curve thus becomes subject to a large error. It is for this reason that the model represented by equation 3.8 has been simplified by setting $\alpha = 1$. This decreases the number of parameters and essentially fits the nephron with the minimum transit time. The approximation may imply that the calculated mean transit time of the renal parenchyma may be associated with a small error. This is also the case when performing non-parametric deconvolution since the juxtamedullary nephron is not accounted for (NIMMON *et al.*, 1981; BRITTON & NIMMON, 1989). The IAD of a single nephron ($\alpha = 1$) is shown in Figure 5.4 and corresponds to deconvolutions typically observed in the literature. Figure 5.7 indicates that the single nephron model seems to sufficiently characterise the dominant behaviour of the kidney.

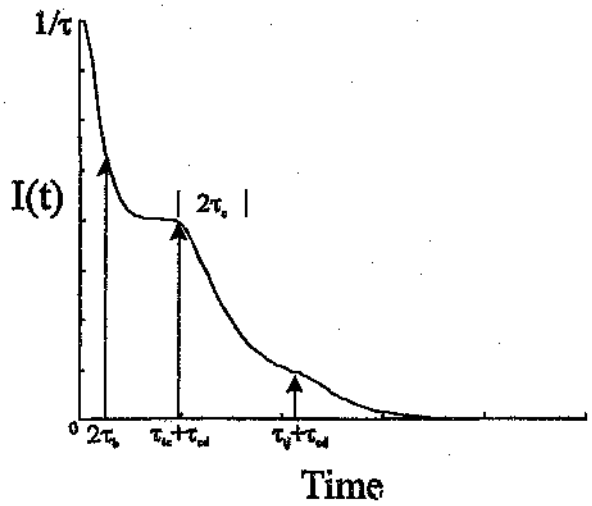

Figure 5.3: Internal Age Density of Medullary and Juxtamedullary Nephrons in parallel

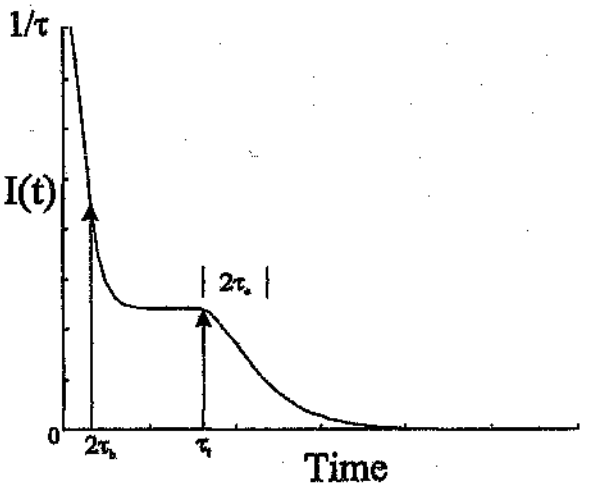

Figure 5.4: Internal Age Density for a single nephron

By combining the delay components of the nephron and taking the limit as $\alpha \rightarrow 1$, equation 5.6 reduces to:

$$h_{\text{combined}}(t) = f\delta(t-\tau_t)\frac{te^{-t/\tau_{cc}}}{\tau_{cc}^2} + (1-f)\frac{te^{-t/\tau_b}}{\tau_b^2} \tag{5.7}$$

where

τ_t :- Mean transit time through the shortest nephron and shortest length of collecting duct ie. $\tau_{tc} + \tau_{cd}$, s

$h_{\text{combined}}(t)$:- Residence time density (RTD) of the average renal parenchyma, s^{-1}

The distribution of nephron lengths is lumped into parameter τ_{cc}. τ_{cc} also includes the segregated mixing effects associated with the points where the distal tubules meet the collecting duct and where the urine meets in the inner calyces.

Based on equation 5.7, the simplified flow representation of the parenchyma is presented in Figure 5.5.

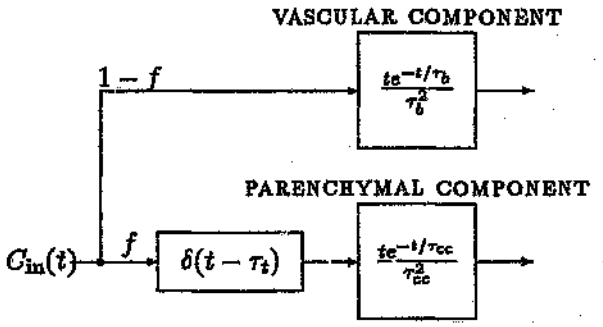

Figure 5.5: Simplified Flow Representation of the Parenchyma

5.3 Clinical Parameters and Indices

The mean transit time of the parenchymal model, including the vascular components, may be calculated using equation 3.21 as follows:

$$\begin{aligned} \mathrm{KMTT}_{\mathrm{total}} &= \int_0^\infty t\, h_{\mathrm{combined}}(t)dt && (5.8)\\ &= \frac{1-f}{\tau_b^2}\int_0^\infty t^2 e^{-t/\tau_b}dt + \frac{f}{\tau_{cc}^2}\int_0^\infty t(t-\tau_t)e^{-(t-\tau_t)/\tau_{cc}}dt && (5.9)\\ &= 2(1-f)\tau_b + f(\tau_t + 2\tau_{cc}) && (5.10) \end{aligned}$$

As we are only interested in the mean parenchymal transit time, the contribution of the vascular component may be removed by setting $f = 1$ in the above equations. It therefore follows that,

$$\begin{aligned} \mathrm{KMTT}_{\mathrm{paren}} &= \tau_t + 2\times\tau_{cc} && (5.11)\\ &= \tau_t + \mathrm{MTT}_{cc} && (5.12) \end{aligned}$$

As defined by Britton *et al.* (1987), the Minimum Transit Time (MinTT) corresponds to the length of the plateau in the renal retention function. This corresponds to τ_t as derived previously in the model. Recall that τ_t is the transit time through the shortest nephron and shortest length of collecting duct.

Britton *et al.* (1987) also defines the parenchymal transit time index, PTTI, as:

$$\mathrm{PTTI} = \mathrm{KMTT}_{\mathrm{paren}} - \mathrm{MinTT} \qquad (5.13)$$

As outlined by BRITTON *et al.* (1987), the MinTT is removed from the mean parenchymal transit time, to account for variations in urine flow between patients. equation D.5 in Appendix D demonstrates the non-linear relationship between urine flow and minimum parenchymal transit time.

The PTTI can be calculated from the model parameters using equation 5.13,

$$\begin{aligned} \text{PTTI} &= \tau_t + 2\tau_{cc} - \tau_t = 2 \times \tau_{cc} && (5.14) \\ &= \text{MTT}_{cc} && (5.15) \end{aligned}$$

The published results indicate that prolongation of PTTI is a sensitive indicator of the presence of obstructive nephropathy (BRITTON *et al.*, 1979). A common interpretation of a raised PTTI is that it indicates not only prolongation of transit time, but also an increase in the spread of these transit times. From equation 5.14, it appears as if the PTTI is independent of the prolongation of transit time. Any prolongation of transit time will be incorporated into the model parameter, τ_t.

This result differs from the conventional interpretation of the PTTI, and raises the question of the PTTI's validity as a measure of the tubular transit time prolongation. In the initial stages of obstructive uropathy, the rate of reabsorption can be assumed to be approximately constant for all nephrons and the PTTI will be within the normal range. As the disease progresses and tubular dysfunction develops, there will be a distribution of reabsorption rates in the nephrons. This distribution of reabsorption rates will manifest itself as an increase in the spread of transit times. The model parameter, τ_{cc}, will reflect this increase as an apparent change in the length distribution of nephrons and mixing points (Appendix D.1). The PTTI described by equation 5.14 will then indicate an obstructive nephropathy.

From equations 5.6 and 5.7, the renal model contains information about the filtration fraction, f. The glomerular filtration rate (GFR) (GUYTON 1986, PP 398) is 'the quantity of glomerular filtrate formed each minute in all nephrons of both kidneys', i.e. the sum of the individual kidney glomerular filtration rates:

$$\text{GFR} = \text{GFR}_{\text{left}} + \text{GFR}_{\text{right}} \qquad (5.16)$$

The individual glomerular filtration rates GFR_{left} and GFR_{right} can be related to the respective filtration fractions, f_{left} and f_{right}, by the renal arterial flowrates to each kidney. GUYTON (1986, PP 395) defines the normal renal fraction (NRF) as the fraction of cardiac output (CO) that flows to both kidneys (approximately 21%). Assuming an equal split of renal arterial blood flow, the GFR may thus be approximated by equation 5.17.

$$GFR = CO \times \frac{NRF}{2} \times (f_{left} + f_{right}) \quad (l.min^{-1}) \tag{5.17}$$

5.4 Data Pre-Processing

5.4.1 Renal Background Elimination

Chapter 4 showed that typical background activity/time curves behave in a similar manner to aorta activity/time curves. One can then pose the question whether the aorta curves cannot be used to determine renal background. This assumes that the tissue above and below the imaged parenchyma is vascular in nature. If this is true, then the arguments of Chapter 4 can be used to determine a background measure for renal studies. This is done for a particular kidney according to the following steps:

1. The aorta curve is time shifted so that the peak in the aorta and subrenal background activity/time curves correspond. This accounts for the fact that it takes a certain amount of time for the tracer to flow to the background tissue. The peak in the subrenal tissue activity/time curve contains this information.

2. The time shifted aorta is scaled so that the average of this curve corresponds to the average of the measured background histogram. This scales the values of the time shifted aorta activity/time curve so that they have a similar radioactive contribution to the subrenal background tissue.

3. 75% of the time shifted, scaled aorta is used as background. The value of 75% results from the fact that in the lateral subrenal region, the thickness of the

body is approximately 10cm, while the kidney is approximately 2.5cm thick (THIBODEAU, 1987).

The aorta and background peak at different times. This implies that there is a delay time associated with the flow of blood from the aorta to the afferent arterioles. This time delay, τ_{delay} has to be included in the model of the renal parenchyma. The adjustment to equation 5.7 is made by:

$$h_{adjusted}(t) = h_{combined}(t) * \delta(t - \tau_{delay}) \tag{5.18}$$

The value of τ_{delay} is determined from experimental background data.

5.4.2 Parameter Estimation

To obtain the initial model parameter estimates, conventional non-parametric deconvolution was performed [4] to approximate the renal retention function. Initial estimates of the model parameters f, τ_b, τ_{cc} and τ_t were calculated as follows,

- The filtration fraction, f, is typically 19% (GUYTON, 1986, PP 398).
- The blood time constant, τ_b, was estimated at 4s.
- τ_t (MinTT), was estimated by detecting the end of the plateau in the renal retention function.
- The parenchymal time constant, τ_{cc}, was found using the result that the Mean Parenchymal Transit Time $KMTT_{paren} = \tau_t + 2 \times \tau_{cc}$, and the $KMTT_{paren}$ was estimated as the time at which the plateau reached half its initial height.

The non-parametric deconvolution method does not to have to be very accurate, as the initial estimates provide only a rough starting point for the model parameters. In this case, a filtered fast Fourier transform (FFT) method (NIMMON *et al.*, 1981) was selected to perform the non-parametric deconvolution.

[4] According to the techniques outlined in section 2.3.2

5.5 Results

The simulation of the model described by equations 3.16 and 5.7 was performed according to the techniques outlined in section 3.4.3. The clinical indices were determined using MinTT = τ_t and equations 5.11 and 5.14. A typical fit of the simulated model is shown in Figure 5.6 and the corresponding parameters for the case studies are shown in Table 5.1. The simulated model fit to all the subjects tabulated in Table 5.1 is displayed in Appendix Q.1. The χ^2 goodness-of-fit test (section 2.3.3) shows that the renal model represents the distribution function of all the data displayed in Appendix Q.1 ($P < 0.05$). The parenchymal IAD from equation 3.16 is compared to the IAD obtained from the non-parametric deconvolution of the parenchymal activity/time curve with the background corrected aorta activity/time curve in Figure 5.7. The mean absolute correlation matrix for the fitted model parameters is shown in Table 5.2. An attempt was made to try and

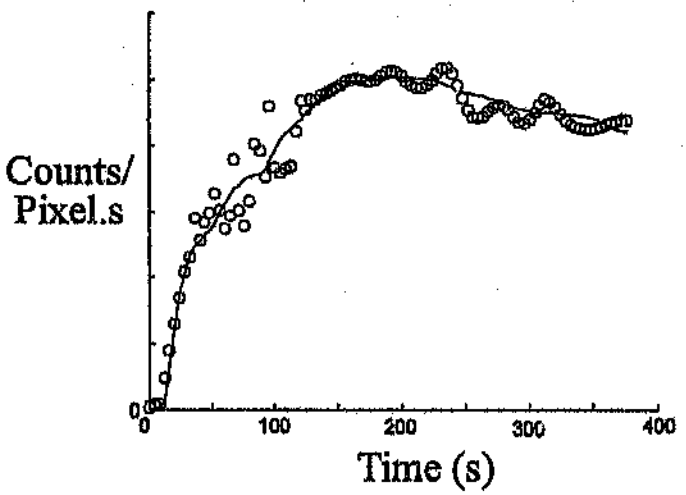

Figure 5.6: Typical fit of the model to the experimental renal parenchymal activity/time curve. ——— Model, ○ Experimental data

scale the renal activity/time data in a similar manner to that performed on the liver activity/time data (section 8.5). These attempts were unsuccessful (Appendix G.1).

Table 5.1: Renal parameter values for twelve normal kidneys and four diseased kidneys. *Significantly different from normal, $P < 0.05$. SEM represents the standard error of the mean.

	Fitted Parameters				Calculated Parameters		
Normal	τ_{cc} (s)	τ_t (s)	MTT_b (s)	f	MinTT (s)	$KMTT_{paren}$ (s)	PTTI (s)
1	12.9	112.3	7.2	0.228	112.3	138.1	25.8
2	19.2	111.4	8.8	0.230	111.4	149.9	38.5
3	24.9	38.2	4.3	0.117	38.2	88.0	49.9
4	16.7	68.0	7.9	0.216	68.0	101.4	33.4
5	17.2	93.4	2.3	0.164	93.4	127.8	34.3
6	34.9	69.2	2.1	0.143	69.2	139.1	69.9
7	37.7	43.7	8.3	0.208	43.7	119.1	75.4
8	16.8	62.7	5.9	0.286	62.7	96.2	33.6
9	13.6	141.7	6.6	0.293	141.7	168.9	27.1
10	13.3	135.5	8.2	0.305	135.5	162.0	26.6
11	14.8	122.7	6.6	0.206	122.7	152.2	29.5
12	14.5	125.7	6.1	0.211	125.7	154.7	29.0
Mean	19.71	93.70	6.18	0.2171	93.70	133.13	39.42
SEM	2.439	10.43	0.642	0.0168	10.43	7.739	4.877
$P < 0.05$ (±)	16.89	72.32	4.45	0.1164	72.32	53.62	33.79
% Variation	12.4	11.1	10.4	7.7	11.1	5.8	12.4

	Fitted Parameters				Calculated Parameters		
Pathology	τ_{cc} (s)	τ_t (s)	MTT_b (s)	f	MinTT (s)	$KMTT_{paren}$ (s)	PTTI (s)
Left 1	21.5	63.7	18.0*	0.139	63.7	106.7	43.0
Right 1	60.8*	65.9	15.4*	0.129	65.9	187.5*	121.6*
Left 2	23.4	107.3	20.8*	0.145	107.3	154.1	46.8
Right 2	∞*	∞*	35.6*	0.000*	∞*	∞*	∞*

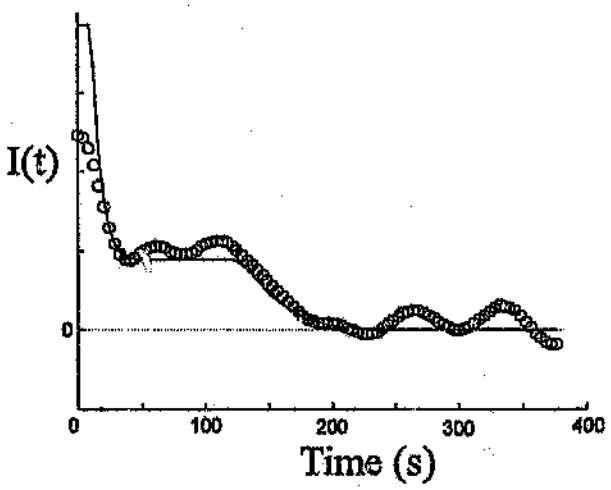

Figure 5.7. Model Internal Age Density (IAD) compared to Experimental IAD. ——— Model $I(t)$, ○ Filtered and deconvolved experimental data

Table 5.". The mean absolute correlation matrix of the four independent fitted model parameters τ_{cc}, τ_t, MTT_b and f respectively, for the values in Table 5.1, together with the corresponding standard error of the mean for each matrix component r_{ij}.

1 ± 0	0.949 ± 0.000	0.173 ± 0.002	0.269 ± 0.008
0.949 ± 0.000	1 ± 0	0.282 ± 0.003	0.382 ± 0.015
0.173 ± 0.002	0.282 ± 0.003	1 ± 0	0.443 ± 0.019
0.269 ± 0.008	0.382 ± 0.015	0.443 ± 0.019	1 ± 0

5.6 Discussion

For the purposes of the discussion, the important renal parameters listed in Table 5.1 are graphically displayed in Figure 5.8.

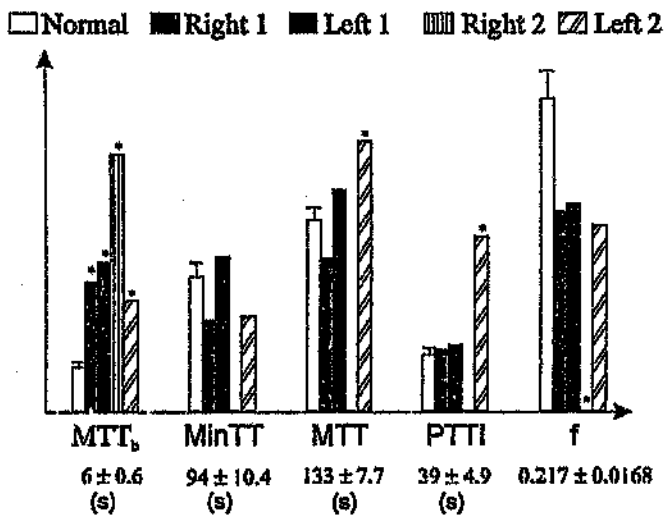

Figure 5.8: Some of the important renal parameters tabulated in Table 5.1. *Significantly different from normal, $P < 0.05$. Error bars indicate the standard error of the mean for the normal subjects. The other results are for the patients with known pathologies.

5.6.1 Normal Subjects

Figures 5.6 and 5.7 show a reasonable correlation between the parametric model and the experimental data. It is likely that the discrepancies between the model and the deconvolved curve in Figure 5.7 are due to the *Gibbs phenomenon* of the FFT and the noise in the experimental data since there has been an attempt to to account for uncertainty in the aorta and parenchymal backgrounds (Chapter 4). This indicates that the flow and mixing in the renal parenchyma can be adequately described by equations 3.16 and 5.7. The variation between the individual kidneys for the parameters displayed in Table 5.1, while quite large, are likely to represent normal variation between individuals.

The correlation matrix is a measure of a model's sensitivity to parameter variation and a measure of the association between variables. The correlation matrix of fitted parameters in Table 5.2 seems to indicate that the values in Table 5.1 are relatively accurate since all of the off diagonal elements do not exceed 0.9 (BECK & ARNOLD, 1977; Appendix I.1). This suggests that a four parameter model is adequate and hence reinforces the likelihood that equations 3.16 and 5.7 adequately describe the renal parenchyma.

From examination of the correlation matrix element $r_{21} = 0.949$, it is clear that there is a relatively high degree of correlation between the collecting duct and inner calyces mean transit time parameter, τ_{cc} ($MTT_{cc} = 2 * \tau_{cc}$), and the mean transit time through the shortest nephron and shortest length of collecting duct, τ_t. The correlation between these parameters is also apparent if one examines the first two columns of Table 5.1; As τ_{cc} increases, τ_t decreases and *vice versa*. There is therefore a functional relationship between these parameters. If one examines the model structure it is clearly evident why these parameters are likely to be related. The mean transit time through the parenchymal component of the model, $KMTT_{paren}$, (Figure 5.5) is the sum of the mean transit time through the shortest nephron and shortest length of collecting duct, τ_t, and the collecting duct and inner calyces mean transit time parameter, τ_{cc} (equation 5.11). Thus while the estimates of these two parameters may change, $KMTT_{paren}$ is likely to be relatively invariant. The data in Table 5.1 reflects this effect where the % variation of $KMTT_{paren}$ within the normal population is almost half that of τ_{cc} and τ_t. This indicates that $KMTT_{paren}$ is likely to be a relatively accurate parameter. τ_{cc} is related to the parenchymal transit time index, PTTI, by equation 5.14 and thus any uncertainty in τ_{cc} is reflected in the PTTI. Although there is less confidence in PTTI and τ_t than in $KMTT_{paren}$, the values of PTTI are consistently smaller than the values of τ_t. This is in agreement with the values reported in the literature using non-parametric deconvolution (BRITTON & NIMMON, 1989). Thus while τ_{cc} and τ_t (and thus PTTI and MinTT) are useful parameters which have an anatomical significance, the estimates of these parameters are strongly correlated and so they should be used in conjunction with $KMTT_{paren}$ for the diagnosis of pathology using the techniques discussed in this thesis.

The other values of the correlation matrix are relatively small. This implies that

there is very little correlation between the parameters which describe the parenchymal component of the renal model and the vascular component. Thus changes in the parenchymal model parameters have little effect on the vascular model parameters. Similarly, the changes in both the parenchymal and vascular parameters of the renal model have little influence on the filtration fraction. All these facts imply that the filtration fraction, the parenchymal component and the vascular components of the model are independent of one another. This is reflected in the the data tabulated in Table 5.1. Thus MTT_b, $KMTT_{paren}$ and f are independent of one another and are likely to be relatively accurate estimates.

The ideal objective is to derive physiological parameter values by applying the mathematical model of the renal parenchyma to experimental data. In order to decide whether the model described above satisfies this requirement, we examine the normal value of the renal filtration fraction. The renal filtration fraction is a physiological parameter that represents the fraction of plasma in the afferent arteriole that is filtered. This parameter can be directly associated with the anatomical structure of the glomerulus and its pathology. The normal value of the filtration fraction is quoted in the literature as $f = 0.19$ (GUYTON, 1986 PP398). This value is comparable to the normal mean value of f presented in Table 5.1. Thus the model of the renal parenchyma described above appears to have physiological significance. This necessary requirement of model allows one to postulate that any significant deviation from the normal parameter values is likely to indicate renal pathophysiology.

There is some disagreement as to the normal values of the parenchymal mean transit time, $KMTT_{paren}$, and the parenchymal transit time index, PTTI, discussed in the literature and the values displayed in Table 5.1. The normal range for PTTI discussed in the literature is 10–156s (BRITTON & NIMMON, 1989) while the normal range for $KMTT_{paren}$ is 40–240s (BRITTON & NIMMON, 1989). The normal ranges for PTTI and $KMTT_{paren}$ from Table 5.1 are 6–73s and 80–187s ($P < 0.05$). According to the PTTI and $KMTT_{paren}$ criteria discussed in the literature (BRITTON & NIMMON, 1989) the pathologies displayed in Table 5.1 fall within normal values. The values that have been determined in the literature use non-parametric deconvolution which may have a subjective component to the analysis (Chapters 3 and 4). This may explain the discrepancy between the normal range of values reported

in the literature and those displayed in Table 5.1. The blood transit time parameter, MTT_b, has not been measured or discussed in the literature. It is however possible to postulate how this parameter might change with pathology and the next subsection explores this issue in further detail.

The twelve normal kidneys in Table 5.1 represent six different people and the paired nature of the parameters is evident. Height and weight information were not recorded for the subjects that were selected for renal evaluation (section 2.3) and it was therefore not possible to determine whether a relationship existed between transit time and height or mass. It is likely that such a relationship exists and an investigation on a large sample of subjects has already started. The hypothesis for such a study is that the amount of renal filtration is likely to be directly related to blood volume. There are many empirical relationships in the literature between blood volume and height/weight data. The effect of sex on renal parameter values has not been investigated in this thesis. This issue is likely to be resolved when the effect of blood volume on renal parametet values is investigated.

5.6.2 Renal Pathology

The parameters associated with the pathologies in Table 5.1 have been obtained by applying the above techniques to two renal hypertensive patients with possible renal hypertension. When the renal artery is partially obstructed as in the case of renal hypertension, the flow and pressure of blood to the glomerulus decreases. The decrease in renal perfusion pressure stimulates renin release and the generation of intrarenal angiotensin II. This in turn causes the vasoconstriction of the efferent arteriole which further reduces renal blood flow. Furthermore, the constriction of the efferent arteriole increases the resistance to outflow from the glomerulus and thus raises the glomerular filtration rate. This control mechanism attempts to maintain normal glomerular filtration rate. The decreased blood flow to the kidney increases the transit time of blood within the renal vasculature. During the initial stages of renal hypertension, the filtration fraction increases.

As a consequence of increased filtration, the plasma colloid osmotic pressure within

the glomerulus increases (since none of the plasma proteins are filtered by the glomerulus). The increased colloid osmotic pressure directly decreases the glomerular filtration rate and a progressive pathology develops where the arterial obstruction increases, the osmotic pressure across the tubular membrane cells increases and the glomerular filtration rate and filtration fraction ultimately decrease. The increased osmotic pressure across the tubular cells with decreased blood flow eventually causes necrosis of the tubular cells. Scar tissue forms which obstructs the nephrons. These changes in the anatomical structure of the kidney should manifest themselves as changes in the model parameters displayed in Table 5.1.

The renal blood transit time, MTT_b, is significantly prolonged ($P < 0.05$) in all the renal hypertensive patients. The change in this parameter is consistent with the above discussion where renal vascular obstruction and efferent arterial constriction combine to reduce the flowrate and thus increase blood transit time through the kidney. The change in MTT_b is thus consistent with the changing pathophysiology.

The parenchymal transit time index, PTTI, is related to the collecting duct and inner calyces time constant, τ_{cc}. This parameter also accounts for the length distribution of nephrons. As the renal hypertension pathology progresses, a number of nephrons become obstructed both partially and completely. The transit time within such nephrons is likely to increase and this in turn is likely to be reflected as an apparent increase in the length distribution of nephrons. The elevated PTTI of the right kidneys of the patients is significantly elevated ($P < 0.05$) and is thus consistent with these arguments. The left kidneys still appear to have some normal function and the small change in the PTTI of these kidneys reflects this function. The change in PTTI is thus consistent with the changing pathology of the nephrons while also addressing the altered physiology of these nephrons.

The minimum transit time, MinTT, corresponds to the minimum time that it takes for the tracer to flow from the glomerulus through the shortest nephron and section of collecting duct ie. MinTT= τ_t. During the development of the renal pathology, it is likely that there exists a nephron whose function is essentially normal. The minimum transit time is thus unlikely to be a sensitive measure of renal hypertensive pathology unless the kidney is completely obstructed. It is thus not surprising that

the values for all the active diseased kidneys are within normal limits. The most obvious value of the above techniques is to aid and assess the pathophysiology of early pathology since the identification of gross pathology is often obvious. The assessment of early renal pathology using the minimum transit time is thus likely to have limited benefit.

According to the above discussion, the filtration fraction, f, should increase in early renal hypertensive patients and decrease as the pathology develops. In the active diseased kidneys, the filtration fraction is on the low side of normal. This already indicates that the pathology of the renal hypertensives is sufficiently advanced. It is possible that patients may not present with clinical symptoms of renal hypertension until there is significant renal tissue damage and a decreased filtration fraction. Thus f in conjunction with MTT_b may be very important indicators of impending renal disease. One might postulate that diabetics may benefit substantially by regularly monitoring f and MTT_b. If the filtration fraction rises above normal and then steadily declines in such patients then perhaps preventative action could be taken to avert permanent renal tissue damage. The application of the above techniques to such a group of subjects is an area of future research. The significant change of the filtration fraction obtained using the renal model is consistent with the pathology as outlined above. This is further evidence that the renal model developed in this chapter has physiological consistency.

The value of f for kidney 3 in Table 5.1 is relatively low. Further investigation revealed that the subject had a below normal glomerular filtration rate. This is also evidence that the renal model appears to predict normal and abnormal cases adequately.

5.7 Conclusions

The chapter proposes a parametric model for the study of the renal retention function. This parametric model is less perturbed by noise artifacts which may be present in deconvolved data than previous models and therefore has the potential benefit of providing more accurate clinical indices. The technique may also improve the

understanding of the physiology and pathology of the renal process. The parametric model of the renal parenchyma appears to consistently describe both normal and abnormal pathophysiology. The model response corresponds to both the measured and deconvolved renal data.

The filtration fraction, f, is likely to be sensitive to renal background subtraction. The values of f obtained from the experimental data, corresponds with those reported in the literature. For this reason, the renal background determined from the aorta activity/time curve appears to be a reasonable approximation, as it does not underestimate the intravascular background within the renal parenchymal activity/time curve (section 2.2.1). The renal blood transit time parameter, MTT_b, has been shown to be a potentially useful clinical index for the determination of renal vascular disease.

The parenchymal transit time index, PTTI, mean parenchymal transit time, $KMTT_{paren}$, filtration fraction, f, and mean blood transit time, MTT_b, all appear to be sensitive measures of organ pathology. Diagnostic information obtained using the PTTI must however be correlated with $KMTT_{paren}$. The minimum transit time, MinTT, has been shown to be a poor indicator of renal pathology.

In conclusion, parametric deconvolution of the renal retention function has been shown to be robust and provides consistent physiological information not provided by the conventional non-parametric methods. Further clinical research is however required to validate the use of the model parameters as clinical indices. In addition, clinical work is required to refine the estimate of the ratio of background tissue thickness to organ tissue thickness.

Chapter 6

An Anatomical and Physiological Model of the Spleen

6.1 Introduction

Hepatic function can be characterised by the activity/time curves obtained from dynamic imaging of the spleen, liver and aorta. In this chapter, anatomical and physiological information is used to determine a model for the *Internal Age Density* (IAD) of the Spleen. The modelling approach characterises the spleen in terms of anatomical and physiological parameters. The model is fitted to experimental data obtained from eight normal, healthy volunteers. Statistical methods are then used to verify the model.

6.2 Anatomy and Physiology of the Spleen

Consider a section though the spleen as shown in Figure 6.1. Blood with tracer enters the spleen through the splenic artery which then branches into the trabecular arteries. The trabecular arteries follow the connective tissue trabeculae. Central arteries then branch off into the *spleen parenchyma* and are surrounded by a sheath of lymphocytes [1]. The concentration at each trabecular artery split point is the same and if we assume that the length distribution of branch vessels is small, ar . he flow

[1] Also termed white pulp arteries

velocity is relatively high, then the concentration of the tracer as a function of time for every central artery will be roughly the same. If the lengths differed substantially and the flowrate was small then each central artery would have an input that differed from the next by a delay time (Chapter 3). Thus we may consider a series of parallel systems such as the unit shown in Figure 6.1.

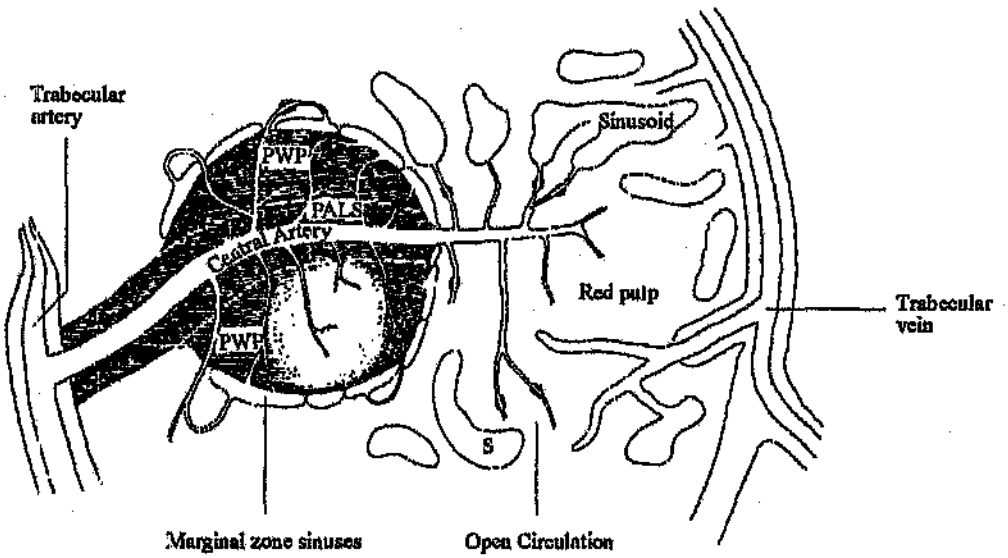

Figure 6.1: A section through the Spleen; **S**, Venous sinuses; **PWP**, peripheral white pulp; **PALS**, periarterial lymphatic sheath. (Redrawn from Greep R.O., Weiss L.: *Histology*, 3rd ed. McGraw-Hill, 1973)

There are two types of blood circulation in the spleen parenchyma namely:

Open Circulation Blood leaves the vascular compartment. Blood can move from the central artery and open into the peripheral white pulp (referred to as white pulp hereafter), marginal zone sinuses or the red pulp. Blood percolates from the white pulp of lymphatic tissue into the marginal zone sinuses where macrophages engulf foreign material. The blood then percolates through the red pulp into the venous sinuses.

Closed Circulation Blood remains within in the blood vessels. In this case the blood in the central arteries empties directly into the venous sinuses.

The venous sinuses join to form the trabecular veins which empty into the splenic vein.

6.3 Flow in the Spleen

A flow representation of the proposed model of the spleen is shown in Figure 6.2. A blood fraction, q, remains in the closed circulation. The rest of the blood flows into the open circulation. A fraction of open circulation blood, κ, flows into the white pulp while the rest flows into the red pulp. The open and closed circulation meet in the sinusoid where mixing occurs. The parallel sinusoids join the trabecular veins. We assume that there is a large length distribution of trabecular veins before they all combine to form the splenic vein.

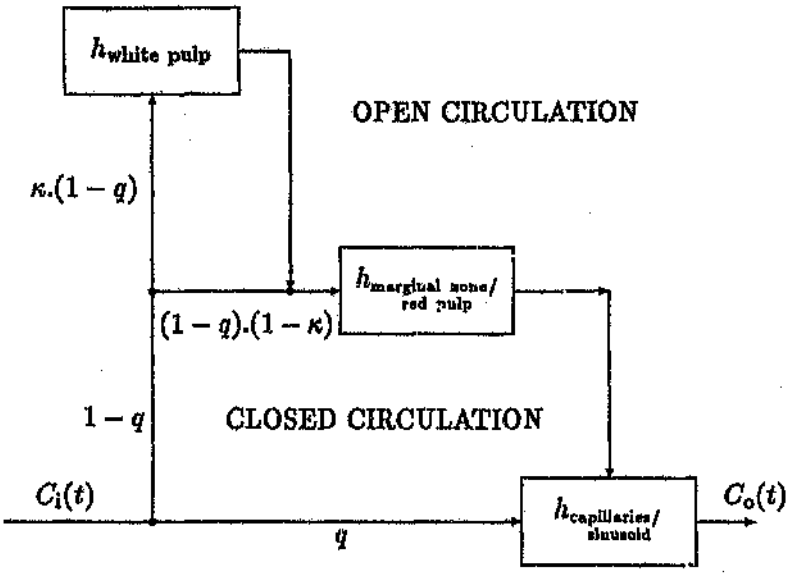

Figure 6.2: Flow Model of the Spleen

6.3.1 Flow in the Open Circulation

Blood that enters the white pulp percolates between the cells into the marginal zone sinuses. The marginal zone sinuses essentially define a border between the white pulp and the red pulp. Blood from the central artery also empties into the marginal zone sinuses and mixes with the blood from the white pulp. The mixing and bypass has not been included in the model because of increased complexity which would add more parameters to the model. Instead, it is assumed that marginal zone sinuses are the point of distinction between the white and red pulps and that no appreciable mixing occurs here. Thus blood that flows into the marginal zone sinuses from the central artery is assumed to behave in the same manner as blood from branches of the central artery that terminate in the red pulp.

6.3.2 Flow Fractions in the Spleen

To develop bounds on the split fractions, q and κ we consider blood flow in the open circulation. One conceptually expects that blood flow through the white pulp, into the marginal sinuses and then through the red pulp must encounter a greater resistance to flow than blood flowing through the red pulp only. It is thus likely that $q > 0.5$ and $\kappa < 0.5$.

6.4 Mixing in the Spleen

LEVENSPIEL (1972) has shown that flow in a packed bed system (a column of particles) can be approximated by plug flow with a small amount of dispersion. In such a system the fluid flows through a tortuous path in the packed column. The degree of dispersion depends on the diameter of the bed, the fraction of volume unoccupied by solid material and the flowrate into the system. In this thesis, we assume that blood flow through the red and white pulp tissue of the spleen closely approximates the flow of fluid in packed beds. Thus we assume that the splenic tissue is arranged like particles of solid and that the blood percolates through this structure in close contact with the splenic tissue. The degree of dispersion is assumed

to be small and the flow of blood through the splenic tissue is approximated as plug flow in nature. Thus (Chapter 3):

$$h_{ms\rightarrow rp}(t) = \delta(t - \tau_{\rm mr}) \tag{6.1}$$

$$h_{wp\rightarrow rp}(t) = \delta(t - \tau_{\rm w}) \tag{6.2}$$

where

$\delta(t)$:- *Dirac's* delta

$\tau_{\rm mr}$:- Blood transit time through the red pulp of the spleen

$\tau_{\rm w}$:- Blood transit time through white pulp of the spleen

$h_{ms\rightarrow rp}$:- Residence time density (RTD) of blood flow through the red pulp of the spleen, s^{-1}

$h_{wp\rightarrow rp}$:- Residence time density (RTD) of blood flow through the white pulp of the spleen, s^{-1}

All the blood meets in the venous sinusoids where mixing occurs in the venous capillary network because of the length distribution of vessels. Thus the mixing in the venous sinusoids coupled with the mixing effects associated with the length distribution of trabecular veins is modelled by the gamma distribution (equation 1.6) with $z = 3$, thus:

$$h_{\substack{\text{capillaries/}\\ \text{sinusoid}}}(t) = \frac{t^2}{2\tau_s^3} e^{\frac{-t}{\tau_s}} \tag{6.3}$$

where

$\tau_{\rm s}$:- Time constant associated with blood flow in the venous sinusoids and trabecular veins of the spleen

$h_{\substack{\text{capillaries/}\\ \text{sinusoid}}}(t)$:- Residence time density (RTD) of blood mixing in the venous sinus and venous capillary network of the spleen, s^{-1}

Blood in the closed circulation is assumed to bypass the splenic white and red pulp and flow directly into the venous sinuses (Figure 6.2). Combining equations 6.1, 6.2 and 6.3 according to Figure 6.2 gives:

$$h_{\rm spleen}(t) = \begin{array}{l}(\kappa(1-q)\delta(t-\tau_w) * \delta(t-\tau_{\rm mr}) + (1-q)(1-\kappa)\delta(t-\tau_{\rm mr})) * \frac{t^2 e^{-t/\tau_s}}{2\tau_s^3} \\ + \; q\frac{t^2 e^{-t/\tau_s}}{2\tau_s^3}\end{array} \tag{6.4}$$

where $*$ denotes convolution. The mean transit time for the spleen can be determined using equation 3.6 which gives:

$$\begin{aligned} \tau_{\text{spleen}} &= \int_0^\infty t\, h_{\text{spleen}}(t)dt \\ &= (1-q)(k\tau_w + \tau_{\text{mr}}) + 3\,\tau_s \end{aligned} \tag{6.5}$$

As discussed above, the deconvolution of splenic activity/time curves with aorta activity/time curves (Chapter 4) gives the IAD of the spleen (equation 3.16). The relationship between $h_{\text{spleen}}(t)$ and the $I_{\text{spleen}}(t)$ is discussed in Chapter 3.

6.5 Results

The simulation of the model described by equations 6.4 was performed according to the techniques outlined in section 3.4.3. A typical fit of the spleen model to the experimental data is shown in Figure 6.3. The model parameters determined from the minimisation of the sum of squares between the model and experimental data are tabulated in Table 6.1. The simulated model fit to all the subjects tabulated in Table 6.1 is displayed in Appendix R.1. The χ^2 goodness-of fit test (section 2.3.3) shows that the spleen model represents the distribution function of all the data displayed in Appendix R.1 ($P < 0.05$). The spleen model IAD from equation 6.4 is compared to the experimental spleen IAD (deconvolution of the spleen activity/time curve with the background corrected aorta activity/time curve (Chapter 4)) in Figure 6.4. The mean absolute correlation matrix of fitted parameters for the normal subjects is shown in Table 6.2. An attempt was made to try and scale the spleen activity/time data in a similar manner to that performed on the liver activity/time data (section 8.5). These attempts were unsuccessful (Appendix G.1).

6.6 Discussion

For the purposes of the discussion, the important splenic parameters listed in Table 6.1 are graphically displayed in Figure 6.5.

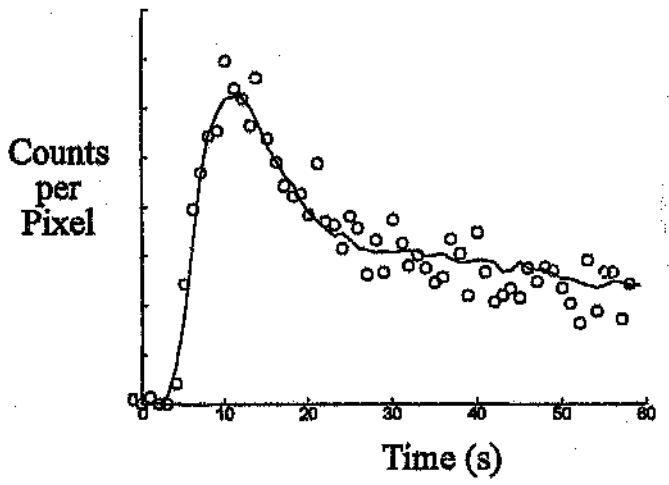

Figure 6.3: Typical fit of the model to the experimental spleen activity/time curve. ——— Model, ○ Experimental data

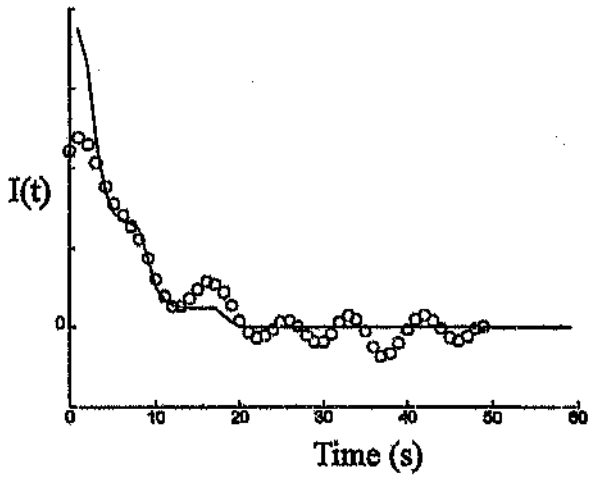

Figure 6.4: Model Internal Age Density (IAD) compared to Experimental IAD. ——— Model $I(t)$, ○ Filtered and deconvolved experimental data

Table 6.1: Spleen parameter values for eight normal healthy volunteers and two diseased spleens. *Significantly different from normal, $P < 0.05$. SEM represents the standard error of the mean.

	Fitted Parameters				Calculated Parameters
Normal	q	κ	τ_{mx} (s)	τ_w (s)	τ_{spleen} (s)
1	0.52	0.33	1.7	12.2	4.8
2	0.48	0.13	8.8	20.2	7.9
3	0.47	0.12	6.6	8.5	6.0
4	0.62	0.27	8.2	12.3	6.3
5	0.86	0.09	6.8	20.4	3.2
6	0.66	0.20	6.4	9.1	4.8
7	0.70	0.11	5.9	35.6	4.0
8	0.93	0.18	4.9	12.5	2.5
Mean	0.656	0.179	6.17	16.3	5.07
SEM	0.069	0.034	0.888	3.67	0.701
$P < 0.05$ ($\pm$)	0.340	0.169	4.35	18.0	3.43
% Variation	10.6	19.2	14.4	22.5	13.8

	Fitted Parameters				Calculated Parameters
Pathology	q	κ	τ_{mx} (s)	τ_w (s)	τ_{spleen} (s)
1	0.39	0.27	5.8	36.1*	11.3*
2	0.14*	0.48*	13.0*	40.0*	29.8*

Table 6.2: The mean absolute correlation matrix of the four independent fitted model parameters q, κ, τ_{mr} and τ_w respectively, for the values in Table 6.1, together with the corresponding standard error of the mean for each matrix component r_{ij}.

1.000 ± 0.000	0.398 ± 0.121	0.838 ± 0.032	0.291 ± 0.114
0.398 ± 0.121	1.000 ± 0.000	0.423 ± 0.124	0.693 ± 0.052
0.838 ± 0.032	0.423 ± 0.124	1.000 ± 0.000	0.239 ± 0.133
0.291 ± 0.114	0.693 ± 0.052	0.239 ± 0.133	1.000 ± 0.000

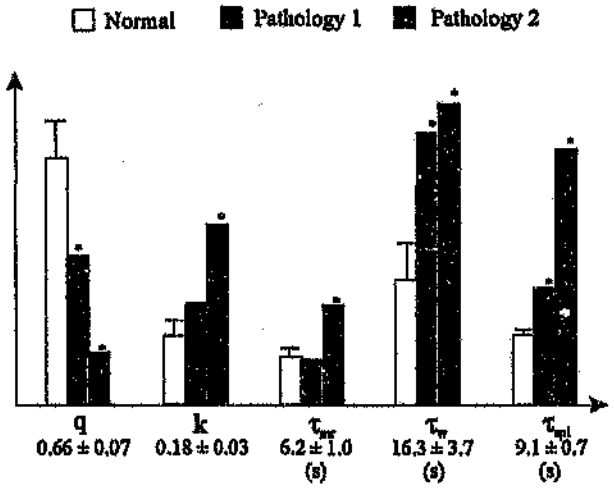

Figure 6.5: Some of the important splenic parameters tabulated in Table 6.1. *Significantly different from normal, $P < 0.05$. Error bars indicate the standard error of the mean for the normal subjects. The other results are for the patients with known pathologies.

6.6.1 Normal Subjects

The close fit between the parametric model and the experimental data in Figures 6.3 and 6.4 indicate that the flow and mixing in the spleen is adequately described by the IAD corresponding to equation 6.4. The discrepancies between the model and the deconvolved curve in Figure 6.4 are likely due to the *Gibbs phenomenon* of the FFT (the oscillations and the discontinuity at $t = 0$) and the noise in the experimental data since the uncertainty in aorta and parenchymal tissue backgrounds have largely been accounted for (Chapter 4). The variation between the individual spleens for the parameters displayed in Table 6.1 appears to represent normal variation between individuals.

The correlation matrix is a measure of a model's sensitivity to parameter variation and a measure of the association between variables. The correlation matrix of fitted parameters in Table 6.2 seems to indicate that the values in Table 6.1 are relatively accurate since all of the off diagonal elements do not exceed 0.9 (BECK & ARNOLDS, 1977; Appendix I.1). This reinforces the likelihood that the four parameter model of equation 6.4 adequately describes the splenic parenchyma.

Upon closer examination of the correlation matrix element $r_{31} = 0.838$, it is clear that there is evidence of some correlation between the fraction of blood that flows through the closed circulation of the spleen, q, and the blood transit time through the red pulp of the spleen, τ_{mr}. The correlation between these parameters is visible if one examines the first and third columns of Table 6.1; As most of the values of τ_{mr} increase, q decreases and *vice versa*. If one examines the relationship between these parameters and the experimental data it is clearly evident that these two parameters affect the early part of the splenic activity/time curve, while the blood transit time through the white pulp of the spleen, τ_w, affects the latter part of the curve. The fraction of blood that flows through the white pulp of the open circulation of the spleen, κ, affects the relative contribution of the red and white pulp to the different parts of this curve. Thus while q and τ_{mr} are correlated, κ and τ_w are not strongly correlated to either of these parameters. The mean transit time through the spleen, τ_{spleen}, is the sum of the relative amounts of transit time through the closed circulation and the red and white pulps of the open circulation

(equation 6.5). Thus τ_{spleen} is likely to be relatively well estimated. The transit time data in Table 6.1 reflects this effect where the % variation of τ_{spleen} within the normal population is less than that of τ_{mr} and τ_{w}. This indicates that τ_{spleen} is likely to be a relatively accurate parameter. Although there is less confidence in τ_{mr} and τ_{w} than in τ_{spleen}, the values of τ_{mr} are consistently smaller than the values of τ_{w}. This is in agreement with the arguments presented above. Furthermore, the normal values of q and κ from Table 6.1 agree with the arguments presented in section 6.3.2. Thus while τ_{mr}, τ_{w}, q and κ are useful parameters which have a physiological significance, these parameters should in all likelihood be used in conjunction with τ_{spleen} for the diagnosis of pathology.

The % variation of τ_{w} and κ in Table 6.1 are significantly higher than the other tabulated parameters. As discussed above the value of κ determines the amount of blood that flows through the open circulation as opposed to the closed circulation. The actual fraction of total splenic blood flow that flows through the white pulp of the spleen is $\kappa(1-q)$ which has an average value of 0.117 ± 0.02. Thus only about 12% of the total blood flow through the spleen flows through the white pulp. The value of τ_{w} is thus determined using a fairly small component of the experimental data and it is likely that this parameter might have a larger error than other parameter values. This is reflected in Table 6.1. The splenic transit time values are not excessively large.

An attempt was made to try and correlate the parameter variation in Table 6.1 with weight and/or sex. There was no obvious relationship. This in itself is surprising because of the scaling relationship determined for the hepatic vascular system in Chapter 8, Figure 8.3. This provides some evidence that the explanation for the scaling relationship of hepatic vascular system is to be found elsewhere.

The ideal objective of the mathematical model of the spleen is to derive physiological parameter values from the experimental data. There appear to be no measurements in the literature of splenic transit time or the relative blood flow through open and closed circulations. It is thus difficult to decide whether the model of the spleen is physiologically sound. It is however possible to postulate how these parameters might change with pathology and the next subsection explores this issue in further

detail.

6.6.2 Splenic Pathology

The closed circulation blood flow fraction, q, is reduced in the first pathology and significantly decreased in the second portal hypertensive patient ($P < 0.05$). It thus appears that more blood flows through the open circulation than the closed circulation in portal hypertensive spleens. This in turn suggests an enlargement of open circulation. The fraction of open circulation blood that flows into the white pulp, κ, is also elevated in the first portal hypertensive subject and significantly elevated in the second subject ($P < 0.05$). Thus more blood "appears" to flow through the white pulp in the portal hypertensive spleens than in the normal subjects. The increase in the value of κ suggests a greater enlargement of the white pulp as opposed to the red pulp in the portal hypertensive spleens. The white pulp mean transit time, τ_w, is significantly elevated in both portal hypertensives ($P < 0.05$) and the marginal zone and red pulp transit time, τ_{mr}, are not elevated in the first portal hypertensive while it is significantly elevated in the second subject ($P < 0.05$). The spleen mean transit time τ_{spleen} appears to be a sensitive measure of spleen abnormality in the two portal hypertensives.

In portal hypertension the spleen demonstrates the histologic features of fibrocongestive splenomegaly (GRIFFITH & JANNEY, 1990). The red pulp is expanded with areas of fibrosis and the sinuses may be open and dilated or narrowed in areas of dense fibrosis (GRIFFITH & JANNEY, 1990). The increase in the values of q and τ_{mr} would be consistent with an increased red pulp size. The white pulp is often atrophic because expansion of the red pulp and fibrosis of the marginal zone sinuses is often present (GRIFFITH & JANNEY, 1990). Thus blood flow out of the white pulp is likely to be obstructed with an increased τ_w. If the volume of white pulp decreases and τ_w increases, then the flowrate of blood through the white pulp should decrease and the value of κ should decrease. The value of κ has however increased in the portal hypertensive subjects. The apparent discrepancy in this parameter can be explained and conceptually defended on the grounds that the model of the spleen is based on normal spleen tissue. It is thus likely that the increased value of κ and

τ_w in the portal hypertensive subjects may reflect a combination of flow through the white pulp and the increasing fibrosed regions of the red pulp.

In order to really be able to say more about these pathologies, more work on both normal and pathological spleens will need to be done.

6.7 Conclusions

The flow and mixing in the spleen is adequately described by the IAD corresponding to equation 6.4. The spleen parameter values for the first portal hypertensive indicate a developing progression of the observed pathology. The spleen parameter values for the portal hypertensive subjects concur with the degree of splenomegaly observed clinically. The fraction of blood that flows through the closed circulation of the spleen, q, the fraction of blood that flows through the white pulp of the open circulation of the spleen, κ, the blood transit time through the red pulp of the spleen, τ_{mr}, the blood transit time through white pulp of the spleen, τ_w, and the mean transit time through the spleen, τ_{spleen} all appear to be relatively sensitive measures of organ pathology. Diagnostic information obtained using q, κ, τ_{mr} and τ_w must however be correlated with τ_{spleen}.

The transit time parameters indicate that the hepatic vascular obstruction associated with portal hypertension has reduced the total flow through the spleen.

Chapter 7

Deconvolution and Imaged Multiple Input Organs

7.1 Introduction

Chapter 3 showed that the deconvolution of single-input organs gave rise to the IAD of the organ. Unfortunately the deconvolution of liver activity/time curves with aorta activity/time curves does not give rise to the internal age density (IAD) of the liver because it has multiple inputs. It is thus necessary to extend the analysis of Chapter 3 to account for multiple input, imaged systems.

7.2 Dynamic Imaging of the Liver

Chapter 3 introduced the use of residence time density theory for tracer imaging experiments. The chapter examined single input systems and derived equation 7.1, describing the relationship between the input to a system and the measured organ activity/time curve. In other words, the convolution of the transient input to the system with the internal age density of the system gives the volume averaged concentration or the measured area normalised organ activity/time curve (Chapter 3).

$$C_{\text{in}} * I(t) = \frac{\int_0^V C(t,v)dv}{V} \qquad (7.1)$$

As discussed above, the liver is a multiple input system; the hepatic artery and

portal vein both enter the liver. The hepatic artery is essentially fed from the aorta with a delay as it flows towards the liver. The portal venous supply contains blood that has already circulated from the aorta, through the gut and spleen. A schematic representation of this system is shown in Figure 7.1. The relative amounts of blood from the portal vein and the hepatic artery is given by the split fraction, r. In the following analysis, the gut/spleen RTD will be represented by h_{gs}.

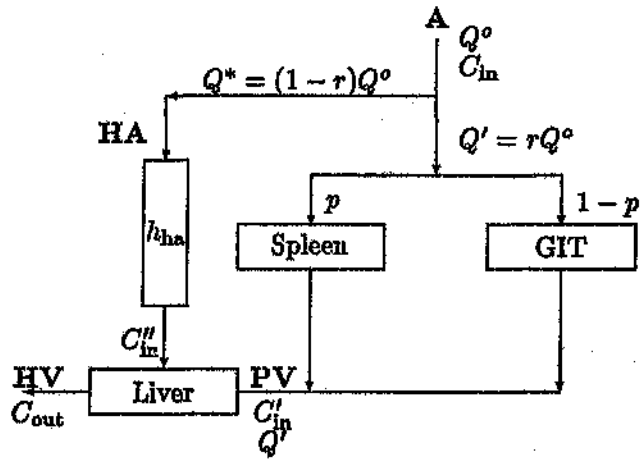

Figure 7.1: The Hepatic Vascular System; **HA** Hepatic Artery, **PV** Portal Vein, **HV** Hepatic Vein, Q denotes Volumetric Flowrate, C denotes concentration, r is the fraction of Q^o that flows to the spleen and GIT, p is the portal blood flow (Q') that flows through the spleen, h_{ha} is the RTD of the hepatic artery (section 8.3).

We begin the analysis in the same way as Chapter 3. In a recirculating system, at any time, mass balance holds and so:

$$\text{Mass In of Tracer} - \text{Mass Out of Tracer} = \text{Accumulated Mass of Tracer} \qquad (7.2)$$

We perform a mass balance for the tracer flowing into the liver in Figure 7.1. Thus in some small time interval, $t \rightarrow t + dt$:

$$Q^* C''_{in}.dt + Q' C'_{in}.dt - Q^o C_{out}.dt = \int_0^V C(v, t+dt)dv - \int_0^V C(v,t)dv \qquad (7.3)$$

where

$Q^*C''_{\text{in}}$:- Mass flow into the liver by the hepatic artery

$Q'C'_{\text{in}}$:- Mass flow into the liver by the portal vein

Q^oC_{out} :- Mass flow out of the liver by the hepatic vein

$\int_0^V C(v,t)dv$:- Mass of tracer in the system at time t (imaged)

Q^o :- Total blood flow into the liver, $m^3.s{-}1$

Dividing by dt and taking limits gives:

$$Q^*C''_{\text{in}} + Q'C'_{\text{in}} - Q^oC_{\text{out}} = \frac{d}{dt}\left\{\int_0^V C(t,v)dv\right\} \tag{7.4}$$

But by mass balance for constant density, ρ (Chapter 3):

$$Q^* = (1-r)Q^o \tag{7.5}$$

$$Q' = rQ^o \tag{7.6}$$

$$C'_{\text{in}} = C_{\text{in}} * h_{\text{gs}}(t) \tag{7.7}$$

$$C''_{\text{in}} = C_{\text{in}} * h_{\text{ha}}(t) \tag{7.8}$$

where

h_{gs} :- Residence time density (RTD) of the splenic and gastrointestinal regions (equation 8.3), s^{-1}

r :- Fraction of blood that flows into the liver through the portal vein, dimensionless

p :- Fraction of portal blood that flows through the spleen as opposed to the gastrointestinal tract, dimensionless

$h_{\text{ha}}(t)$:- RTD of the hepatic artery (section 8.3), s^{-1}

$*$:- Denotes convolution

Similarly, by mass balance over the whole hepatic vascular system in Figure 7.1:

$$C_{\text{out}} = C_{\text{in}} * h_{\text{hvs}}(t) \tag{7.9}$$

where

$h_{\text{hvs}}(t)$:- Residence time density of the hepatic vascular system in Figure 7.1 (hepatic artery, spleen and gastrointestinal tract), s^{-1}

C_{in} :- Concentration of tracer flowing into the hepatic vascular system through the aorta

C_{out} :- Concentration of tracer flowing out the hepatic vascular system in the hepatic vein

By substituting equations 7.5, 7.6, 7.7, 7.8 and 7.9 into equation 7.4 and solving (Appendix E.1) we find:

$$\left\{\frac{\int_0^t [(1-r)h_{\text{ha}} + rh_{\text{gs}} - h_{\text{hvs}}]\,dt}{\tau_{\text{liver}}}\right\} * C_{\text{in}} = \frac{\int_0^V C(t,v)dv}{V_{\text{liver}}} \tag{7.10}$$

where

τ_{liver} :- Volume of the liver divided by the total volumetric flowrate into the liver (V_{liver}/Q^o), s

$\delta(t)$:- *Dirac's* delta

Equation 7.10 is general for imaging any tracer in the liver. The equation is valid for a time-invariant recirculating system (Chapter 3). The extension of equation 7.10 for imaging systems with any number of system inputs would follow the above analysis. We define the Liver Probability Density Function, $LPDF(t)$ as:

$$LPDF(t) = \left\{\frac{\int_0^t [(1-r)h_{\text{ha}} + rh_{\text{gs}} - h_{\text{hvs}}]\,dt}{\tau_{\text{liver}}}\right\} \tag{7.11}$$

The RTD, $h_{\text{hvs}}(t)$ depends on the anatomy and physiology of the liver, spleen and gastrointestinal tract. Equation 7.10 represents the relationship between the measured liver activity/time curves and the measured aorta time/activity curve. The result is derived only from mass balance. From Appendix E.1:

$$\lim_{t\to 0}\left\{\frac{\int_0^t [(1-r)h_{\text{ha}} + rh_{\text{gs}} - h_{\text{hvs}}]\,dt}{\tau_{\text{liver}}}\right\} = 0 \tag{7.12}$$

$$\lim_{t\to \infty}\left\{\frac{\int_0^t [(1-r)h_{\text{ha}} + rh_{\text{gs}} - h_{\text{hvs}}]\,dt}{\tau_{\text{liver}}}\right\} = 0 \tag{7.13}$$

$$\frac{\int_0^t [(1-r)h_{\text{ha}} + rh_{\text{gs}} - h_{\text{hvs}}]\,dt}{\tau_{\text{liver}}} \geq 0 \tag{7.14}$$

and,

$$\begin{aligned} \int_0^\infty \int_0^{t'} [(1-r)h_{\text{ha}} + rh_{\text{gs}} - h_{\text{hvs}}]\, dtdt' &= \frac{(\tau_{\text{hvs}} - \tau_{\text{ha}}) - r(\tau_{\text{gs}} - \tau_{\text{ha}})}{\tau_{\text{liver}}} \\ &= 1 \end{aligned} \tag{7.15}$$

where

τ_{ha} :- Transit time of blood travelling down the hepatic artery (section 8.3), s

The numerator of equation 7.15 corresponds to the liver mean transit time, LMTT ie.

$$LMTT = \tau_{\text{liver}} = (\tau_{\text{hvs}} - \tau_{\text{ha}}) - r(\tau_{\text{gs}} - \tau_{\text{ha}}) \tag{7.16}$$

It is clear from equation 7.10 that the deconvolution of liver activity/time curves give rise to a complex combination of splenic, gastrointestinal and liver dependencies. Unlike the single input systems described above, there is no obvious correlation between types of mixing and the effect it has on the deconvolved curve. The only direct information that one can glean by deconvolution is the time at which tracer first appears in the liver, τ_{ha}, and the mean transit time.

Thus a parametric flow model of the portal and hepatic vascular systems becomes desirable (as a means to explain and quantify the deconvolved hepatic activity/time curve). The rest of this thesis is devoted to the development of such models and the application of these models to experimental data.

7.3 Conclusion

The relationship between the aorta and organ activity/time measurements was investigated for multiple input organs, in particular the liver. This analysis provides a mathematical framework describing the deconvolution of imaged multiple input organs. It was shown that deconvolution of liver activity/time curves gives rise to a complex combination of splenic, gastrointestinal and liver dependencies. Unlike single input systems (Chapter 3), it was shown that there is no obvious correlation between the type of mixing and the effect it has on the liver deconvolved c: ve.

Furthermore, the only direct information that one can glean from such a curve is the time at which tracer first appears in the liver and the mean transit time of the combined system.

A parametric flow model of the portal and hepatic vascular systems thus become desirable as a means to explain and quantify the deconvolved hepatic activity/time curve.

Chapter 8

An Anatomical and Physiological Model of the Liver

8.1 Introduction

Various researchers (FLEMING *et al.*, 1983; GIANPAOLO *et al.*, 1989; O'CONNOR *et al.*, 1992) have used various methods of processing scintigraphic imaging data in an attempt to identify hepatic blood supply abnormalities. The methods make broad assumptions in relating the hepatic arterial perfusion time to the peak time of the renal or splenic activity/time curves. There appears to be no experimental evidence to confirm these assumptions. Other researchers (ACKROYD *et al.*, 1986; CARLISLE *et al.*, 1992; DOI *et al.*, 1988; HORN *et al.*, 1990) have used doppler ultrasound techniques to measure portal and hepatic arterial flows. These techniques have to determine a vessel cross sectional area to convert the measured blood velocities to flowrates. The measurements vary depending on the technical ability of the operator and as a result, the accuracy of blood flowrate measurements vary widely (PAULSON *et al.*, 1992). Compartmental modelling approaches have also been used (GAMBHIR *et al.*, 1989) however they have difficulty in characterising unmixed systems and many pitfalls exist when extending compartmental flow models to include non-linear reaction kinetics (ZWIETERING, 1959).

As has been mentioned before, imaging techniques such as scintigraphic imaging suffer from noise in the experimental data. This gives rise to noisy deconvoluted

curves. Many researchers have used filtering techniques to reduce the effect of noise, but this in turn may obscure physiological information. Furthermore, the deconvolution of liver activity/time curves gives rise to a complex curve where there is no obvious correlation between the type of blood flow in the liver and the deconvolved curve. It is the purpose of this chapter to develop an anatomic and physiologically based theory as a means of understanding hepatic blood flow from the deconvolved liver curve.

8.2 The Gastrointestinal Tract (GIT) and Portal System

The identification of the GIT residence time density is impractical using scintillation techniques [1]. Anatomical information suggests that the blood supply of the GIT consists of a large distribution of blood vessels. If the distribution of vessels is large

3 in equation 1.6) and the time constant of this system is τ_{gi}, then the GIT

idence time density is given by:

$$h_{gi} = \frac{t^2 e^{t/\tau_{gi}}}{2\tau_{gi}^3} \tag{8.1}$$

The mean transit time of the GIT can be determined from equation 3.6 ie.:

$$\mathrm{MTT}_{gi} = \int_0^\infty t \, \frac{t^2 e^{-t/\tau_{gi}}}{2\tau_{gi}^3} dt = 3\tau_{gi} \tag{8.2}$$

where

h_{gi} :- Gastrointestinal tract residence time density (RTD), s^{-1}

MTT_{gi} :- Mean transit time of the GIT

The portal vein has a large diameter and we expect the velocity of blood in the vessel to be relatively low. For this reason, a delay time for flow up the portal vein is introduced, τ_{pv}. Combining this information with equation 8.1, h_{spleen} from Chapter 6 and the information in Figure 7.1, h_{gs} is given as:

$$h_{gs} = \left[p h_{spleen} + (1-p) \frac{t^2 e^{t/\tau_{gi}}}{\tau_{gi}^3} \right] * \delta(t - \tau_{pv}) \tag{8.3}$$

[1] Other imaging techniques with better resolutions could be better determinants of the GIT residence time density.

where

p :- Fraction of portal blood that flows through the spleen as opposed to the gastrointestinal tract

The mean gastrointestinal/splenic transit time can be determined using equation 3.6:

$$\begin{aligned} \tau_{gs} &= \int_0^\infty t\, h_{gs}(t)dt \\ &= (\tau_{spleen} - 3\,\tau_{gi} - \tau_{pv})\,p + 3\,\tau_{gi} + \tau_{pv} \end{aligned} \tag{8.4}$$

and τ_{spleen} is given in equation 6.5.

8.3 Anatomy and Flow Physiology of the Liver

There are different structural interpretations of liver tissue. The actual choice of structural unit for flow modelling is unimportant, however the liver lobule representation has been chosen in this thesis to analyse the flow. A typical liver lobule is shown in Figure 8.1.

Venous blood from the portal vein breaks up into small portal venules. The portal blood carried in these vessels enters the liver lobule at the beginning of the liver sinusoid (Figure 8.1). The blood flows down the liver sinusoids which are passages lined with hepatocytes. We postulate that blood flows slowly down the sinusoid in order for a reasonable transfer of material between blood plasma and hepatocyte to occur. Experimental evidence suggests that this is the case. *Post mortem* studies in orally poisoned patients indicate a marginalisation of the hepatocytes along the liver sinusoid (WILLIAMS *et al.*, 1989). If the flow was fast, one would expect a uniform disease state of hepatocytes along the sinusoid. Blood at the end of the sinusoid enters the central vein which joins the sublobular vein. Many sublobular veins combine to form the hepatic vein.

Blood can also enter the liver lobule through an arterial supply. The hepatic artery branches off into hepatic arterioles. These enter the liver sinusoids and mix with the portal blood. The hepatic arterioles enter a sinusoid laterally all along from the origin of the sinusoid up to Zone III (RAPPAPORT & SCHNEIDERMAN, 1976; HASE & BRIM, 1966; MCCUSKEY, 1966) and it has been reported that hepatic arterial

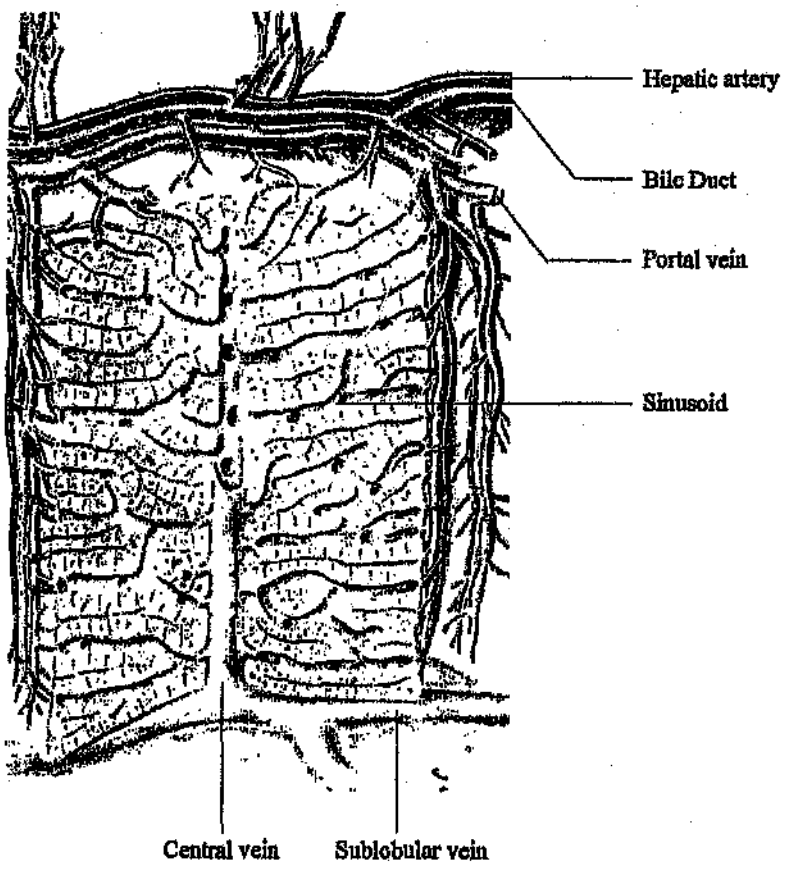

Figure 8.1: Anatomical Structure of the Liver Lobule. (Redrawn from Bourne G.: *An Introduction to Functional Histology*, Churchill, 1953

blood may enter the sinusoids even up to the central vein (ELIAS & PETTY, 1953). The blood then follows the same pathway as the venous blood described above.

The pressure in the hepatic artery is much greater than the pressure in the portal vein. The pressure where the venous and arterial blood mix must be equal. This is accomplished by muscular tissue which lines the hepatic arterioles. These muscles contract or relax to control hepatic arterial pressure (and thus flow) by changing vascular resistance. As the portal flowrate and pressure change, hepatic arterial blood supply can be manipulated (RAPPAPORT & SCHNEIDERMAN, 1976). RAPPAPORT and SCHNEIDERMAN (1976) visualised arteriolar sphincter like structures that permitted intermittent spurts of arterial blood to pass into the sinusoids of the liver. Thus blood in the hepatic artery may not flow unimpeded through the liver, and this in turn suggests a delay time for blood as it flows down the hepatic artery. For this reason $h_{ha}(t)$ in equation 7.10 is given by:

$$h_{ha}(t) = \delta(t - \tau_{ha}) \tag{8.5}$$

where

τ_{ha} :- Transit time of blood travelling down the hepatic artery (section 8.3), s

A flow representation of the liver lobule is given in Figure 8.2. The liver lobule is represented by venous blood in plug flow (Chapter 3) with lateral arterial flow along the sinusoid.

8.4 Development of the Model of the Liver

Equation 7.10 related the gastrointestinal tract RTD, the hepatic vascular RTD, h_{hvs}, and the measured aorta activity/time curve to measured hepatic activity/time curves. To determine a parametric form for $h_{hvs}(t)$, consider the anatomical representation of the liver lobule shown in Figure 8.1. Blood with tracer enters the liver through the hepatic artery and portal vein. These two vessels branch off into arterioles and venules respectively. The length distribution of arterioles and venules

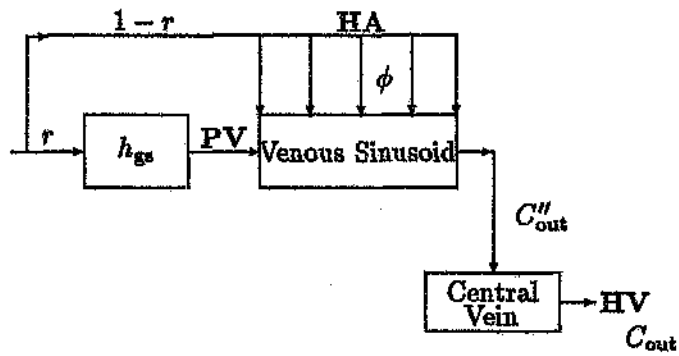

Figure 8.2: A Flow and Mixing Model of the Liver Lobule; **HA** Hepatic Artery, **PV** Portal Vein, **HV** Hepatic Vein, r is the fraction of blood that enters the liver from the portal vein, ϕ is the flow per unit volume of sinusoid that enters from the hepatic artery, h_{gs} represents the Residence Time Density of the splanchnic and gastrointestinal systems.

is assumed to be small. If the lengths differed substantially, each lobule would have an input that differed from the next by some time delay.

From Figure 8.1, the blood from the portal venules flows through the venous sinusoids into the central vein. Hepatic arterial blood also mixes with the portal blood supply along the length of the sinuses. We thus postulate from the anatomy that the hepatic flow into the sinusoids behaves like the maximum mixedness system of ZWIETERING (1959). Now the central veins of many lobules eventually join together to form hepatic venules and ultimately the hepatic vein. There is a distribution of lengths of the venous sinusoids, central veins and hepatic venules before they all combine to form the hepatic vein. The RTD of the length distributed system is given by the gamma density (THOMPSON *et al.*, 1964). We define $h_{cv}(t)$ to be this density with time constant, τ_{cv}. A value of $z = 2$ has thus been used in equation 1.6 [2]. Thus:

$$h_{cv}(t) = \frac{te^{-t/\tau cv}}{\tau_{cv}^2} \tag{8.6}$$

A blood flow and mixing representation of the liver lobule is shown in Figure 8.2.

It is now necessary to determine h_{hvs} for equation 7.10. We begin by assuming that the flowrate of portal blood to the hepatic sinusoid is Q' and that the hepatic arterial

[2] A physically measured density could be substituted

blood flow per unit length of lobule sinusoid is constant, ϕ. The mathematical statement is given as (Figure 7.1):

$$\frac{dQ}{dv} = \phi \tag{8.7}$$

$$Q(v=0) = Q' = rQ^o \tag{8.8}$$

We perform a transient mass balance of the tracer in the sinusoid with the sinusoid volume, V, and volume flowrate, $Q(v)$. The notation used is that associated with Figures 8.2 and 7.1. Consider equation 7.2 and some volume element dv:

$$QC|_v - QC|_{v+dv} + \phi dv C''_{\text{in}} = dv\frac{\partial C}{\partial t} \tag{8.9}$$

Dividing by dv and taking the $\lim_{dv\to 0}$ gives:

$$-\frac{\partial QC}{\partial v} + \phi C''_{\text{in}} = \frac{\partial C}{\partial t} \tag{8.10}$$

From equation 8.7 and equation 8.8:

$$Q(v) = Q' + \phi v \tag{8.11}$$

By substituting equation 8.11 into equation 8.10 we get:

$$-Q\frac{\partial C}{\partial v} - C\phi + \phi C''_{\text{in}} = \frac{\partial C}{\partial t} \tag{8.12}$$

The boundary and initial conditions for this equation are:

$$C(t=0,v) = 0 \tag{8.13}$$

$$C(t, v=0) = C'_{\text{in}} = C_{\text{in}} * h_{gs} \tag{8.14}$$

To solve the equation, we make the substitution:

$$y = ln(Q' + \phi v) \tag{8.15}$$

Thus:

$$\frac{dy}{y} = \frac{dv}{Q' + \phi v} \tag{8.16}$$

By substituting equations 7.8, 7.9, 8.5 and 8.16 into equation 8.12 and solving using the boundary and initial conditions of equation 8.13 and equation 8.14 we get (Appendix F.1):

$$h_{\mathrm{hve}}(t) = \left\{ \begin{array}{l} \frac{(1-r)e^{-t(1-r)/\tau_{\mathrm{sinus}}}}{\tau_{\mathrm{sinus}}} * \delta(t-\tau_{\mathrm{ha}}) - \\ \frac{r(1-r)e^{-t(1-r)/\tau_{\mathrm{sinus}}} * \delta(t-(\lceil \tau_{\mathrm{sinus}}/(1-r) \rceil ln(1/r)+\ldots,t+}{\tau_{\mathrm{sinus}}} \\ rh_{\mathrm{gs}} * \delta(t-\lceil \tau_{\mathrm{sinus}}/(1-r) \rceil ln(1/r)) \end{array} \right\} * \frac{te^{-t/\tau_{\mathrm{cv}}}}{\tau_{\mathrm{cv}}^2} \qquad (8.17)$$

where

τ_{sinus} :- Mean transit time of the hepatic sinusoid ($\frac{V_{\mathrm{sinus}}}{Q_e}$), s

The mean hepatic vascular system transit time can be determined using equation 3.6:

$$\begin{aligned} \tau_{\mathrm{hve}} &= \int_0^\infty t\, h_{\mathrm{hve}}(t)dt \\ &= (\tau_{\mathrm{ha}} + 2\tau_{\mathrm{cv}})(1-r) + \tau_{\mathrm{sinus}} + r(\tau_{\mathrm{gs}} + 2\tau_{\mathrm{cv}}) \end{aligned} \qquad (8.18)$$

Equations 8.17 and 8.18 can now be used in equations 7.10 and 7.16 respectively to examine the liver activity/time data. The LPDF can be obtained using equation 3.16.

8.5 Results

The liver activity/time data has been scaled by both the time at which the maximum in the data occurs (t_{max}) and the maximum value. The effect of this scaling is shown in Figure 8.3 and the modification of equations 7.10, 8.17 and 8.3 to analyse scaled data is discussed in Appendix J.1. This scaling technique did not appear to apply to the spleen or the renal parenchyma activity/time curves (Appendix G.1).

The simulation of the model described by equations 7.10, 8.17 and 8.3 was performed according to the methods outlined by Chapter 3, section 3.4.3.

The splenic parameter values obtained in Table 6.1 have been used in conjunction

with equations 7.10, 8.17 and 8.3 to fit the hepatic vascular model to the experimental liver activity/time data. A typical fit of the model is shown in Figure 8.4. The parameters determined from the minimisation of the sum of squares between the model and experimental data are presented in Tables 8.1 and 8.2. The parameter τ_{ha} is fixed from the deconvolution of the experimental liver and background corrected aorta activity/time (Chapter 4) curves as shown in Figure 8.5. The simulated model fit to all the subjects tabulated in Tables 8.1 and 8.2 is displayed in Appendix R.1. The χ^2 goodness-of-fit test (section 2.3.3) shows that the hepatic vascular model represents the distribution function of all the data displayed in Appendix R.1 ($P < 0.05$). The mean absolute correlation matrix of fitted parameters for the normal subjects is shown in Table 8.3.

The deconvolution of liver activity/time data with the background corrected aorta activity/time curve (Chapter 4) is compared to the model LPDF (equations 7.10 and 8.17) in Figure 8.5.

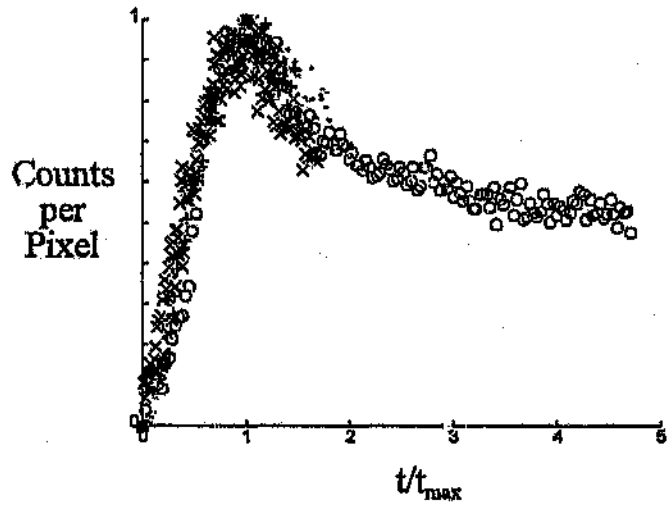

Figure 8.3: Eight liver activity/time curves scaled according to the maximum value and maximum time

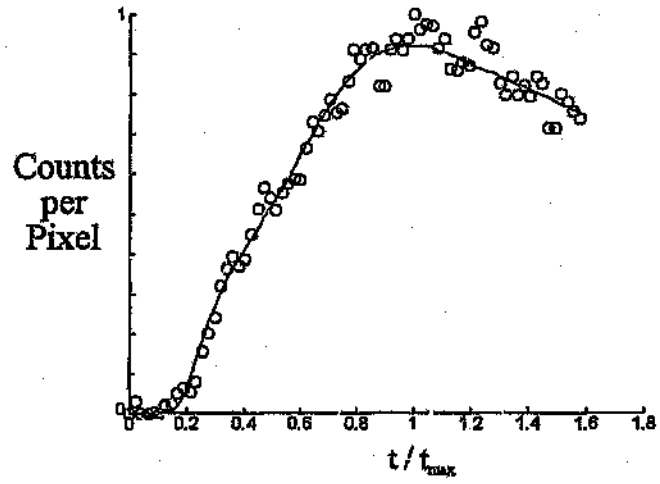

Figure 8.4: Typical fit of the liver model to the experimental liver activity/time curve. ——— Model, o Experimental data

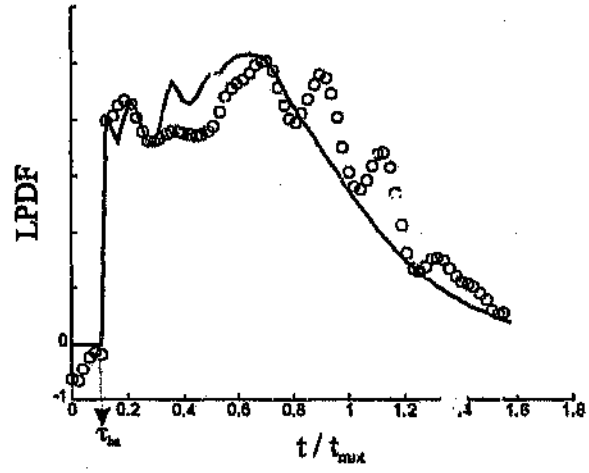

Figure 8.5: Model Liver Probability Density Function (LPDF) compared to the experimental LPDF (Deconvolution of liver activity/time data). ——— Model, o Filtered and deconvolved experimental data

Table 8.1: Liver time scaled parameter values for eight normal healthy volunteers and two diseased livers. $\tau_\phi = 1/\phi$ and is related to r and τ_{sinus} in Appendix F.1. *Significantly different from normal, $P < 0.05$. SEM represents the standard error of the mean.

	Fitted Parameters					Calculated Parameters					
Normal	r	p	τ_{sinus}	τ_{pv}	MTT_{gi}	τ_{ha}	τ_ϕ	τ_{gs}	τ_{hvs}	LMTT	t_{max} (s)
1	0.72	0.28	0.157	0.137	0.503	0.026	0.409	0.480	0.538	0.183	76
2	0.73	0.16	0.176	0.077	0.453	0.136	0.476	0.474	0.604	0.221	44
3	0.88	0.10	0.259	0.046	0.495	0.091	1.827	0.507	0.774	0.319	33
4	0.73	0.20	0.159	0.072	0.453	0.037	0.430	0.443	0.530	0.196	54
5	0.78	0.19	0.216	0.124	0.509	0.081	0.762	0.528	0.699	0.270	37
6	0.73	0.23	0.399	0.145	0.454	0.085	1.101	0.485	0.820	0.441	47
7	0.73	0.16	0.158	0.131	0.453	0.108	0.429	0.512	0.615	0.212	37
8	0.71	0.13	0.132	0.055	0.418	0.043	0.319	0.417	0.482	0.174	47
Mean	0.752	0.180	0.207	0.098	0.467	0.076	0.719	0.480	0.633	0.252	47.9
SEM	0.022	0.023	0.036	0.016	0.013	0.016	0.210	0.015	0.050	0.037	5.6
$P < 0.05$ (±)	0.109	0.113	0.175	0.079	0.064	0.076	1.030	0.073	0.243	0.181	27.2
% Variation	2.9	12.8	17.2	16.5	2.8	20.4	29.2	3.1	7.8	14.6	11.8

	Fitted Parameters					Calculated Parameters					
Pathology	r	p	τ_{sinus}	τ_{pv}	MTT_{gi}	τ_{ha}	τ_ϕ	τ_{gs}	τ_{hvs}	LMTT	t_{max} (s)
1	0.64*	0.20	0.231	0.061	0.691*	0.010	0.412	0.657*	0.703	0.279	42
2	0.40*	0.12	0.821*	0.059	1.117*	0.211	0.539	1.266*	1.581*	0.952*	15

Table 8.2: Liver unscaled parameter values for eight normal healthy volunteers and two diseased livers. $\tau_\phi = 1/\phi$ and is related to r and τ_{sinus} in Appendix F.1. *Significantly different from normal, $P < 0.05$. SEM represents the standard error of the mean.

	Fitted Parameters					Calculated Parameters				
Normal	r	p	τ_{sinus} (s)	τ_{pv} (s)	MTT_{gi} (s)	τ_{ha} (s)	τ_ϕ (s)	τ_{gs} (s)	τ_{hvs} (s)	LMTT (s)
1	0.72	0.28	11.9	10.4	38.2	2.0	31.1	36.5	40.9	13.9
2	0.73	0.16	7.7	3.4	19.9	6.0	21.0	20.8	26.6	9.7
3	0.88	0.10	8.5	1.5	16.3	3.0	60.3	16.7	25.6	10.5
4	0.73	0.20	8.6	3.9	24.4	2.0	23.2	23.9	28.6	10.6
5	0.78	0.19	8.0	4.6	18.8	3.0	28.2	19.5	25.9	10.0
6	0.73	0.23	18.7	6.8	21.3	4.0	51.7	22.8	38.5	20.7
7	0.73	0.16	5.9	4.8	16.7	4.0	15.9	18.9	22.8	7.9
8	0.71	0.13	6.2	2.6	19.6	2.0	15.0	19.6	22.7	8.2
Mean	0.752	0.180	9.44	4.74	21.93	3.25	30.80	22.36	28.93	11.44
SEM	0.022	0.023	1.71	1.13	2.880	0.567	6.798	2.52	2.84	1.71
$P < 0.05$ (±)	0.109	0.113	8.37	5.53	14.11	2.78	33.31	12.29	13.91	8.37
% Variation	2.9	12.8	18.1	23.8	13.1	17.5	22.1	11.2	9.8	14.9

	Fitted Parameters					Calculated Parameters				
Pathology	r	p	τ_{sinus} (s)	τ_{pv} (s)	MTT_{gi} (s)	τ_{ha} (s)	τ_ϕ (s)	τ_{gs} (s)	τ_{hvs} (s)	LMTT (s)
1	0.64*	0.20	9.7	2.6	29.0	0.4	17.3	27.6	29.5	11.7
2	0.40*	0.12	12.5	0.89	17.0	3.2	8.2	19.2	24.0	14.5

Table 8.3: The mean absolute correlation matrix of the five independent fitted model parameters τ_{sinus}, τ_{pv}, τ, p, and MTT_{gi} respectively, for the values in Table 8.1, together with the corresponding standard error of the mean for each matrix component r_{ij}.

1.000 ± 0.000	0.756 ± 0.079	0.696 ± 0.116	0.460 ± 0.127	0.696 ± 0.104
0.756 ± 0.079	1.000 ± 0.000	0.550 ± 0.122	0.629 ± 0.137	0.582 ± 0.140
0.696 ± 0.116	0.550 ± 0.122	1.000 ± 0.000	0.496 ± 0.110	0.768 ± 0.086
0.460 ± 0.127	0.629 ± 0.137	0.496 ± 0.110	1.000 ± 0.000	0.552 ± 0.120
0.696 ± 0.104	0.582 ± 0.140	0.768 ± 0.086	0.552 ± 0.120	1.000 ± 0.000

8.6 Discussion

For the purposes of the discussion, the fitted hepatic vascular parameters and some of the important calculated parameters listed in Table 8.1 are graphically displayed in Figure 8.6.

8.6.1 Normal Subjects

Figures 8.4 and 8.5 show a reasonable correlation between the parametric model and the experimental data. The discrepancies between the model and the deconvolved curve in Figure 8.5 are probably due to the *Gibbs phenomenon* of the FFT (the discontinuity in the model curve is evident at $t = \tau_{ha}$) and the poisson noise in the experimental data since the uncertainty in aorta background has largely been accounted for using the techniques in Chapter 4.

Thus the flow and mixing in the liver and portal system appears to be adequately described by equations 7.10, 8.17 and 8.3.

The variation between individuals for the parameters displayed in Tables 8.1 and 8.2 is likely to represent the normal population variation.

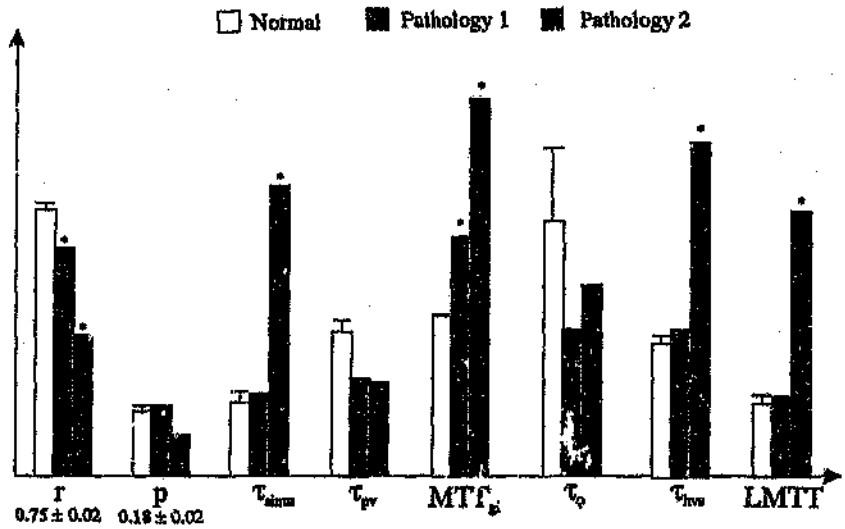

Figure 8.6: Some of the important hepatic parameters tabulated in Table 8.1. *Significantly different from normal, $P < 0.05$. Error bars indicate the standard error of the mean for the normal subjects. The other results are for the patients with known pathologies.

As discussed previously, the correlation matrix is a measure of a model's sensitivity to parameter variation and a measure of the association between variables. The correlation matrix of fitted parameters in Table 8.3 indicates that the values in Tables 8.1 and 8.2 are relatively accurate since all of the off diagonal elements do not exceed 0.9 (BECK & ARNOLD, 1977; Appendix I.1). This reinforces the likelihood that equations 8.17 and 8.3 adequately describe the hepatic vascular system.

Upon closer examination of the correlation matrix element $r_{12} = 0.756$, it is clear that there is some degree of correlation between the mean transit time of the hepatic sinusoid, τ_{sinus} ($\frac{V_{sinus}}{Q^{\bar{v}}}$), and the delay time for blood flow up the portal vein, τ_{pv}. The correlation between these parameters is visible if one examines the third and fourth columns of Table 8.1; As τ_{sinus} increases τ_{pv} increases and *vice versa*. If one examines the model structure it is clearly evident why these parameters are likely to be related. The mean transit time of the hepatic vascular system, τ_{hvs}, is the sum of the mean transit time through the hepatic arterial and portal components of the hepatic vascular system. This parameter thus includes a linear combination of these

two correlated parameters. Thus while τ_{sinus} and τ_{pv} may change, τ_{hvs} is likely to be more accurate. The data in Table 8.1 reflects this effect where the % variation of τ_{hvs} within the normal population is more than half that of τ_{sinus} and τ_{pv}. This indicates that τ_{hvs} is likely to be a relatively accurate parameter. Although there is less confidence in τ_{sinus} and τ_{hvs} than in τ_{hvs}, the values of the τ_{sinus} are consistently larger than the values of τ_{pv}. Thus while τ_{sinus} and τ_{pv} are useful parameters which have an anatomical significance, these parameters should be used in conjunction with τ_{hvs} for the diagnosis of pathology using the techniques discussed in this thesis.

There is some correlation between the fraction of blood that enters the liver from the portal vein, r, and the mean transit time of the gastrointestinal tract, MTT_{gi} ($r_{35} = 0.768$). The complexity of the model precludes the identification of the relationship between these parameters. As will be seen in the next subsection, as portal obstruction occurs, r decreases and MTT_{gi} increases. r has a direct effect on the modelling of early part of the experimental activity/time curve when most of the blood in the liver is derived from the hepatic arterial blood supply. MTT_{gi} however, affects the time at which the portal blood arrives at the liver and therefore affects the modelling of the latter part of the experimental data. The mean transit time of the hepatic vascular system, τ_{hvs}, is the sum of the mean transit time through the hepatic arterial and portal components of the hepatic vascular system. This parameter thus includes a linear combination of these parameters. This is further evidence that τ_{hvs} is likely to be an important diagnostic parameter that is more accurate due to the correlation between the parameters. The % variation of r and MTT_{gi} within the normal population is small and this indicates that while these parameter are to some extent correlated, they are likely to be relatively accurate diagnostic parameters.

The ideal objective of the mathematical model of the hepatic vascular system is to derive physiological parameter values from the experimental data. In order to decide whether the model described above satisfies this requirement, we examine the normal values of the fraction of blood that flows into the liver through the portal vein, r, the fraction of portal blood that flows through the spleen as opposed to the gastrointestinal tract, p, and the liver mean transit time, $LMTT$ tabulated in Table 8.2. The other parameter values tabulated in Table 8.2 have not traditionally

been measured and reported in the literature.

The fraction of blood that enters the liver from the portal vein, r, describes the relationship between the portal and hepatic arterial blood supplies to the liver. The value of r, from Table 8.1 agrees with experimental measurements reported in the literature (GUYTON, 1986 :- $r = 0.76$; PAULSEN & KLINTMALM, 1992 :- $r = 0.71 \pm 0.02$; DOI *et al.*, 1988 :- $r = 0.74 \pm 0.02$). Thus the model of the hepatic vascular system described in this thesis appears to be physiological meaningful. This requirement of the model allows one to suggest that any significant deviation from the normal parameter values is likely to indicate hepatic vascular pathology. The development of the mathematical model of the hepatic vascular system based on anatomical information has thus yielded a physiological parameter value from the experimental data.

The fraction of portal blood that flows through the spleen as opposed to the gastrointestinal tract, p, from Table 8.1 also agrees with experimental measurements reported in the literature (GUYTON, 1986 :- $p = 0.20$). Thus the development of the mathematical model of the hepatic vascular system based on anatomical information has yielded another physiological parameter value from the experimental data. Obstructions or enlargements of the splenic or gastrointestinal systems are thus likely to manifest themselves in a change in this parameter.

The liver mean transit time, LMTT, from Table 8.2 is also in agreement with experimental measurements reported in the literature (GUYTON, 1986 :- LMTT= 12.4s (Volume=300ml, Volumetric Flowrate=1450ml/min)).

The above physiological parameters namely r, p and LMTT provide convincing evidence that the hepatic vascular model based on anatomy is theoretically sound. The above analysis indicates that both flow fraction and transit time parameters have physiological significance. This suggests that r, p and LMMT are likely to have important diagnostic and prognostic implications for the the management of patients with portal pathology. An important component of the hepatic vascular system is a satisfactory model of the spleen. The physiological significance of the above parameter values indirectly implies a satisfactory physiological description of

the spleen.

8.6.2 Hepatic Vascular Pathology

Figure 8.3 and Table 8.1 indicate the importance of scaling liver activity/time curves using t_{max}. The unscaled mean transit times for the portal hypertensives in Table 8.2 do not differ significantly from the normal values. This is in stark contrast to the mean transit times of portal hypertensives in Table 8.1. It thus appears that the identification of hepatic abnormalities, based on transit time analysis, can only be performed using scaled hepatic activity/time curves. Thus the comparison of normal and portal hypertensive transit times has been limited to the values in Table 8.1. Transit times are related to the flowrate and volume of the system by equation 3.6. In fact a transit time can be thought of as the reciprocal of the flowrate per unit volume of the system. This implies that transit times associated with the liver might be related to another physical parameter (eg. weight). An attempt was made to try and correlate t_{max} with weight and/or sex. There appeared to be no obvious relationship and the significance of this parameter as a physiological or pathological index remains obscure. Chapter 6 showed that this scaling relationship did not hold true for the spleen. An explanation for this scaling therefore lies elsewhere. The identification of such an explanation or the determination of other relationships have not been addressed in this thesis and provides an interesting research topic for further investigation. The scaling of data for the identification of hepatic pathology using tracer studies has not previously been addressed in the literature.

The fraction of total hepatic blood flow through the portal vein, r, is significantly decreased in both portal hypertensives ($P < 0.05$). The gastrointestinal tract mean transit time, τ_{gi}, in Table 8.1 is significantly elevated in both portal hypertensive subjects ($P < 0.05$) and the fraction of blood flow in the portal vein that flowed through the spleen, p, is not significantly different. Also, the hepatic vascular mean transit time, τ_{hvs}, is significantly elevated in the second portal hypertensive subject ($P < 0.05$). These results suggest that any obstruction is likely to be hepatic in nature since the ratio of splenic blood flow to gastrointestinal blood flow is unaltered while portal flow is reduced. This agrees with the mechanical obstruction of blood

flow through the liver by fibrosis, thrombosis and nodular regeneration associated with portal hypertension (LAMONT & ISSELBACHER, 1977).

The hepatic arterial flowrate per unit volume, $\phi = \frac{1}{\tau_\phi}$, is increased (although not very significantly) in the portal hypertensive subjects. This suggests that while the portal flow decreases, hepatic arterial flow may increase. These results concur with a number of authors who have reported small increases in hepatic arterial flow with decreased portal flow (ACKROYD *et al.*, 1966; PRICE *et al.*, 1965; DOI *et al.*, 1988).

The other parameter values for the first portal hypertensive, namely τ_{sinus}, τ_{ha} and $LMTT$ in Table 8.1 are not significantly different from the normal values. This indicates that the first portal hypertensive subject has a developing pathology which supports the evidence indicated by the spleen parameter values discussed in Chapter 6.

The parameters values, τ_{sinus}, τ_{ha} and $LMTT$ in Table 8.1 for the second portal hypertensive are all significantly different from the normal values ($P < 0.05$). This indicates advanced portal hypertension.

The portal vein delay time, τ_{pv} is not significantly different in either portal hypertensive. This may indicate that this parameter is not a sensitive measure of organ pathology.

8.7 Conclusions

A hepatic vascular model has been developed in an attempt to quantify liver physiology from imaging data. The model has been applied to a both normal subjects and organ pathologies. The model parameters appear to describe normal physiology and pathophysiology accurately. In particular the parameters $r = 0.75 \pm 0.02$, $p = 0.18 \pm 0.02$ and $LMTT = 13.4 \pm 1.7s$ for normal subjects correspond to *in vivo* measurements furnished in the literature. The physiological significance of r, p and LMTT provide convincing evidence that the hepatic vascular model based on anatomy is theoretically sound. This in turn implies that the model of the spleen developed in Chapter 6 is likely to have physiological significance.

The trends of parameter ϕ in portal hypertension agree with experimental values presented in the literature. The transit time parameters and flow fraction parameter values indicate that the sinusoidal obstruction associated with portal hypertension has reduced the total flow through the liver. These results are consistent with results obtained in the previous chapter. A detailed clinical research program is however required to validate the use of the model parameters as clinical indices.

Chapter 9

Conclusions

9.1 Deconvolution and Imaged Single Input Organs

In Chapter 3, the relationship between the aorta and organ activity/time measurement was investigated for single input organs. Equation 3.16 was derived and shown to be generally applicable for any imaging experiment of a single input organ in a recirculating system. Chapter 3 also developed the relationship between input-output and input-content measurements of a system.

The noise generating nature of deconvolution was addressed and it was concluded that a parametric model of an organ be used, without filtering, to determine the organ Internal Age Density. The Prediction Error Identification Method (PEM) was chosen to compare experimental data with that predicted by mathematical models.

9.2 Identification of an Aorta Background for Organ Scintigraphic Studies

In Chapter 4, the negative artifact seen in many organ deconvolution studies was addressed. It was concluded that this negative artifact was probably due to background tissue activity present in the aorta measurement. In particular, scintigraphic imaging techniques measure more material as the aorta than is actually present within

this artery. It was shown that no background tissue region could be chosen that represents the tissue anterior and posterior of the imaged aorta since any background tissue is vascular in nature and thus contains small arteries which have similar characteristics to the aorta. Two theoretical models of tissue background activity were developed which removed this negative component. This analysis appears to explain a discrepancy which has appeared in the literature for some time.

9.3 An Anatomical and Physiological Model of the Kidney

In Chapter 5 a parametric model of the renal retention function was developed. This parametric model was shown to be less perturbed by noise artifacts which are generally present in deconvolved data. Thus the parametric model provided a more accurate estimation of clinical indices than those discussed in the literature. The parametric model of the renal parenchyma appeared to consistently describe both normal and pathophysiology. Normal parameter values such as the filtration fraction, f, were shown to correspond to independent measurements reported in the literature. The filtration fraction for normal subjects was found to be 0.217 ± 0.017

The renal blood transit time parameter, τ_b, was shown to be a potentially useful clinical index for the determination of renal vascular disease. Further clinical research is however required to validate the use of the model parameters as clinical indices. In addition, further clinical work is required to remove the contribution of renal background tissue inherent in the renogram.

9.4 An Anatomical and Physiological Model of the Spleen

In Chapter 6 a parametric model of the spleen was developed. The parametric model of the spleen appeared to adequately describe both normal and abnormal physiologies. The spleen parameter values for portal hypertensives concurred with

the degree of splenomegaly observed clinically. The spleen mean transit time τ_{spleen} was shown to be a sensitive clinical measure of spleen pathology. It was thus shown that the parametric model could facilitate in the diagnosis of splenic disorders, where flow is affected.

9.5 Deconvolution and Imaged Multiple Input Organs

In Chapter 7 the relationship between the aorta and organ activity/time measurement was investigated for multiple input organs, in particular the liver. This chapter provided the first mathematical description for the deconvolution of imaged multiple input organs. It was shown that deconvolution of liver activity/time curves give rise to a complex combination of splenic, gastrointestinal and liver blood flow dependencies. Unlike the single input systems, it was shown that there is no obvious correlation between the type of mixing and the effect it has on the liver deconvolved curve. Furthermore, the only direct information that one can glean from such a curve, is the time at which tracer first appears in the liver. A conclusion of this chapter was that a parametric flow model of the hepatic vascular system was desirable to explain and quantify the deconvolved hepatic activity/time curve.

9.6 An Anatomical and Physiological Model of the Liver

In Chapter 8 a parametric model of the hepatic vascular system was developed. The parametric model of the hepatic vascular system appeared to adequately describe both normal and abnormal physiologies. A number of parameters were found to correspond to *in vivo* measurements reported in the literature. In particular the portal flow fraction was determined as 0.752 ± 0.022, the splenic blood flow fraction was determined as 0.180 ± 0.023 and the liver mean transit time was determined as 11.4 ± 1.7 seconds. It was concluded that the model was therefore an adequate flow description of the hepatic vascular system.

It was shown that the scaling of liver activity/time curves by both the time at which the maximum in the curve occurred, t_{max}, and the maximum value was fundamental to the identification of organ pathologies. The parameters r, MTT_{gi}, τ_{hvs}, τ_{gs}, LMTT and τ_{ϕ} were shown to be sensitive and consistent measures of liver pathology when the liver data was scaled appropriately.

9.7 Conclusion

The physics of imaging radioactive tracers such as ^{99m}Tc-DTPA has been identified and related to residence time density theory (RTD). This theory permits the identification of parameters that describe organ physiology from the deconvolution of aorta and organ activity/time curves. Residence time density theory places limits on the behaviour of the deconvolved curves. These limits are related to the properties of probability density functions and conservation of mass. The RTD theory has been applied to three major abdominal organs; the Kidney, the Spleen and the Liver. In all three cases residence time density models have been developed in an attempt to quantify the organ physiology more accurately. These models have been applied to a reasonably large sample or normal subjects to determine normal parameter values. The models have also been applied to a small number of organ pathologies. The residence time density models appear to clearly identify the organ pathologies and discriminate between the effect of these pathologies on the organ physiology.

In conclusion, parametric deconvolution of the kidney, liver and spleen has been shown to be a robust technique which provides physiological information not provided by the conventional non-parametric methods. Further clinical research is however required to validate the use of the model parameters as clinical indices.

Appendix A

A.1 The Internal Age Density and Imaged Single-Input Organs

In this appendix, the relationship between an imaged single input organ and I(t) is investigated. To do this we begin with Equation 3.15:

$$QC_{\text{in}} - QC_{\text{out}} = \frac{d}{dt}\left\{\int_0^V C(t,v)dv\right\} \tag{A.1}$$

Taking Laplace transforms with initial condition $C(v, t \leq 0) = 0$ we get:

$$\bar{C}_{\text{in}}(s) - \bar{C}_{\text{out}}(s) = \frac{s}{Q}\int_0^V \bar{C}(s,v)dv \tag{A.2}$$

where

$\bar{C}_{\text{in}}(s)$:- Laplace transform of $C_{\text{in}}(t)$

$\bar{C}_{\text{out}}(s)$:- Laplace transform of $C_{\text{out}}(t)$

Now by mass balance Equation 3.12 gives:

$$C_{\text{out}}(t) = \int_0^t C_{\text{in}}(t-t')h(t')dt' = C_{\text{in}} * h \tag{A.3}$$

or in the Laplace transform domain

$$\bar{C}_{\text{out}}(s) = \bar{C}_{\text{in}}(s)\bar{h}(s) \tag{A.4}$$

Substituting Equation A.4 into Equation A.2 gives:

$$\bar{h}(s) = 1 - \frac{s\int_0^V \bar{C}(s,v)dv}{Q\bar{C}_{\text{in}}(s)} \tag{A.5}$$

But from Equation 3.8:

$$I(t) = \frac{H(t)}{\tau} = \frac{1 - \int_0^t h(t)dt}{\tau} \tag{A.6}$$

By taking Laplace transforms and rearranging this equation we get:

$$\bar{h}(s) = 1 - \tau s\bar{I}(s) = 1 - \frac{Vs}{Q}\bar{I}(s) \tag{A.7}$$

Substituting Equation A.7 into Equation A.5 gives:

$$\tau\bar{I}(s) = \frac{\int_0^V \bar{C}(s,v)dv}{Q\bar{C}_{\text{in}}(s)} \tag{A.8}$$

From Equation 3.6, $\tau = \frac{V}{Q}$ and substituting into Equation A.8 and taking inverse Laplace transforms we finally get:

$$C_{\text{in}} * I(t) = \frac{\int_0^V C(t,v)dv}{V} \tag{A.9}$$

Or in words, the convolution of the internal age density with the inlet concentration is equal to the volume averaged concentration.

If $h(t) \geq 0$ and $\int_0^\infty h(t)dt = 1$ (LEVENSPIEL, 1972) then from Equation 3.8, $1 - \int_0^\infty h(t)dt \geq 0$ and thus $I(t) \geq 0$. Also as $t \to \infty$, $\int_0^\infty h(t)dt \to 1$ and $1 - \int_0^\infty h(t)dt \to 0$. Thus $\lim_{t\to\infty} I(t) = 0$. We can also consider the integral of I(t), $\int_0^\infty I(t)dt$. To do this we begin by integrating Equation 3.8 to give:

$$\int_0^\infty I(t)dt = \int_0^\infty \frac{H(t)}{\tau}dt \tag{A.10}$$

From ZWIETERING (1959), $\int_0^\infty [H(t)]dt = \tau$. If we substitute this result into Equation A.10 then $\int_0^\infty I(t)dt = 1$

Appendix B

B.1 Attenuation and Concentration

Let:

$C(x,y,z,t)$ = activity concentration within an organ, MBq/ml

S_o = gamma camera sensitivity, cps/MBq

μ = gamma ray attenuation coefficient, m^{-1}

$D(x,y,t)$ = image count density, cps/m^2

Then,

$$D(x,y,t) = \int S_o e^{-\mu z} C(x,y,z,t) dz \tag{B.1}$$

and the total count rate from a region of interest is given by:

$$\text{Organ Count Rate} = \int\int D(x,y,t) dx dy \tag{B.2}$$

$$= \int\int\int S_o e^{-\mu z} C(x,y,z,t) dx dy dz \tag{B.3}$$

$$= S_o e^{-\mu d} \int_0^V C(v,t) dv \tag{B.4}$$

where

d :- Mean depth of the kidney and attenuation is assumed to be approximately constant throughout the imaged organ

The organ count rate is thus directly proportional to the total amount of tracer within the organ. The organ count rate is typically normalised with respect to the region of interest area, A, and thus:

$$\text{Area Normalised Organ Count Rate} = S_o e^{-\mu d} \frac{\int_0^V C(v,t) dv}{A} \tag{B.5}$$

$$= \frac{S_o d e^{-\mu d}}{d} \frac{\int_0^V C(v,t)dv}{V} \qquad \text{(B.6)}$$

Thus the Area Normalised Organ Count Rate is proportional to the average concentration within the organ. This normalised organ count rate is the same as the average image count density, $\overline{D(x,y,t)}$.

Appendix C

C.1 Flow in a Length Distributed System

Consider Figure C.1. If one has n parallel plug flow capillaries then the fraction of particles that spend some mean residence time, τ_i, or less in the system is given by:

$$H(\tau_i) = \int_0^t \sum_{i=1}^{n} q_i \delta(t - \tau_i) dt \tag{C.1}$$

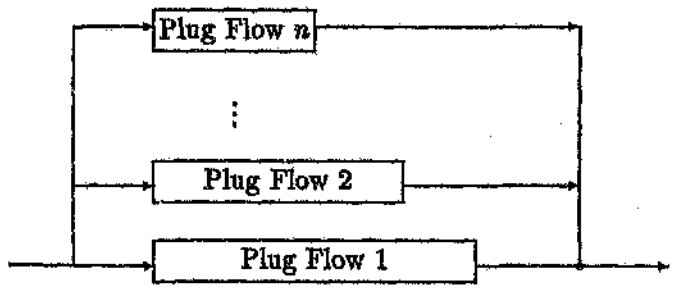

Figure C.1: Parallel Plug Flow System

where

q_i :- Fraction of material flowing through plug flow i

$\delta(t)$:- Dirac's delta (LEVENSPIEL, 1972))

τ_i :- Transit time associated with plug flow i

Since $\int_0^\infty \delta(t - \tau_i) dt = 1$ we find that:

$$H(\infty) = \sum_{i=1}^{n} q_i = 1 \tag{C.2}$$

Each q_i is associated with some length $\tau_i = \frac{A}{Q} L_i$, where Q is the flowrate in the system and A is the cross sectional area of a capillary which is assumed to be approximately constant for most capillaries (GUYTON, 1986). If the flowrate, Q, through each plug flow is approximately the same ($q_i = \frac{Q}{n_{tot}}$), and the cross sectional area of each plug flow system is similar then the fraction of molecules that spent mean residence time τ_i in the system, $H(\tau_i)$, depends on the number of tubes with length L_i. A density function, $g(L)$, can then be defined as the length distribution of capillaries and is analogous to the RTD of such a system.

Appendix D

D.1 Descending Loop of Henle

Consider the side stream system shown in Figure D.1. This figure depicts movement of water in the descending loop of Henle where although the tracer remains in the tubule, the carrier water medium is actively transported out of the tubule. We assume a constant net flow out the tube per unit volume, a, and consider a mass balance over volume element v to $v + \Delta v$.

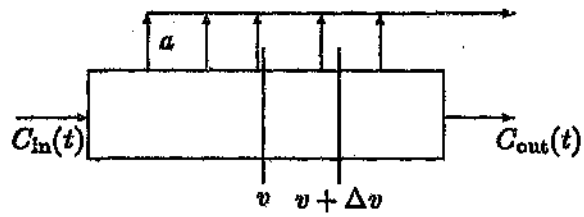

Figure D.1: Side stream system representing tracer in the loop of Henle and movement of water out of the tubule

$$\text{Mass In of Tracer} - \text{Mass Out of Tracer} = \text{Accumulated Mass of Tracer} \quad \text{(D.1)}$$

so

$$QC\,|_v - QC\,|_{v+\Delta v} = \Delta v \frac{\partial C}{\partial t} \quad \text{(D.2)}$$

Dividing and taking limits as $\Delta v \rightarrow 0$ gives:

$$-\frac{\partial QC}{\partial v} = \frac{\partial C}{\partial t} \tag{D.3}$$

Similarly if the density of the fluid, ρ, is constant then we can perform a flowrate balance which gives:

$$\frac{\partial Q}{\partial v} = -a \tag{D.4}$$

If we fix the initial and boundary conditions as:

- $C(t, v = 0) = C_{\text{in}}(t)$
- $C(t, v = V) = C_{\text{out}}(t)$
- $C(t = 0, v) = 0$
- $Q(v = 0) = Q^{Ho}$

and solving Equations D.3 and D.4 simultaneously with the initial and boundary conditions, we find:

$$C_{\text{out}}(t) = C_{\text{in}}(t) * \frac{Q^o}{Q^o - aV}\delta(t - \frac{ln[\frac{Q^o}{Q^o - aV}]}{a}) \tag{D.5}$$

Note that this is not the residence time density of water molecules in the tube because this implicitly assumes that the tracer flows with the carrying fluid. Mass balance is however conserved for the tracer in the tube because $Q^{Ho}C_{\text{in}} = (Q^{Ho} - aV)C_{\text{out}}$. We also note that the tracer is delayed by some time $\frac{1}{a}$ times the dimensionless time scaling factor $ln[\frac{Q^{Ho}}{Q^{Ho} - aV}]$. Thus the tracer is only delayed and no mixing of this tracer occurs. Should a be described by a distribution of reabsorption rates across a number of nephrons, this would manifest itself in an apparent change in the length distribution of nephrons. The RTD of the descending loop of Henle can still be defined in terms of some other constant flowing medium (RTD is still defined) and is thus given by:

$$h_{LH}(t) = C_{\text{in}}(t) * \delta(t - \tau_{LH}) \tag{D.6}$$

where

h_{LH} :- Loop of Henle residence time density (RTD), s^{-1}

τ_{LH} :- Loop of Henle mean transit time

τ_{LH} is not the mean residence time of the water in the descending loop but we note that as τ_{LH} becomes greater, the flowrate per unit volume, a must get larger. This may be a useful clinical parameter for diagnosis.

Appendix E

E.1 Dynamic Imaging of the Liver

Equation 7.4 gives:

$$Q^* C''_{\text{in}} + Q' C'_{\text{in}} - Q^o C_{\text{out}} = \frac{d}{dt}\left\{\int_0^V C(t,v)dv\right\} \tag{E.1}$$

and

$$Q^* = (1-r)Q^o \tag{E.2}$$

$$Q' = rQ^o \tag{E.3}$$

$$C'_{\text{in}} = C_{\text{in}} * h_{\text{gs}}(t) \tag{E.4}$$

$$C''_{\text{in}} = C_{\text{in}} * h_{\text{ha}} \tag{E.5}$$

$$C_{\text{out}} = C_{\text{in}} * h_{\text{hvs}}(t) \tag{E.6}$$

where

$h_{\text{hvs}}(t)$:- Residence time density of the hepatic vascular system in Figure 7.1 (hepatic artery, spleen and gastrointestinal tract)

C_{in} :- Input tracer concentration of the aorta

C_{out} :- Output tracer concentration in the hepatic vein

$h_{\text{ha}}(t)$:- RTD of the hepatic artery (section 8.3), s^{-1}

$*$:- Denotes convolution

Taking the laplace transform of equations E.1, E.4, E.5 and E.6, gives:

$$Q^* \bar{C}''_{\text{in}} + Q' \bar{C}'_{\text{in}} - Q^o \bar{C}_{\text{out}} = s\int_0^V \bar{C}(s,v)dv \tag{E.7}$$

$$\bar{C}'_{\text{in}} = \bar{C}_{\text{in}} \bar{h}_{\text{gs}} \tag{E.8}$$

$$\bar{C}''_{\text{in}} = \bar{C}_{\text{in}}\bar{h}_{\text{ha}}(s) \tag{E.9}$$

$$\bar{C}_{\text{out}} = \bar{C}_{\text{in}}\bar{h}_{\text{hvs}}(s) \tag{E.10}$$

If we substitute equations E.2, E.3, E.8, E.9 and E.10 into equation E.7 we get:

$$\{[(1-r)\bar{h}_{\text{ha}}(s) + r\bar{h}_{\text{gs}}] - \bar{h}_{\text{hvs}}\}\,\bar{C}_{\text{in}} = \frac{s}{Q^o}\int_0^V \bar{C}(s,v)dv \tag{E.11}$$

We define a mean residence time of the liver as the volume of the liver divided by the total volumetric flowrate into the liver ie.:

$$\tau_{\text{liver}} = \frac{V_{\text{liver}}}{Q^o} \tag{E.12}$$

If we substitute equation E.12 into equation E.11 for Q^o then:

$$\frac{\{[(1-r)\bar{h}_{\text{ha}}(s) + r\bar{h}_{\text{gs}}] - \bar{h}_{\text{hvs}}\}}{\tau_{\text{liver}}s}\bar{C}_{\text{in}} = \frac{\int_0^V \bar{C}(s,v)dv}{V_{\text{liver}}} \tag{E.13}$$

Taking inverse laplace transforms finally gives:

$$\left\{\frac{\int_0^t [(1-r)h_{\text{ha}} + rh_{\text{gs}} - h_{\text{hvs}}]\,dt}{\tau_{\text{liver}}}\right\} * C_{\text{in}} = \frac{\int_0^V C(t,v)dv}{V_{\text{liver}}} \tag{E.14}$$

The deconvolution of the liver activity/time curve with the aorta activity/time curve thus gives:

$$\frac{\int_0^t [(1-r)h_{\text{ha}} + rh_{\text{gs}} - h_{\text{hvs}}]\,dt}{\tau_{\text{liver}}} \tag{E.15}$$

For simplicity we define, $F(t) = 1 - H(t)$, $F(0) = 0$, $F(\infty) = 1$. $F(t)$ is the probability of a tracer particle spending time t or less in a system. Thus as $t \to 0$ equation E.15 gives:

$$\lim_{t\to 0}\left\{\frac{\int_0^t [(1-r)h_{\text{ha}} + rh_{\text{gs}} - h_{\text{hvs}}]\,dt}{\tau_{\text{liver}}}\right\} = 0 \tag{E.16}$$

and using the integral definitions listed above, as $t \to \infty$,

$$\lim_{t\to \infty}\left\{\frac{\int_0^t [(1-r)h_{\text{ha}} + rh_{\text{gs}} - h_{\text{hvs}}]\,dt}{\tau_{\text{liver}}}\right\} = 0 \tag{E.17}$$

The convolution of two positive functions is always positive. Since h_{gs}, h_{hvs} and h_{ha} are positive, equation E.15 is positive when $0 \leq r \leq 1$. r is a fraction and this condition is always satisfied, thus:

$$\frac{\int_0^t [(1-r)h_{\text{ha}} + rh_{\text{gs}} - h_{\text{hvs}}]\,dt}{\tau_{\text{liver}}} \geq 0 \tag{E.18}$$

If equations E.16 E.17 and E.18 hold, then the infinite integral should also be defined. To show this we integrate equation E.18 and use the information that $\int_0^\infty F(t)dt = \tau$ (LEVENSPIEL, 1972). Integrating equation E.18 gives:

$$\int_0^\infty \frac{\int_0^{t'} [(1-\tau)h_{\text{ha}} + \tau h_{\text{gs}} - h_{\text{hvs}}]\, dt}{\tau_{\text{liver}}} dt' \tag{E.19}$$

$$= \frac{\int_0^\infty [(1-\tau)F_{\text{ha}} + \tau F_{\text{gs}} - F_{\text{hvs}}]\, dt'}{\tau_{\text{liver}}} \tag{E.20}$$

$$= \frac{\int_0^\infty [(1-\tau)F_{\text{ha}} + \tau F_{\text{gs}} + \tau - \tau - F_{\text{hvs}} + 1 - 1]\, dt'}{\tau_{\text{liver}}} \tag{E.21}$$

$$= \frac{\int_0^\infty [(1-\tau)(F_{\text{ha}} - 1) - \tau(1 - F_{\text{gs}}) + (1 - F_{\text{hvs}})]\, dt'}{\tau_{\text{liver}}} \tag{E.22}$$

$$= \frac{(\tau_{\text{hvs}} - \tau_{\text{ha}}) - \tau(\tau_{\text{gs}} - \tau_{\text{ha}})}{\tau_{\text{liver}}} \tag{E.23}$$

The numerator of equation E.23 is equal to τ_{liver} and thus (equations 8.4 and 8.18):

$$\int_0^\infty \frac{\int_0^{t'} [(1-\tau)h_{\text{ha}} + \tau h_{\text{gs}} - h_{\text{hvs}}]\, dt}{\tau_{\text{liver}}} dt' = 1 \tag{E.24}$$

Appendix F

F.1 Development of the Liver Parametric Model

From section 8.4 equation 8.12,

$$-Q\frac{\partial C}{\partial v} - C\phi + \phi C_{\text{in}}'' = \frac{\partial C}{\partial t} \tag{F.1}$$

with boundary conditions for this equation are:

$$C(t=0,v) = 0 \tag{F.2}$$

$$C(t,v=0) = C_{\text{in}}' = C_{\text{in}} * h_{\text{gs}} \tag{F.3}$$

We make the substitution:

$$y = ln(Q' + \phi v) \tag{F.4}$$

and thus:

$$\frac{dy}{\phi} = \frac{dv}{Q' + \phi v} \tag{F.5}$$

Substituting equation F.5 into equation F.1 gives:

$$-\phi\frac{\partial C}{\partial y} - \phi C + \phi C_{\text{in}}'' = \frac{\partial C}{\partial t} \tag{F.6}$$

The laplace transform of equation F.6 gives:

$$-\phi\frac{\partial \bar{C}}{\partial y} - \phi\bar{C} + \phi\bar{C}_{\text{in}}'' = s\bar{C} \tag{F.7}$$

rearranging:

$$\frac{\partial \bar{C}}{\partial y} + \left(\frac{s}{\phi} + 1\right)\bar{C} = \bar{C}_{\text{in}}'' \tag{F.8}$$

Now the integration of equation F.8 gives:

$$\bar{C} = exp\left[-\left(\frac{s}{\phi}+1\right)y\right]\left\{\frac{exp\left[\left(\frac{s}{\phi}+1\right)y\right]}{\frac{s}{\phi}+1}\bar{C}'_{in} + A_1\right\} \tag{F.9}$$

where

A_1 :- Constant of integration

From the boundary condition of equations F.3,

$$\bar{C}(s, v = 0; y = ln(Q')) = \bar{C}'_{in} = \bar{C}_{in}\bar{h}_{gs} \tag{F.10}$$

Substituting equation F.10 into equation F.9,

$$\bar{C}_{in}\bar{h}_{gs} = \frac{1}{\frac{s}{\phi}+1}\bar{C}''_{in} + A_1 exp\left[-\left(\frac{s}{\phi}+1\right)ln(Q')\right] \tag{F.11}$$

also from equation E.9,

$$\bar{C}''_{in} = \bar{C}_{in}\bar{h}_{ha}(s) \tag{F.12}$$

Thus A_1 is given by:

$$A_1 = \bar{C}_{in} exp\left[\left(\frac{s}{\phi}+1\right)ln(Q')\right]\left\{\bar{h}_{gs} - \frac{\bar{h}_{ha}(s)}{\frac{s}{\phi}+1}\right\} \tag{F.13}$$

We now define:

$$\frac{1}{\phi} = \tau_\phi \tag{F.14}$$

$$\frac{V_{sinus}}{Q'} = \frac{V_{sinus}}{\tau Q^o} = \frac{\tau_{sinus}}{\tau} \tag{F.15}$$

Substituting for A into equation F.9, re-substituting for y and simplifying gives:

$$\bar{h}_{hvs} = \frac{\bar{C}(s, v = V_{sinus})}{\bar{C}_{in}} = \left\{\begin{array}{c} \frac{\bar{h}_{ha}}{(1-e^{-(\tau_\phi s+1)ln(1+\tau_{sinus}/\tau\tau_\phi)})}\tau_\phi s + 1 \\ \\ + \\ \\ \bar{h}_{gs}e^{-(\tau_\phi s+1)ln(1+\tau_{sinus}/\tau\tau_\phi)} \end{array}\right\} \tag{F.16}$$

Inverting the laplace transform and re-organising:

$$h_{hvs}(t) = \left\{\begin{array}{c} \frac{e^{-t/\tau_\phi}}{\tau_\phi} * h_{ha} - \frac{\tau e^{-t/\tau_\phi} * \delta(t-(\tau_\phi ln(1+\tau_{sinus}/\tau\tau_\phi)+\tau_{ha}))}{\tau\tau_\phi+\tau_{sinus}} + \\ \\ \frac{\tau\tau_\phi h_{gs} * \delta(t-\tau_\phi ln(1+\tau_{sinus}/\tau\tau_\phi))}{\tau\tau_\phi+\tau_{sinus}} \end{array}\right\} \tag{F.17}$$

The mixing in the central vein is not included and thus the true residence time density of the hepatic vascular system is:

$$h_{\text{hvs}}(t) = \left\{ \begin{array}{l} \frac{e^{-t/\tau_\phi}}{\tau_\phi} * h_{\text{ha}} - \frac{re^{-t/\tau_\phi} * \delta(t-(\tau_\phi ln(1+\tau_{\text{sinus}}/r\tau_\phi)+\tau_{\text{ha}}))}{r\tau_\phi+\tau_{\text{sinus}}} + \\ \\ \frac{r\tau_\phi h_{\text{gs}} * \delta(t-\tau_\phi ln(1+\tau_{\text{sinus}}/r\tau_\phi))}{r\tau_\phi+\tau_{\text{sinus}}} \end{array} \right\} * \frac{te^{-t/\tau_{\text{cv}}}}{\tau_{\text{cv}}^2} \quad \text{(F.18)}$$

where

τ_{cv} :- Mean transit time of the blood in the central vein

The fraction of hepatic arterial relative to portal flow is not directly available from the model. To include this relationship, we consider a flowrate balance [1] in Figure 8.2.

Now by mass balance with constant density:

$$(1-r)Q^\circ = \phi V_{\text{sinus}} \quad \text{(F.19)}$$

or re-arranging for r and substituting equation F.14,

$$r = 1 - \frac{V_{\text{sinus}}}{\tau_\phi Q^\circ} \quad \text{(F.20)}$$

and so substituting equation F.15 into equation F.20 and re-arranging for τ_ϕ:

$$\tau_\phi = \frac{\tau_{\text{sinus}}}{1-r} \quad \text{(F.21)}$$

Equations F.21 and 8.5 can be substituted into equation F.18 to finally give:

$$h_{\text{hvs}}(t) = \left\{ \begin{array}{l} \frac{(1-r)e^{-t(1-r)/\tau_{\text{sinus}}}}{\tau_{\text{sinus}}} * \delta(t-\tau_{\text{ha}}) - \\ \\ \frac{r(1-r)e^{-t(1-r)/\tau_{\text{sinus}}} * \delta(t-[(\tau_{\text{sinus}}/(1-r)]ln(1/r)+\tau_{\text{ha}}))}{\tau_{\text{sinus}}} + \\ \\ rh_{\text{gs}} * \delta(t-[\tau_{\text{sinus}}/(1-r)]ln(1/r)) \end{array} \right\} * \frac{te^{-t/\tau_{\text{cv}}}}{\tau_{\text{cv}}^2} \quad \text{(F.22)}$$

[1] Constant density of blood is assumed

Appendix G

G.1 Scaling of the Spleen and Kidney Activity/Time Curves

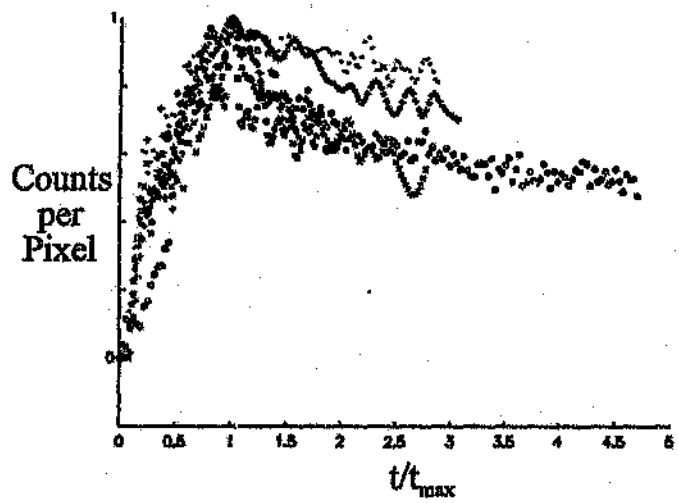

Figure G.1: Eight Kidney activity/time curves scaled according to the maximum value and maximum time

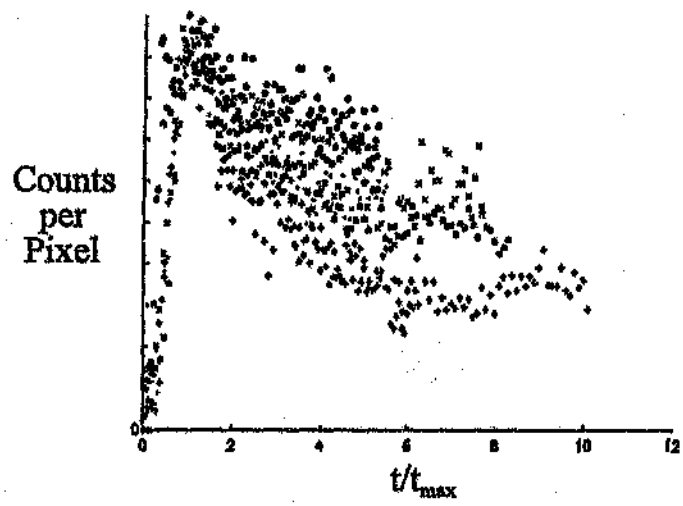

Figure G.2: Eight Spleen activity/time curves scaled according to the maximum value and maximum time

Appendix H

H.1 Fast Fourier Transforms (FFT) and Deconvolution

The discreet fast fourier transform of some vector, $\vec{v}$, of length $\mathcal{N}$ is given as:

$$\mathcal{F}\{\vec{v}\} = \vec{V} \tag{H.1}$$

$$V(k) = \sum_{i=1}^{\mathcal{N}} v(i)\omega_{\mathcal{N}}^{(i-1)(k-1)} \tag{H.2}$$

where the $\mathcal{N}$-th root of unity is given by,

$$\omega_{\mathcal{N}} = e^{-2\pi j/\mathcal{N}} \tag{H.3}$$

and j is the root of minus one ($\sqrt{-1}$).

The Inverse Fast Fourier Transforms (IFFT) is then defined as,

$$v(j) = (1/\mathcal{N}) \sum_{k=1}^{\mathcal{N}} V(k)\omega_{\mathcal{N}}^{-(j-1)(k-1)} \tag{H.4}$$

Convolution of two vectors in the time domain gives rise to a product of vectors in the fourier domain ie. (KREYSZIG, 1983),

$$\mathcal{F}\left\{\vec{a} * \vec{b}\right\} = \vec{A}.\vec{B} \tag{H.5}$$

Appendix I

I.1 The Correlation Matrix

The formulations that appear in this appendix can be found in BECK AND ARNOLD (1977).

We define the sensitivity coefficient, X_i, for some model parameter, β_i, as,

$$X_i = \frac{\partial f(t,\beta)}{\partial \beta_i} \tag{I.1}$$

where

X_i :- Sensitivity vector for parameter i (Appendix I.1)

t :- Independent variable for model f

We can then define the sensitivity matrix, $\mathbf{X}$, by

$$\mathbf{X} = \begin{bmatrix} X_{11} & \cdots & X_{1p} \\ X_{21} & \cdots & X_{2p} \\ \vdots & & \vdots \\ X_{m1} & \cdots & X_{mp} \end{bmatrix} \tag{I.2}$$

$X_{jk}(i)$ is the sensitivity coefficient for the jth dependent variable in in $f(t,\beta)$, for the kth parameter at the ith time. If t has length ten, and there are three model parameters, then $\mathbf{X}$ has dimensions 10×3.

For ordinary least squares (OLS), the covariance matrix can be approximated as (BECK AND ARNOLD, 1977)

$$\mathbf{P} = \mathrm{cov}(\beta) \approx \left(\mathbf{X}^{\mathbf{T}}\mathbf{X}\right)^{-1} s^2 \tag{I.3}$$

where

s^2 :- Approximate constant variance of measurement errors (Appendix I.1)

$$s^2 \approx \frac{OLS}{n-p} \tag{I.4}$$

OLS can be obtained from *SS* Equation 3.29, n is the number of experimental data points and p is the number of model parameters.

The approximate correlation matrix of fitted parameters can be determined from this variance covariance matrix. The ij element of the correlation matrix is given by

$$r_{ij} = \frac{P_{ij}}{(P_{ii}P_{jj})^{0.5}} \tag{I.5}$$

The diagonal elements of r are all unity and the off diagonal elements lie in the interval $[-1, 1]$.

Whenever all the off diagonal elements exceed 0.9 in magnitude, the parameter estimates are highly correlated and tend to be inaccurate (BECK AND ARNOLD, 1977). The correlation matrix also provides information about correlation between pairs of parameters. The closer an element of the correlation matrix is to unity, the higher the correlation between the pair of parameters associated with that element of the correlation matrix (BECK AND ARNOLD, 1977). When the correlation between parameters is small, the minimisation of ε should converge rapidly near the minimum.

Appendix J

J.1 Scaling Residence Time Density Models

Given a RTD, $h(t)$, which needs to be reformulated in terms of a variable θ where $\theta = t/t_m$ and t_m is a constant. By mass balance, the fraction of material that spends time between t and $t + dt$ in the system must be equal to the fraction of material that that spends between θ and $\theta + d\theta$,

$$h(t)dt = h(\theta)d\theta \tag{J.1}$$

Substituting θ for t,

$$h(\theta t_m)t_m d\theta = h(\theta)d\theta \tag{J.2}$$

Simplifying this equation gives:

$$h_\theta = t_m h_t(\theta t_m) \tag{J.3}$$

Appendix K

K.1 Private Communications

```
Received: from shannon.ee.wits.ac.za by witsvma.wits.ac.za
          (IBM VM SMTP V2R1)
        with TCP; Thu, 20 Aug 92 12:04:35 RSA
Received: by shannon.ee.wits.ac.za (/\==/\ Smail3.1.22.1 #22.3)
id <m0mL9Ag-0000vRC@shannon.ee.wits.ac.za>; Thu, 20 Aug
        92 11:51 EET
Received: From WITS_EE2/WORKQUEUE by cerberus.ee.wits.ac.za
          via Charon 3.4 with IPX id 100.920820114266.320;
          20 Aug 92 11:43:18 +0200
Message-ID: <MAILQUEUE-101.920820114245.304@odie>
To:           004fin@witsvma.wits.ac.za
From:         "Roy Eric Lurie"  <LURIE@odie.ee.wits.ac.za>
Date:         20 Aug 92 11:42:45 SAT
Subject:      Reply for Sabine van Huffel
X-pmrqc:      1
X-mailer:     Pegasus Mail v2.3 (R2).
```

David,

Here is the reply from Sabine van Huffel. This basically confirms that no-one really knows why the deconvolution goes negative. We should probably reference this in our paper as "Personal communications"

- Roy

------- Forwarded Message Follows -------

Date: Thu, 20 Aug 92 09:57:40-0100

From: vanhuffe@esat.kuleuven.ac.be

To: lurie@odie.ee.wits.ac.za

Dear Roy,

I just received your e-mail. I will give you a quick answ since I am very busy for the moment and do not have time to treat your questions more carefully.

The fact that the concentration of tracer can become negative is of course an artifact of the background subtraction. This is just a consequence of the fact that you don't work with exact data but with noisy data and hence we work with some statistical assumptions that are never satisfied exactly but only on average. The problem that the retention function may become negative is a due to the fact that the real-life data do not fit the model assumptions and the fact that the background noise can not be measured exactly. You can impose constraints and require that the solution is nonnegative but I don't think more explanation can be given to this phenomenon.

Concerning SVD techniques for background subtraction: I know there are some papers in image processing that use SVD in order to restore the image and subtract the background noise but I don't find the references right now. What I mean is that you can put the data of the nuclear images in a matrix, perform the SVD and lower the rank of this matrix appropriately and then work with the rank-reduced images. If done appropriately, the rank reduction should correspond with background subtraction. Influencing parameters are the matrix size, correcting the singular values, ... I didn't try it out for the computation of the renal retention function.

Sabine

========== RFC 822 Headers ==========

Date: Thu, 20 Aug 92 10:57:10 +0200

Message-Id: <9208200857.AA08242@celine.esat.kuleuven.ac.be>

Received: by celine.esat.kuleuven.ac.be Thu, 20 Aug 92 10:57:10 +0200

Roy Eric Lurie] Control Department
lurie@odie.ee.wits.ac.za] Electrical Engineering
(011)716-5406 (w)] University of Witwatersrand
(011)403-1929 (fax)] South Africa 2050

Appendix L

L.1 Renal Computer Programs in Matlab™ for Windows™

L.1.1 Renal Global Program

```
% ------------------------------------------------------------------
% KIDNEY.M  (Non-parameric model)
%
% This file
% 1) Loads and Cleans the data from the ascii file
% 2) Bounds the data using BOUND.M
% 3) Interpolates the data to 1 seconds
% 4) Deconvolves the data using : Filtered FFT Method
% 5) Fits the renal model to the experimental data
% 6) Displays the results and compares the model IAD with the
%    deconvolved data
%
% D.R Fine and R.E.Lurie 21-07-93

% Prompt the user for the file name of the data to be
% analysed. The data is assumed to be :
%
% file name1 = Left Parencema  0 - 120 sec in 2 sec intervals
%      name2 = Right Parencema 0 - 120 sec in 2 sec intervals
%      name3 = Aorta           0 - 120 sec in 2 sec intervals
%      name1 = Left Parencema  120 - 1780 sec in 15 sec intervals
%      name2 = Right Parencema 120 - 1780 sec in 15 sec intervals
%      name3 = Aorta           120 - 1780 sec in 15 sec intervals

% Clear the Workspace
clear
clear global
pack
format compact
clc
clg
global Pathname
echo off
```

```
%Get the Present Directory
oldpath = pwd;

% Get the file name
Fname = 0;
while Fname==0,
  [Fname,Pathname] = uigetfile('*.asc','Select a Data File');
end,
Fname = Fname(1:findstr(lower(Fname),'.asc')-1);
Fname(find((Fname>='0')&(Fname<='9'))) = [];

% Get Left Parenchyma Data
eval(['load ',Fname,'1.asc']);
eval(['load ',Fname,'10.asc']);
%eval(['T = [',Fname,'1(:,2) ; ' ,Fname,'10(:,2)];']);
eval(['T1 = ',Fname,'1(:,2);']);
eval(['T2 = ',Fname,'10(:,2);']);
T = [T1; T2];
dec1 = T1(2) - T1(1);
dec2 = T2(2) - T2(1);
lenfil = [length(T1) length(T2)];

eval(['L = [',Fname,'1(:,3) ; ' ,Fname,'10(:,3)];']);
eval(['clear ',Fname,'1']);
eval(['clear ',Fname,'10']);

% Get Left Parenchyma Background Data
eval(['load ',Fname,'8.asc']);
eval(['load ',Fname,'17.asc']);
eval(['Lbg = [',Fname,'8(:,3) ; ' ,Fname,'17(:,3)];']);
eval(['clear ',Fname,'8']);
eval(['clear ',Fname,'17']);

% Get Right Parenchyma Data
eval(['load ',Fname,'2.asc']);
eval(['load ',Fname,'11.asc']);
eval(['R = [',Fname,'2(:,3) ; ' ,Fname,'11(:,3)];']);
eval(['clear ',Fname,'2']);
eval(['clear ',Fname,'11']);

% Get Right Parenchyma Background Data
eval(['load ',Fname,'9.asc']);
eval(['load ',Fname,'18.asc']);
eval(['Rbg = [',Fname,'9(:,3) ; ' ,Fname,'18(:,3)];']);
eval(['clear ',Fname,'9']);
eval(['clear ',Fname,'18']);


% Get Aorta Parenchyma
eval(['load ',Fname,'3.asc']);
eval(['load ',Fname,'12.asc']);
eval(['A = [',Fname,'3(:,3) ; ' ,Fname,'12(:,3)];']);
eval(['clear ',Fname,'3']);
eval(['clear ',Fname,'12']);

cd(oldpath);
```

```
hold off

aa = A;
ll = L;
rr = R;
tt = T;
retur = 0;
retu = ['retur=1;'];

% Interpolate 4s second data to 1s and decimate all the data to 2s
% Marginally filter the data using the technique of Diffy and
% Corfield (1976)
[aa, tt]   = decinter(T,aa,6,5,3,[dec1 dec2 4],'Aorta',lenfil);
ll         = decinter(T,ll,6,5,3,[dec1 dec2 4],'Left',lenfil);
rr         = decinter(T,rr,6,5,3,[dec1 dec2 4],'Right',lenfil);
lbg        = decinter(T,Lbg,6,5,3,[dec1 dec2 4],'Right',lenfil);
rbg        = decinter(T,Rbg,6,5,3,[dec1 dec2 4],'Right',lenfil);

% Truncate Data
hold off
plot(tt,aa,tt,ll*max(aa)/max(ll),tt,rr*max(aa)/max(rr),'EraseMode','none')
title('Select Experiment END point ')
[x,y] = ginput(1);
[temp,maxind] = min((tt-x).^2);
aa = aa(1:maxind);
rr = rr(1:maxind);
ll = ll(1:maxind);
tt = tt(1:maxind);
lbg=lbg(1:maxind);
rbg=rbg(1:maxind);

% Plot all the data and save the interpolated and decimated data
clg
hold off
lft = ['Healthy = ''l'';'];
rft = ['Healthy = ''r'';'];
blnk = [' '];

hold off
plot(tt,ll*max(aa)/max(ll),'-',tt,rr*max(aa)/max(rr),'--',tt,aa,'-.',
     'EraseMode','none'), grid, title('Interpolated and Data Bounded :
  CHOOSE THE HEALTHY KIDNEY ("Cont" to continue)'),
  xlabel('Seconds'), hold on, drawnow
uicontrol('Units','normal','Position',[.91 .9 .08 .06],'String','Cont',
          'callback',retu)
uicontrol('Units','normal','Position',[.91 .6 .08 .06],'String','Left',
          'callback',lft)
uicontrol('Units','normal','Position',[.91 .4 .08 .06],'String','Right'
          ,'callback',rft)
while retur == 0 , waitforbuttonpress; end
uicontrol('Units','normal','Position',[.91 .6 .08 .06],'String','',
          'callback',blnk)
uicontrol('Units','normal','Position',[.91 .4 .08 .06],'String','',
          'callback',blnk)
retur = 0;
```

```
eval(['save ',Pathname,'kidbound aa ll rr tt'])

% ------------------------------------------------------------------
% Minimise the aorta background and determine the initial guesses using
% filtered FFT Method.  Also determine the amount of renal background
% from the aorta curve

len=length(aa);
options(1) = 0;   % Do not print the results after each itteration
options(3) = 1; % Termination criteria for minimised function
options(14) = 20; % Maximum number of iterations
bgfactor = 0.25;
[val maxa]=max(aa);
hold off
plot(tt,aa,tt,lbg*max(aa)/max(lbg)),title('Select the Aorta
     Peak and Corresponding BKG Peak'),drawnow
maxbg = ginput(2);
blooddelay = maxbg(2,1)-maxbg(1,1);
[val dirac]=min((tt-blooddelay).^2);
lbg=[zeros(dirac,1); aa(:)];
lbg=lbg(1:length(aa))*mean(Lbg)/mean(aa);
rbg=[zeros(dirac,1); aa(:)];
rbg=rbg(1:length(aa))*mean(Rbg)/mean(aa);
fA      = fft(aa);
fL      = fft(ll-lbg*bgfactor);
fR      = fft(rr-rbg*bgfactor);
HLfft2  = fili(real(ifft(fL./fA)),10);
HRfft2  = fili(real(ifft(fR./fA)),10);

hold off
if Healthy == 'l'
  factor     = max(ll)/max(aa);
  ll         = ll/factor;
  rr         = rr/factor;
  lbg        = lbg/factor;
  rbg        = rbg/factor;
  Aortafix   = 100;
  bgndasymp  = 0.6667*aa(len);
  ind1       = min(find(HLfft2<0));
  [minv ind2] = min((tt-1.5*tt(ind1)).^2);
  plot(tt,HLfft2/factor,'co','Erasemode','none'), axis(axis), grid,
       ylabel('Left'), xlabel('Seconds'), title('Filtered FFT'),hold on
  Plothandle = plot(tt,HLfft2/factor,'y-','EraseMode','xor');
  x=log([Aortafix,bgndasymp]);
  x = fminu('aortamin',x,options,[],ll,aa,tt,Plothandle,[ind1 ind2]);
else
  factor    = max(rr)/max(aa);
  ll         = ll/factor;
  rr         = rr/factor;
  lbg        = lbg/factor;
  rbg        = rbg/factor;
  Aortafix   = 100;
  bgndasymp  = 0.6667*aa(len);
  ind1       = min(find(HRfft2<0));
  [minv ind2] = min((tt-1.5*tt(ind1)).^2);
```

```
  plot(tt,HRfft2/factor,'co','Erasemode','xor'), axis(axis), grid,
       ylabel('Left'), xlabel('Seconds'), title('Filtered FFT'),hold on
  Plothandle = plot(tt,HRfft2/factor,'y-','EraseMode','xor');
  x=log([Aortafix,bgndasymp]);
  x = fminu('aortamin',x,options,[],rr,aa,tt,Plothandle,[indi ind2]);
end
Aortafix  = exp(x(1));
bgndasymp = exp(x(2));
aanew=aa-(1-exp(-tt'/Aortafix))*bgndasymp;
bgfactor  = 0.75;
ll        = ll-lbg*bgfactor;
rr        = rr-rbg*bgfactor;
ll = fixup(tt,ll,aa,'Left');
rr = fixup(tt,rr,aa,'Right');
eval(['save ',Pathname,'kidbound aa ll rr tt'])
eval(['save ',Pathname,'aortapara Aortafix bgndasymp'])
fA        = fft(aanew);
HLfft2    = fili(real(ifft(fL./fA)),10);
HRfft2    = fili(real(ifft(fR./fA)),10);
meanLTT   = calcmean(tt,HLfft2,'Left');
uicontrol('Units','normal','Position',[.91 .9 .08 .06],'String',
          'Cont','callback',retu)
while retur == 0 , waitforbuttonpress; end, retur = 0;
meanRTT = calcmean(tt,HRfft2,'Right');
uicontrol('Units','normal','Position',[.91 .9 .08 .06],'String',
          'Cont','callback',retu)
while retur == 0 , waitforbuttonpress; end, retur = 0;

eval(['save ',Pathname,'means meanLTT meanRTT'])
eval(['save ',Pathname,'ret HLfft2 HRfft2'])
% ------------------------------------------------------------------------
% Fit the model to the experimental data

% Setup the optimisation parameters
options(1) = 0;     % Do not print the results after each itteration
options(3) = 1e-4; % Termination criteria for minimised function
options(14) = 40;  % Maximum number of iterations
eval(['load ',Pathname,'kidbound'])
eval(['load ',Pathname,'means'])

ll=ll(1:len);
lbg=lbg(1:len);
rr=rr(1:len);
rbg=rbg(1:len);
tt=tt(1:len);
aa=aa(1:len);

len = length(tt);

hold off
eval(['load ',Pathname,'aortapara'])

% Initial objective function value
Error = 1e12;
eval(['save ',Pathname,'errLeft Error'])
pp = ll;
```

```
string = 'Left';

%Initial Guesses
fraction = 0.20;
minttest=75;
taublood=3;
taupara=23;

x = [taupara minttest taublood fraction]; % initial guess

eval(['save ',Pathname,'ansLeft x'])
x = log(x);
hold off
plot(tt,ll,'co','EraseMode','none'),axis(axis),title(string),
     xlabel('Time'),ylabel('Activity'),hold on
Plothandle = plot(tt,ll,'y-','EraseMode','xor');
[val iind] = max(aa);
iind=[iind blooddelay];

% Call the minimization routine
x = fminu('jeffloop(x,P1,P2,P3,P4,P5,P6,P7,P8)',x,options,[],
          tt,aa,pp,bgndasymp,Acortafix,string,Plothandle,iind);
s = ['load ',Pathname,'ansleft, x = log(x); x =
    fminu(''jeffloop(x,P1,P2,P3,P4,P5,P6,P7,P8)'',
 x,options,[],tt,aa,pp,bgndasymp,Acortafix,string,
 Plothandle,iind);'];
uicontrol('Units','normal','Position',[.91 .2 .08 .06],'String',
          'Again','callback',s)
sv = ['save ',Pathname,'ans',string];
uicontrol('Units','normal','Position',[.91 .4 .08 .06],'String',
          'Save','callback',sv)
pr = ['print'];
uicontrol('Units','normal','Position',[.91 .6 .08 .06],'String'
         ,'Print','callback',pr)
uicontrol('Units','normal','Position',[.91 .9 .08 .06],'String'
         ,'Cont','callback',retu)
while retur == 0 , waitforbuttonpress; end, retur = 0;

Error = 1e12;
eval(['save ',Pathname,'errRight Error'])
pp = rr;
string = 'Right';

% Initial Guessed
fraction = 0.20;
taublood=3;
taupara=23;
minttest=75;

x = [taupara mintteat taublood fraction]; % initial guess
eval(['save ',Pathname,'ansRight x'])
x = log(x);
hold off
plot(tt,rr,'co','EraseMode','none'),axis(axis),title(string),
     xlabel('Time'),ylabel('Activity'),hold on
Plothandle = plot(tt,rr,'y-','EraseMode','xor');
```

```
x = fminu('jeffloop(x,P1,P2,P3,P4,P5,P6,P7,P8)',x,options,[],
          tt,aa,pp,bgndasymp,Aortafix,string,Plothandle,iind);
s = ['load ',Pathname,'ansright, x = log(x);
    x = fminu(''jeffloop(x,P1,P2,P3,P4,P5,P6,P7,P8)'',x,options,
 [],tt,aa,pp,bgndasymp,Aortafix,string,Plothandle,iind);'];
uicontrol('Units','normal','Position',[.91 .2 .08 .06],'String',
          'Again','callback',s)
sv = ['save ',Pathname,'ans',string];
uicontrol('Units','normal','Position',[.91 .4 .08 .06],'String',
          'Save','callback',sv)
uicontrol('Units','normal','Position',[.91 .6 .08 .06],'String',
          'Print','callback',pr)
uicontrol('Units','normal','Position',[.91 .9 .08 .06],'String',
          'Cont','callback',retu)
while retur == 0 , waitforbuttonpress; end, retur = 0;
% ------------------------------------------------------------------
% Evaluate the PARAMETRIC vs NON-PARAMETRIC kidney reponse

eval(['load ',Pathname,'kidbound'])  % Load non-parametric time data
eval(['load ',Pathname,'ret'])       % Load non-parametric retention funcs
eval(['load ',Pathname,'aortapara']) % Load assymtote

% Left kidney
eval(['load ',Pathname,'ansleft'])

pp       = 11;
len      = length(tt);
Tau1     = x(1);        % Parenchemal Time Const
Delay1   = x(2);        % Parenchemal Delay Const
Tau2     = x(3);        % Blood Time Const
q        = x(4);        % Fixed vascular split factor
Tsample1 = tt(2)-tt(1); % Sample Time
len      = length(tt);  % Vector Length
string   = 'Left';

% Build normal system

% Parenchemal 2nd order system with delay
[A1,B1,C1,D1] = tf2ss(q,nconv([Tau1 1],2));       % Parenchemal model
[Ad1,Bd1,Cd1,Dd1] = c2dt(A1,B1,C1,Tsample1,
                    Delay1+blooddelay);           % Discrete

% Vascular 2nd order system without delay

Num2 = 1-q;
Den2 = nconv([Tau2 1],2);
[A2,B2,C2,D2] = tf2ss(Num2,Den2);      % Blood model
[Ad2,Bd2,Cd2,Dd2] = c2dt(A2,B2,C2,Tsample1,blooddelay); % Discrete

[Ad,Bd,Cd,Dd] = parallel(Ad1,Bd1,Cd1,Dd1,Ad2,Bd2,Cd2,Dd2,1,1,1,1);

% Convert to Internal Age distribution

% Invert sign of Matrix
Cdd = -Cd;
```

```
Ddd = -Dd;
% 1 in state space
Done = 1;
[Aret,Bret,Cret,Dret] = parallel(Ad,Bd,Cdd,Ddd,0,0,0,Done,1,1,1,1);
% Integrate (ie. multiply by '1/s')
[Aint,Bint,Cint,Dint] = tf2ss(1,[1 0]);
[Aint,Bint] = c2d(Aint,Bint,Tsample1);
% Connect
[Aret,Bret,Cret,Dret] = series(Aret,Bret,Cret,Dret,Aint,Bint,
                               Cint,Dint,1,1);

% Remove aorta background function
aanew=aa-(1-exp(-tt'/Aortafix))*bgndasymp;

% Simulate Retention function
yret = dlsim(Aret,Bret,Cret,Dret,aanew);

% Calc Impulse Retention function
yretimp = dimpulse(Aret,Bret,Cret,Dret,1,len);

% Calc Output Retention Function
youtimp = dimpulse(Ad,Bd,Cd,Dd,1,len);

K = sum(yret)/sum(pp);
IntR = integ(yretimp,Tsample1);
IntR = integ(yretimp,Tsample1);
Index = find(HRfft2<=0);
if ~isempty(Index),
   Index = min(Index);
else
Index = length(HLfft2);
end,
IntF = integ(HLfft2(1:Index),Tsample1);
IntR = IntR(len);
IntF = IntF(Index);

hold off
clg
plot(tt,yret,'-',tt,pp*K,'x','EraseMode','none'), title([ string ,
     ' Parenchema : Parametric Model']);
xt = max(tt)/3;
yt = max(yret)/3;
text(xt,1.16*yt,['Tau1 =  ' num2str(x(1)) ', Delay =
     ' num2str(x(2))])
text(xt,1.0*yt,['Tau3 =  ' num2str(x(3))  ', GFF   =
    ' num2str(x(4))]),hold on, drawnow
uicontrol('Units','normal','Position',[.91 .6 .08 .06],'String',
          'Print','callback',pr)
uicontrol('Units','normal','Position',[.91 .9 .08 .06],'String',
          'Con ' 'callback',retu)
while retur == 0 , waitforbuttonpress; end, retur = 0;

hold off
plot(tt,yretimp/IntR,'-',tt,HLfft2/IntF,'o','EraseMode','none'),
title('Internal Age Distibutions'), hold on, drawnow;
uicontrol('Units','normal','Position',[.91 .6 .08 .06],
```

```
          'String','Print','callback',pr)
uicontrol('Units','normal','Position',[.91 .9 .08 .06],
          'String','Cont','callback',retu)
while retur == 0 , waitforbuttonpress; end, retur = 0;

eval(['save ',Pathname,'lftrprt2 tt K IntR IntF pp yret
     yretimp youtimp HLfft2'])


% Right kidney
eval(['load ',Pathname,'ansright'])

pp = rr;

len      = length(tt);
Tau1     = x(1);         % Parenchemal Time Const
Delay1   = x(2);         % Parenchemal Delay Const
Tau2     = x(3);         % Blood Time Const
q        = x(4);         % Fixed vascular split factor
Tsample1 = tt(2)- t(1); % Sample Time
len      = length(tt);   % Vector Length
string   = 'Right';

% Build normal system

% Parenchemal 2nd order system with delay

[A1,B1,C1,D1] = tf2ss(q,nconv([Tau1 1],2));          % Parenchemal model
[Ad1,Bd1,Cd1,Dd1] = c2dt(A1,B1,C1,Tsample1
                         ,Delay1+blooddelay);        % Discrete

% Vascular 2nd order system without delay
Num2 = 1-q;
Den2 = conv([Tau2 1],[Tau2 1]);
[A2,B2,C2,D2] = tf2ss(Num2,Den2);     % Blood model
[Ad2,Bd2,Cd2,Dd2] = c2dt(A2,B2,C2,Tsample1,blooddelay);% Discrete

[Ad,Bd,Cd,Dd] = parallel(Ad1,Bd1,Cd1,Dd1,Ad2,Bd2,Cd2,Dd2,1,1,1,1);

% Convert to Internal Age distribution

% Invert sign of Matrix
Cdd = -Cd;
Ddd = -Dd;
% 1 in state space
Done = 1;
[Aret,Bret,Cret,Dret] = parallel(Ad,Bd,Cdd,Ddd,0,0,0,Done,1,1,1,1);
% Integrate (ie. multiply by '1/s')
[Aint,Bint,Cint,Dint] = tf2ss(1,[1 0]);
[Aint,Bint] = c2d(Aint,Bint,Tsample1);
% Connect
[Aret,Bret,Cret,Dret] = series(Aret,Bret,Cret,Dret,
                               Aint,Bint,Cint,Dint,1,1);

% Remove aorta background function
aanew=aa-(1-exp(-tt'/Aortafix))*bgndasymp;
```

```
% Simulate Retention function
yret = dlsim(Aret,Bret,Cret,Dret,aanew);

% Calc Impulse Retention function
yretimp = dimpulse(Aret,Bret,Cret,Dret,1,len);

% Calc Output Retention Function
youtimp = dimpulse(Ad,Bd,Cd,Dd,1,len);

K = sum(yret)/sum(pp);
IntR = integ(yretimp,Tsample1);
Index = find(HRfft2<=0);
if ~isempty(Index),
   Index = min(Index);
else
Index = length(HLfft2);
end,
IntF = integ(HRfft2(1:Index),Tsample1);
IntR = IntR(len);
IntF = IntF(Index);

hold off
plot(tt,yret/K,'-',tt,pp,'x','EraseMode','none'),
     title([ string , ' Parenchema : Parametric Model']);
xt = max(tt)/3;
yt = max(yret)/3;
text(xt,1.16*yt,['Tau1 =  ' num2str(x(1)) ', Delay = ' num2str(x(2))])
text(xt,1.0*yt,['Tau3 =  ' num2str(x(3))  ', GFF   = ' num2str(x(4))])
     ,hold on, drawnow
uicontrol('Units','normal','Position',[.91 .6 .08 .06],'String',
          'Print','callback',pr)
uicontrol('Units','normal','Position',[.91 .9 .08 .06],'String',
          'Cont','callback',retu)
while retur == 0 , waitforbuttonpress; end, retur = 0;

hold off
plot(tt,yretimp/IntR,'-',tt,HRfft2/IntF,'o','EraseMode','none'),
title('Internal Age Distibutions'), hold on, drawnow;
uicontrol('Units','normal','Position',[.91 .6 .08 .06],
          'String','Print','callback',pr)

eval(['save ',Pathname,'rghrprt3 tt K IntR IntF pp yret yretimp
     youtimp HRfft2'])
eval(['save ',Pathname,'blooddelay'])
% ------------------------------------------------------------------
```

L.1.2 Renal Objective Function

```
% ------------------------------------------------------------------
function Error = jeffloop(x,tt,aa,pp,bgndasymp,Aortafix,
                          string,Plothandle,iind);
% The file KIDLOOP determines the summ of squares between the kidney
```

```
% model and the experimental data
%
% D.R. Fine and R.E.Lurie 21-07-93

x=exp(x);

if x(2) < 0
  x(2) = 2;
end
if x(2) > 200
  keyboard;
end


global Pathname

len      = length(tt);
Tau1     = x(1);        % Parenchymal Time Const
Delay1   = x(2);        % Parenchymal Delay Const
Tau2     = x(3);        % Blood Time Const
q        = x(4);        % Fixed vascular split factor
Tsample = tt(2)-tt(1); % Sample Time

eval(['load ',Pathname,'err',string]);
Lasterror=Error;

% Build normal system

% Parenchymal 2nd order system with delay

[A1,B1,C1,D1] = tf2ss(q,nconv([Tau1 1],2)); %Parenchymal model
[Ad1,Bd1,Cd1,Dd1] = c2dt(A1,B1,C1,Tsample,Delay1+iind(2));% Discrete

% Vascular 2nd order system without delay

Num2 = 1-q;
Den2 = nconv([Tau2 1],2);
[A2,B2,C2,D2] = tf2ss(Num2,Den2);       % Blood model
[Ad2,Bd2,Cd2,Dd2] = c2dt(A2,B2,C2,Tsample,iind(2)); % Discrete

[Ad,Bd,Cd,Dd] = parallel(Ad1,Bd1,Cd1,Dd1,Ad2,Bd2,Cd2,Dd2,1,1,1,1);

% Convert to Internal Age distribution

% Invert sign of Matrix
Cdd = -Cd;
Ddd = -Dd;
% 1 in state space
Done = 1;
[Aret,Bret,Cret,Dret] = parallel(Ad,Bd,Cdd,Ddd,0,0,0,Done,1,1,1,1);
% Integrate (ie. multiply by '1/s')
[Aint,Bint,Cint,Dint] = tf2ss(1,[1 0]);
[Aint,Bint] = c2d(Aint,Bint,Tsample);
% Connect
[Aret,Bret,Cret,Dret] = series(Aret,Bret,Cret,Dret,Aint,Bint,
                               Cint,Dint,1,1);
```

```
% Remove aorta background function
aa=aa-(1-exp(-tt'/Aortafix))*bgndasymp;

% Simulate Retention function
y = dlsim(Aret,Bret,Cret,Dret,aa);

%Int1 = integ(y(iind(1):len),Tsample);
%Int1 = Int1(length(Int1));
%Int2 = integ(pp(iind(1):len),Tsample);
%Int2 = Int2(length(Int2));
%K = Int1/Int2;

K = sum(y)/sum(pp);

% Calculate the sum of squares
Error = y/K - pp;
Error = Error(:)'*Error(:);

xt = max(tt)/3;
yt = max(y)/3;
set(Plothandle,'ydata',y/K)
drawnow

if (Error < Lasterror)
  eval(['save ',Pathname,'err',string,' Error']);
  eval(['save ',Pathname,'Ans',string,' x']);
end
% ------------------------------------------------------------------
```

L.1.3 Interpolate and Decimate Data

```
% ------------------------------------------------------------------
function [data, tt] = decinter(Time,indata,looptimes,Q,n,decifactor,
                      string,lenfil);
%function [data, tt] = decinter(Time,indata,looptimes,Q,n,decifactor,
%                       string,lenfil);

ind = find(indata<=0);
indata(ind) = 0.001*ones(length(ind),1);
data = indata;
hold off
clg
plot(Time,indata,'co','EraseMode','none'),axis(axis),title(['Data Bound,
     Interpolate and Decimate : ' string]),
  xlabel('Time'),ylabel('Activity'),hold on
Plothandle = plot(Time,indata,'y-','EraseMode','xor');

% Diffy and Corfield (1976) Data Bounding Technique
for i = 1:looptimes;
data = bound(indata,Q,n);
set(Plothandle,'ydata',data)
        drawnow
```

```
Q = Q/2;
end,


data = [interp(data(1:lenfil(1)),decifactor(1)) ;
       interp(data(lenfil(1)+1:lenfil(1)+lenfil(2)),decifactor(2))];

data = decimate(data,decifactor(3),'FIR');
t=0:length(data)-1;
tt = decifactor(3)*t;
% ------------------------------------------------------------------
```

L.1.4 Data Bounding Technique

```
% ------------------------------------------------------------------
function [data, tt] = decinter(Time,indata,looptimes,Q,n,decifactor,
                      string,lenfil);
%function [data, tt] = decinter(Time,indata,looptimes,Q,n,decifactor,
%                      string,lenfil);

ind = find(indata<=0);
indata(ind) = 0.001*ones(length(ind),1);
data = indata;
hold off
clg
plot(Time,indata,'co','EraseMode','none'),axis(axis),title(['Data Bound,
     Interpolate and Decimate : ' string]),
  xlabel('Time'),ylabel('Activity'),hold on
Plothandle = plot(Time,indata,'y-','EraseMode','xor');

% Diffy and Corfield (1976) Data Bounding Technique
for i = 1:looptimes;
data = bound(indata,Q,n);
set(Plothandle,'ydata',data)
        drawnow
Q = Q/2;
end,


data = [interp(data(1:lenfil(1)),decifactor(1)) ;
       interp(data(lenfil(1)+1:lenfil(1)+lenfil(2)),decifactor(2))];

data = decimate(data,decifactor(3),'FIR');
t=0:length(data)-1;
tt = decifactor(3)*t;
% ------------------------------------------------------------------
```

Appendix M

M.1 Spleen Programs in Matlab-386^{TM}

M.1.1 Process the Raw Spleen Data

```
% ------------------------------------------------------------------------
% SPLEEN1 processes the raw spleen and aorta data
%
% This file
% 1) Loads and Cleans the data from the ascii file
% 2) Bounds the data using BOUND.M
% 3) Interpolates the data to 1 seconds
% 4) Deconvolves the data using : Filtered FFT Method
%
% D.R. Fine 20-04-93

% Get Aorta
eval(['load Aorta1.asc']);
eval(['load Aorta2.asc']);

% Get Spleen info
eval(['load Spleen1.asc']);
eval(['load Spleen2.asc']);

T=[Spleen1(:,2);Spleen2(:,2)];
A=[Aorta1(:,9);Aorta2(:,3)];
S=[Spleen1(:,3);Spleen2(:,3)];

hold off
clg
subplot(211)
plot(T,A), grid, title(['Aorta : ', Date]);, xlabel('Seconds')
plot(T,S), grid, title(['Original Data: ', Date]),  xlabel('Seconds')

save SPLEEN

% use BOUND.M to non-linear filter the data to remove poisson noise.

aa = A;
```

```
ss = S;
tt = T;

% Shift the data to remove the pre-injection data.
subplot(111)
clg
hold off
blen=120;
plot(tt(1:blen),aa(1:blen),tt(1:blen),ss(1:blen),'+')
title('Select Experiment BEGIN point ')
[x,y] = ginput(1);
[mtemp,minind] = min((tt-x).^2);

% Decimate the initial 0.5s per frame data to 1s data
decifactor = 2;
aa = [decimate(aa(minind:121),decifactor,'FIR') ; aa(122:length(T))];
ss = [decimate(ss(minind:121),decifactor,'FIR') ; ss(122:length(T))];
tt=0:1000;
tt = tt(1:length(aa));

%Use the Diffy and Corfield (1976) technique to bound the data.
looptimes = 6;
keyboard
Q = 5; % Initial standard deviation
ind = find(aa<=0);
aa(ind) = 0.001*ones(length(ind),1);

len=length(aa);
anew=aa;
for i = 1:looptimes;
anew = bound(anew,Q,3);
plot(tt,aa,tt,anew), title('Aorta : Data Bounding'),
Q = Q/2;
end,

Q = 5;
ind = find(ss<=0);
ss(ind) = 0.001*ones(length(ind),1);
snew=ss;
for i = 1:looptimes;
snew = bound(snew,Q,5);
plot(tt,ss,tt,snew), title('Spleen : Data Bounding'),
Q = Q/2;
end,

clg
subplot(211)
plot(tt,aa,'w.',tt,anew), title('Aorta : Data Bounding')
plot(tt,ss,'w.',tt,snew), title('Spleen : Data Bounding'),pause

aa = anew;
ss = snew;

% Select the background tissue component in the spleen data
subplot(111)
clg
```

```
hold off
plot(tt(1:30),aa(1:30),tt(1:30),ss(1:30))
title('Select Subtract Point')
[x,y] = ginput(1);
[ival,iind]    = max(aa);
[scal,sind]    = min((tt-x).^2);
maxind=length(aa);

save iind iind sind

aa = aa(1:maxind);
ss = ss(1:maxind)-ss(sind);
tt = tt(1:maxind);
aa(1)=0;
ss(1)=0;
ind=find(ss<0);
ss(ind)=eps*ones(length(ind),1);

hold off
clg
subplot(211)
plot(tt,aa), grid, title(['Aorta : ', Date]);, xlabel('Seconds')
plot(tt,ss,'-'), grid, title(['Interpolated and Data Bounded : ',
     Date]),  xlabel('Seconds'), pause

save Splnbound aa ss tt

% Perform the Non-Parametric Deconvolution using the filtered FFT Method
fA = fft(aa);
fS = fft(ss);

HSfft2 = fill(real(ifft(fS./fA)),4);

hold off
clg
plot(tt,HSfft2), grid, ylabel('ALL'), xlabel('Seconds'),
     title('Filtered FFT'),

save Sret HSfft2
mind
% ------------------------------------------------------------------
```

M.1.2 Fit Spleen Model to Experimental Data

```
% ------------------------------------------------------------------
% SPLEEN2 fits the model of the spleen to the experimental
% data
%
% D.R. Fine and R.E.Lurie 21-07-93

clear
pack
```

```
options(1)  = 0;   % Do not print the results after each itteration
options(3)  = 3;  % Termination criteria for minimised function
options(14) = 100; % Maximum number of iterations
options(6)  = 1;   % Broyden-Fletcher-Golfarb-Shanno algorithm
options(7)  = 1;  % Cubic Interpolation

load splnbound
load iind
load aortapara

% Initial Guesses.  The parameters are described in the figures within the
% thesis.
q          = 0.80;
f          = 0.20;
Tau_s      = 2;
Tau_p      = 5;
Tau_mp     = 15;

x0         = [q f Tau_p Tau_mp]; % initial guess
len        = length(tt)
% Initial function value
Error      = 1e6;
save errSpleen Error
keyboard
x0         = log(x0);
factor     = max(ss)/max(aa);
save param x0 len Aortafix factor bgndasymp
ss         = ss(1:len)/factor;
tt         = tt(1:len);
aa         = aa(1:len);
string     = 'Spleen';


x = fminu('splnloop(x,P1,P2,P3,P4,P5,P6,P7,P8)',x0,options,[],tt,
           aa,ss,bgndasymp,string,Tau_s,iind,Aortafix);
% ------------ ---------------------------------------- ----------------
```

M.1.3 Objective Function for Model Fitting Program

```
% ------------------------------------------------------------------------
function Error = splnloop(x,tt,aa,pp,bgndasymp,string,Tau_s,
                          iind,Aortafix);
%function Error = splnloop(x,tt,aa,pp,bgndasymp,string,Tau_s,
                           iind,Aortafix);
%
% The file SPLNLOOP determines the summ of squares between the spleen
% model and the experimental data
%
% D.R. Fine 20-04-93

len        = length(tt);
x          = exp(x);
q          = x(1);
```

```
f         = x(2);
Tau_p     = x(3);
Tau_mp    = x(4);
Tsample   = tt(2)-tt(1);      % Sample Time

eval(['load err',string]);
Lasterror= norm(Error);

% Remove aorta background using the aorta parameters
aa = aa - (1-exp(-tt'/Aortafix))*bgndasymp;

G1 = ((2*x(1) - 1))^100;
G2 = ((2*x(2) - 1))^100;

% Put Marginal Zone Plug Flow
[Am,Bm,Cm,Dm]=tf2ss((1-q)*f,nconv([Tau_s/3 1],3));
[Am,Bm,Cm,Dm]=c2dt(Am,Bm,Cm,Tsample,Tau_mp+Tau_p);

% Put Central Artery in the system
[Ac,Bc,Cc,Dc]=tf2ss(q,nconv([Tau_s/3 1],3));
[Ac,Bc,Cc,Dc]=c2dt(Ac,Bc,Cc,Tsample,0);

% Put Red Pulp
[Ar,Br,Cr,Dr]=tf2ss((1-f)*(1-q),nconv([Tau_s/3 1],3));
[Ar,Br,Cr,Dr]=c2dt(Ar,Br,Cr,Tsample,Tau_p);

% put the systems in parallel
[A1,B1,C1,D1]=parallel(Am,Bm,Cm,Dm,Ac,Bc,Cc,Dc,1,1,1,1);
[As,Bs,Cs,Ds]=parallel(A1,B1,C1,D1,Ar,Br,Cr,Dr,1,1,1,1);

% Convert to Internal Age distribution

% Invert sign of Matrix
Cdd = -Cs;
Ddd = -Ds;

% 1 in state space
Done = 1;
[Aret,Bret,Cret,Dret] = parallel(As,Bs,Cdd,Ddd,0,0,0,Done,1,1,1,1);

% Integrate (ie. multiply by '1/s')
[Aint,Bint,Cint,Dint] = tf2ss(1,[1 0]);
[Aint,Bint] = c2d(Aint,Bint,Tsample);

% Connect
[Aret,Bret,Cret,Dret] = series(Aret,Bret,Cret,Dret,
                               Aint,Bint,Cint,Dint,1,1);

y=dlsim(Aret,Bret,Cret,Dret,aa);
IntY=integ(y(iind:len),Tsample);
IntP=integ(pp(iind:len),Tsample);
K = IntY(len-iind)/IntP(len-iind);

% Determine the summ of squares
Error = norm(y(iind:len)-pp(iind:len)*K,2);
```

```
hold off
clg
subplot(111)
plot(tt,y,'-',tt,pp*K,'x'), title([ string ,
     ' Parenchema : Parametric Model']);
xt = max(tt)/3;
yt = max(y)/3;
text(xt,1.16*yt,['q      = ' num2str(q)  ', f     = ' num2str(f)])
text(xt,1.00*yt,['Tau_p  = ' num2str(Tau_p)])
text(xt,0.86*yt,['Tau_mp = ' num2str(Tau_mp)  ',
     Aortafix    = ' num2str(Aortafix)])
text(xt,0.66*yt,['Error  = ' num2str(norm(Error)) ',
     Last Error  = ' num2str(Lasterror)])

if (norm(Error) < Lasterror)
  eval(['save err',string,' Error']);
  eval(['save Ans',string,' x']);
end,
% ---------------------------------------------------------------------
```

M.1.4 Displays Model Fit to Experimental Data

```
% ---------------------------------------------------------------------
% SPLEEN3 displays the model fit to the experimental data
%
%
% D.R. Fine 20-04-93

load splnbound
load Sret
load Anssplcen
load param
load iind
load aortapara

len
keyboard
tt     = tt(1:len);
aa     = aa(1:len);
ss     = ss(1:len)/factor;
q      = x(1);
f      = x(2);
Tau_s  = 2;
Tau_p  = x(3);
Tau_mp = x(4);
Tsample  = tt(2)-tt(1); % Sample Time

% Remove aorta background using the aorta parameters
aa = aa - (1-exp(-tt'/Aortafix))*bgndasymp;

save aorta aa

% Put Marginal Zone Plug Flow
```

```
[Am,Bm,Cm,Dm]=tf2ss((1-q)*f,nconv([Tau_s/3 1],3));
%[Am,Bm,Cm,Dm]=tf2ss((1-q)*f,conv([Tau_mp 1],nconv([Tau_s/3 1],3)));
%[Am,Bm,Cm,Dm]=c2dt(Am,Bm,Cm,Tsample,Tau_p);
[Am,Bm,Cm,Dm]=c2dt(Am,Bm,Cm,Tsample,Tau_mp+Tau_p);

% Put Central Artery in the system
[Ac,Bc,Cc,Dc]=tf2ss(q,nconv([Tau_s/3 1],3));
[Ac,Bc,Cc,Dc]=c2dt(Ac,Bc,Cc,Tsample,0);

% Put Red Pulp
[Ar,Br,Cr,Dr]=tf2ss((1-f)*(1-q),nconv([Tau_s/3 1],3));
[Ar,Br,Cr,Dr]=c2dt(Ar,Br,Cr,Tsample,Tau_p);

% put the systems in paral  l
[A1,B1,C1,D1]=parallel(Am,Bm,Cm,Dm,Ac,Bc,Cc,Dc,1,1,1,1);
[As,Bs,Cs,Ds]=parallel(A1,B1,C1,D1,Ar,Br,Cr,Dr,1,1,1,1);

% Convert to Interna.    distribution

% Invert sign of Matrix
Cdd = -Cs;
Ddd = -Ds;
% 1 in state space
Done = 1;
[Aret,Bret,Cret,Dret] = parallel(As,Bs,Cdd,Ddd,0,0,0,Done,1,1,1,1);
% Integrate (ie. multiply by '1/s')
[Aint,Bint,Cint,Dint]      s(1,[1 0]);
[Aint,Bint] = c2d(Ain.,     ,Tsample);
% Connect
[Aret,Bret,Cret,Dret] = series(Aret,Bret,Cret,Dret,
                               Aint,Bint,Cint,Dint,1,1);

y=dlsim(Aret,Bret,Cret,Dret,aa);
IntY=integ(y(iind:len),Tsample);
IntP=integ(ss(iind:len),Tsample);
K = IntY(len-iind)/IntP(len-iind);

% Generate RTD, E(t)

E=dimpulse(As,Bs,Cs,Ds,1,len);
Int1=integ(E,Tsample);
E=E/Int1(length(E));

% 1-E(s)
Ca=-Cs;
Da=-Ds;
Aone = 0;
Bone = 0;
Cone = 0;
Done = 1;
[A1E,B1E,C1E,D1E]=parallel(As,Bs,Ca,Da,Aone,Bone,Cone,Done,1,1,1,1);

% 1/s
[A1s,B1s,C1s,D1s]=tf2ss(1,[1 0]);
[A1s,B1s,C1s,D1s]=c2dt(A1s,B1s,C1s,Tsample,0);
```

```
% i/s(1-E(s))
[AI,BI,CI,DI]=series(A1s,B1s,C1s,D1s,A1E,B1E,C1E,D1E,1,1);

% I(t)
I=dimpulse(AI,BI,CI,DI,1,len);

% normalise the area and plot the curves
Int2=integ(I,Tsample);
I=I/Int2(length(I));

% normalise the Non-Parametric curve

fA = fft(aa);
fS = fft(ss);
HSfft2 = fili(real(ifft(fS./fA)),4);
ind=len-20;
Int3=integ(HSfft2(1:ind),Tsample);
HSfft2=HSfft2/Int3(length(Int3));

% ********************************************************
hold off
clg
subplot(111)
plot(tt,E),pause;
title('Spleen E(t)');
xlabel('Time (s)');
ylabel('E(t)');
!del E_t.met
meta E_t

plot(tt,y,'-',tt,ss*K,'w.'), title(['Spleen : Parametric Model']);
xlabel('Time (s)');
ylabel('Counts/px.s'),pause;
!del Spleen.met
meta Spleen

plot(tt(2:len-1),I(2:len-1),tt(2:len-10),HSfft2(2:len-10),'w.');
title('I(t): Parametric vs Non-Parametric');
xlabel('Time (s)');
ylabel('I(t)');
xt = max(tt)+30;
yt = max(I)/2;
text(xt,1.0*yt,['q      = ' num2str(q)      ', f
                = ' num2str(f)])
text(xt,1.4*yt,['Tau_s  = ' num2str(Tau_s)  ',     Tau_p
                = ' num2str(Tau_p)])
text(xt,1.8*yt,['Tau_mp = ' num2str(Tau_mp) ', Aortafix
                = ' num2str(Aortafix)])

!del I_t.met
meta I_t

save Allspleen
% ---------------------------------------------------------------
```

Appendix N

N.1 Liver Programs in Matlab-386^{TM}

N.1.1 Process the Raw Liver Data

```
% ------------------------------------------------------------------------
% LIVER1 processes the raw liver
%
% This file
% 1) Loads and Cleans the data from the ascii file
% 2) Bounds the data using BOUND.M
% 3) Interpolates the data to 1 seconds
% 4) Deconvolves the data using : Filtered FFT Method
%
% D.R. Fine 20-04-93

load Splnbound
load Anasspleen
load param
load mind
load aorta
len = length(aa);

% Get GIT info
eval(['load Liver1.asc']);
eval(['load Liver2.asc']);

L   = [Liver1(:,3);Liver2(:,3)];
T   = [Liver1(:,2);Liver2(:,2)];
ll  = L;

save LIVER L

hold off
clg
subplot(111)
plot(T,L), grid
title(['Original Liver Data: ', Date]),  xlabel('Seconds')
```

```
% use BOUND.M to non-linear filter the data to remove poisson noise.
% minind is determined in spleen1.m

decifactor = 2;
ll = [decimate(ll(minind:121),decifactor,'FIR') ; ll(122:length(T))];
tt = 0:1000;
tt = tt(1:length(ll));

looptimes = 6; % See Spleen

Q = 5;
ind = find(ll<=0);
ll(ind) = 0.001*ones(length(ind),1);
lnew=ll;
for i = 1:looptimes;
lnew = bound(lnew,Q,5);
plot(tt,ll,tt,lnew), title('Liver : Data Bounding'),
Q = Q/2;
end,

clg
subplot(111)
plot(tt,ll,'w.',tt,lnew), title('Liver : Data Bounding'),pause
subplot(111)
ll = lnew;
ll=ll(1:len);
tt=tt(1:len);
subplot(111)
clg
hold off
plot(tt(1:30),aa(1:30),tt(1:30),ll(1:30))
% Remove the initial liver background activity
title('Select Subtract Point')
[x,y] = ginput(1);
[scal,sind]    = min((tt-x).^2);

ll = ll(1:len)-ll(sind);
ll(1)=0;
ind=find(ll<0);
ll(ind)=eps*ones(length(ind),1);

% Scale the liver data by the maximum value and the time at which
% this maximum occurs
[lmax,lmaxind]=max(ll);
ll=ll/lmax;
t_max=tt(lmaxind);
tt=tt/t_max;

hold off
clg
subplot(111)
plot(tt,ll,'-'), grid, title(['Interpolated and Data Bounded : ',
     Date]),  xlabel('Seconds'), pause

save Liverbound aa ll tt t_max
```

```
% Perform the Non-Parametric Deconvolution using the filtered FFT Method
fA  = fft(aa);
fL  = fft(ll);
fAs = fft(aa(1:len));

HLfft2 = fill(real(ifft(fL./fA)),4);

hold off
clg
subplot(111)
plot(tt,HLfft2), grid, ylabel('Equivqlent I'), xlabel('Seconds'),
     title('Filtered FFT'),

save Lret HLfft2
% ------------------------------------------------------------------
```

N.1.2 Fit Liver Model to Experimental Data

```
% ------------------------------------------------------------------
% LIVER2 fits the model of the liver to the experimental
% data
%
% D.R. Fine 20-04-93

clear
pack

load splnbound
load liverbound
load anspleen
load iind
load aorta

len = length(aa)
keyboard;
Error = 1e6;
save errLiver Error
ll = ll(1:len);
aa = aa(1:len);
tt = tt(1:len);
tt=tt(:);
ll=ll(:);
pp=ll;
clear Error
clear ss;

% Spleen Model Parameter determined by Spleen2.m
q      = x(1);
f      = x(2);
Tau_s  = 2/t_max;
Tau_p  = x(3)/t_max;
Tau_mp = x(4)/t_max;
xsp = [q f Tau_p Tau_mp Tau_s]; % Spleen Parameter Vector
```

```
%Initial Guesses
Tau_dl   = 0.2;              %Liver Delay time in the sinusoids
Delay_pv = 0.1;              %Central Vein Delay.
r        = 0.76;             %0.76 Fraction to the Portal System
p        = 0.2;              %0.2  Fraction to the Spleen
% igueses.m alows one to choose the hepatic arterial delay time
Delay_ah = iguesses(tt,len,t_max); %hepatic arterial delay time
Tau_gi   = 0.5;              %Mixing in the GIT
Tau_cv   = 2/t_max;          %Central Vein Mixing Constant

x0 = [Tau_dl Delay_pv r p Tau_gi]; % initial guess
keyboard
x0=log(x0);
save Delay_ah Delay_ah
string = 'Liver';

global aa xsp string iind Tau_cv Delay_ah ll
Time = tt;
pp   = ll;
clear tt

          %Levenberg-M- quart to get Final Estimates
[funcval,x,var,iter,Correlation,std]=leasqr(Time,pp,x0,'livloop2',
                                              ie-4,20)
% ------------------------------------------------------------------
```

N.1.3 Objective Function 1 for Model Fitting Program

```
% ------------------------------------------------------------------
function Funceval = livloop(x,tt,aa,ll,xsp,string,iind,Tau_cv,
                            Delay_ah,Delay_pv);
%function Funceval = livloop(x,tt,aa,ll,xsp,string,iind,Tau_cv,
%                            Delay_ah,Delay_pv);
%
% The file LIVLOOP1 determines the summ of squares between the liver
% model and the experimental data for the simplex algorithm.
%
% D.R. Fine 20-04-93

len    = length(tt);
% The spleen values obtained from spleen2.m
q      = xsp(1);
f      = xsp(2);
Tau_s  = xsp(5);
Tau_p  = xsp(3);
Tau_mp = xsp(4);

% Ensures that the values of x are always positive
x=exp(x);

Tau_dl   = x(1);          %Liver Delay time in the sinusoids
Delay_pv = x(2);          %Central Vein Delay.
```

```
r        = x(3);           %0.76 Fraction to the Portal System
p        = x(4);           %0.2  Fraction to the Spleen
Tau_gi   = x(5);           %Mixing in the GIT
Tau_ha   = r*Tau_dl/(1-r); %Residence time associated with
                           %the Hepatic Artery Flow
Tsample  = tt(2)-tt(1);    % Sample Time

eval(['load err',string]);
Lasterror=norm(Error);

% ------------------------Begin of Spleen-----------------------------
% Put Marginal Zone Plug Flow
[Am,Bm,Cm,Dm]=tf2ss(p*(1-q)*f,nconv([Tau_s/3 1],3));
[Am,Bm,Cm,Dm]=c2dt(Am,Bm,Cm,Tsample,Tau_mp+Tau_p+Delay_pv);

% Put Cental Artery in the system
[Ac,Bc,Cc,Dc]=tf2ss(p*q,nconv([Tau_s/3 1],3));
[Ac,Bc,Cc,Dc]=c2dt(Ac,Bc,Cc,Tsample,Delay_pv);

% Put Red Pulp
[Ar,Br,Cr,Dr]=tf2ss(p*(1-f)*(1-q),nconv([Tau_s/3 1],3));
[Ar,Br,Cr,Dr]=c2dt(Ar,Br,Cr,Tsample,Tau_p+Delay_pv);

% put the systems in parallel
[A1,B1,C1,D1]=parallel(Am,Bm,Cm,Dm,Ac,Bc,Cc,Dc,1,1,1,1);
[As,Bs,Cs,Ds]=parallel(A1,B1,C1,D1,Ar,Br,Cr,Dr,1,1,1,1);
% ------------------------End of Spleen-------------------------------

% ------------------------Begin of GIT--------------------------------
% Put Marginal Zone Plug Flow
[A  ,Bgi,Cgi,Dgi]=tf2ss((1-p),nconv([Tau_gi 1],3));
[Agi,Bgi,Cgi,Dgi]=c2dt(Agi,Bgi,Cgi,Tsample,Delay_pv);
% ------------------------End of GIT----------------------------------

% ------------------------Begin of Portal-----------------------------
% Put Spleen and GIT in Parallel
[Apv,Bpv,Cpv,Dpv]=parallel(As,Bs,Cs,Ds,Agi,Bgi,Cgi,Dgi,1,1,1,1);
% ------------------------End of Portal-------------------------------

% ------------------------Begin of Liver------------------------------
% Term1 of formulation
[A11,B11,C11,D11]=tf2ss(1,[Tau_ha 1]);
[A11,B11,C11,D11]=c2dt(A11,B11,C11,Tsample,Delay_ah);

% Term 2 of formulation
[A12,B12,C12,D12]=tf2ss(-r,[Tau_ha 1]);
[A12,B12,C12,D12]=c2dt(A12,B12,C12,Tsample,Delay_ah +
                  Tau_ha*log(1/r));

% Sum Term1 and Term2
[A13,B13,C13,D13]=parallel(A11,B11,C11,D11,A12,B12,C12,D12,1,1,1,1);

% Term3 of formulation added to Terms 1 and 2
[A14,B14,C14,D14]=tf2ss(r,[1e-8 1]);
[A14,B14,C14,D14]=c2dt(A14,B14,C14,Tsample,Tau_ha*log(1/r));
[A14,B14,C14,D14]=series(A14,B14,C14,D14,Apv,Bpv,Cpv,Dpv,1,1);
```

```
[A14,B14,C14,D14]=parallel(A14,B14,C14,D14,A13,B13,C13,D13,1,1,1,1);

% Central Vein Mixing in series with the formulation
[A15,B15,C15,D15]=tf2ss(1,nconv([Tau_cv/2 1],2));
[A15,B15,C15,D15]=c2dt(A15,B15,C15,Tsample,0);
[AL,BL,CL,DL]=series(A15,B15,C15,D15,A14,B14,C14,D14,1,1);
% ------------------------End of Liver-------------------------------
% Convert to Internal Age distribution equivalent using multiple
% input system equation

% 1/s in state space
[Aint,Bint,Cint,Dint]=tf2ss(1,[1 0]);
[Aint,Bint,Cint,Dint]=c2dt(Aint,Bint,Cint,Tsample,0);

[A1,B1,C1,D1]=series(0,0,0,r,Apv,Bpv,Cpv,Dpv,1,1);
[A2,B2,C2,D2]=tf2ss(1-r,[1e-8 1]);
[A2,B2,C2,D2]=c2dt(A2,B2,C2,Tsample,Delay_ah);
[A2,B2,C2,D2]=parallel(A2,B2,C2,D2,A1,B1,C1,D1,1,1,1,1);
[A3,B3,C3,D3]=parallel(A2,B2,C2,D2,AL,BL,-CL,-DL,1,1,1,1);
[A,B,C,D]=series(Aint,Bint,Cint,Dint,A3,B3,C3,D3,1,1);

y=dlsim(A,B,C,D,aa);
Iy=integ(y(iind:len),Tsample);
Ip=integ(ll(iind:len),Tsample);
K = Iy(len-iind)./Ip(len-iind);
% Determine the sum of squares
Funceval = norm((y(1:len)-ll*K),2);

hold off
clg
subplot(111)
plot(tt,y/K,tt,ll,'x');
title(' Liver : Parametric Model');

xt = max(tt)/3;
yt = max(ll)/3;
Error = sum(((y(13:len)/K - ll(13:len)).^2)./(y(13:len)/K));
text(xt,1.16*yt,['r      = ' num2str(r)  ', p           = ' num2str(p)])
text(xt,1.00*yt,['Tau_gi = ' num2str(Tau_gi)  ', Tau_cv    = '
                 num2str(Tau_cv)])
text(xt,0.86*yt,['Tau_dl = ' num2str(Tau_dl)  ', Delay_pv    =
                 ' num2str(Delay_pv)])
text(xt,0.68*yt,['Delay_ah = ' num2str(Delay_ah)])
text(xt,0.46*yt,['Error  = ' num2str(norm(Error)) ', Last Error
                 = ' num2str(Lasterror)])
if Error  < Lasterror
  eval(['save err',string,' Error']);
  eval(['save Ans',string,' x']);
end,
return
% ------------------------------------------------------------------
```

N.1.4 Objective Function 2 for Model Fitting Program

```
% ------------------------------------------------------------------
function Funceval = livloop(tt,x);
%function Funceval = livloop(tt,x);
%
% The file LIVLOOP2 determines the function value for a given
% parameter space for the Levenberg-Marquart Algorithm
%
% D.R. Fine 20-04-93

len    = length(tt);
% The spleen values obtained from spleen2.m
q      = xsp(1);
f      = xsp(2);
Tau_s  = xsp(5);
Tau_p  = xsp(3);
Tau_mp = xsp(4);

% Ensures that the values of x are always positive
x=exp(x);

Tau_dl   = x(1);            %Liver Delay time in the sinusoids
Delay_pv = x(2);            %Central Vein Delay.
r        = x(3);            %0.76 Fraction to the Portal System
p        = x(4);            %0.2  Fraction to the Spleen
Tau_gi   = x(5);            %Mixing in the GIT
Tau_ha   = r*Tau_dl/(1-r); %Residence time associated with
                            %the Hepatic Artery Flow

Tsample = tt(2)-tt(1);

if Tau_dl > 2
  Tau_dl = 1;
  Tau_ha = r*Tau_dl/(1-r);
end

if Delay_pv <= 0
  Delay_pv = eps;
end
if Delay_pv > 2
  Delay_pv = 1;
end

eval(['load err',string]);
Lasterror=norm(Error);

% ------------------------Begin of Spleen-------------------------
% Put Marginal Zone Plug Flow
[Am,Bm,Cm,Dm]=tf2ss(p*(1-q)*f,nconv([Tau_s/3 1],3));
[Am,Bm,Cm,Dm]=c2dt(Am,Bm,Cm,Tsample,Tau_mp+Tau_p+Delay_pv);

% Put Central Artery in the system
[Ac,Bc,Cc,Dc]=tf2ss(p*q,nconv([Tau_s/3 1],3));
[Ac,Bc,Cc,Dc]=c2dt(Ac,Bc,Cc,Tsample,Delay_pv);
```

```
% Put Red Pulp
[Ar,Br,Cr,Dr]=tf2ss(p*(1-f)*(1-q),nconv([Tau_s/3 1],3));
[Ar,Br,Cr,Dr]=c2dt(Ar,Br,Cr,Tsample,Tau_p+Delay_pv);

% put the systems in parallel
[A1,B1,C1,D1]=parallel(Am,Bm,Cm,Dm,Ac,Bc,Cc,Dc,1,1,1,1);
[As,Bs,Cs,Ds]=parallel(A1,B1,C1,D1,Ar,Br,Cr,Dr,1,1,1,1);
% ----------------------------End of Spleen-------------------------------

% ----------------------------Begin of GIT--------------------------------
% Put Marginal Zone Plug Flow
[Agi,Bgi,Cgi,Dgi]=tf2ss((1-p),nconv([Tau_gi 1],3));
[Agi,Bgi,Cgi,Dgi]=c2dt(Agi,Bgi,Cgi,Tsample,Delay_pv);
% ----------------------------End of GIT----------------------------------

% ----------------------------Begin of Portal-----------------------------
% Put Spleen and GIT in Parallel
[Apv,Bpv,Cpv,Dpv]=parallel(As,Bs,Cs,Ds,Agi,Bgi,Cgi,Dgi,1,1,1,1);
% ----------------------------End of Portal-------------------------------

% ----------------------------Begin of Liver------------------------------
% Termi of formulation
[A11,B11,C11,D11]=tf2ss(1,[Tau_ha 1]);
[A11,B11,C11,D11]=c2dt(A11,B11,C11,Tsample,Delay_ah);

% Term 2 of formulation
[A12,B12,C12,D12]=tf2ss(-r,[Tau_ha 1]);
[A12,B12,C12,D12]=c2dt(A12,B12,C12,Tsample,Delay_ah +
                  Tau_ha*log(1/r));

% Sum Termi and Term2
[A13,B13,C13,D13]=parallel(A11,B11,C11,D11,A12,B12,C12,D12,1,1,1,1);

% Term3 of formulation added to Terms 1 and 2
[A14,B14,C14,D14]=tf2ss(r,[1e-8 1]);
[A14,B14,C14,D14]=c2dt(A14,B14,C14,Tsample,Tau_ha*log(1/r));
[A14,B14,C14,D14]=series(A14,B14,C14,D14,Apv,Bpv,Cpv,Dpv,1,1);
[A14,B14,C14,D14]=parallel(A14,B14,C14,D14,A13,B13,C13,D13,1,1,1,1);

% Central Vein Mixing in series with the formulation
[A15,B15,C15,D15]=tf2ss(1,nconv([Tau_cv/2 1],2));
[A15,B15,C15,D15]=c2dt(A15,B15,C15,Tsample,0);
[AL,BL,CL,DL]=series(A15,B15,C15,D15,A14,B14,C14,D14,1,1);
% ----------------------------End of Liver--------------------------------
% Convert to Internal Age distribution equivalent using multiple
% input system equation

% 1/s in state space
[Aint,Bint,Cint,Dint]=tf2ss(1,[1 0]);
[Aint,Bint,Cint,Dint]=c2dt(Aint,Bint,Cint,Tsample,0);

[A1,B1,C1,D1]=series(0,0,0,r,Apv,Bpv,Cpv,Dpv,1,1);
[A2,B2,C2,D2]=tf2ss(1-r,[1e-8 1]);
[A2,B2,C2,D2]=c2dt(A2,B2,C2,Tsample,Delay_ah);
[A2,B2,C2,D2]=parallel(A2,B2,C2,D2,A1,B1,C1,D1,1,1,1,1);
```

```
[A3,B3,C3,D3]=parallel(A2,B2,C2,D2,AL,BL,-CL,-DL,1,1,1,1);
[A,B,C,D]=series(Aint,Bint,Cint,Dint,A3,B3,C3,D3,1,1);

y=dlsim(A,B,C,D,aa);
Iy=integ(y(iind:len),Tsample);
Ip=integ(ll(iind:len),Tsample);
K = Iy(len-iind)./Ip(len-iind);
% Determine the function value
Funceval = y(1:le. )/K;

hold off
clg
subplot(111)
plot(tt,y/K,tt,ll,'x');
title(' Liver : Parametric Model');

xt = max(tt)/3;
yt = max(ll)/3;
Error = sum(((y(13:len)/K - ll(13:len)).^2)./(y(13:len)/K));
text(xt,1.16*yt,['r       = ' num2str(r)  ', p           = ' num2str(p)])
text(xt,1.00*yt,['Tau_gi = ' num2str(Tau_gi)  ', Tau_cv
                  = ' num2str(Tau_cv)])
text(xt,0.86*yt,['Tau_dl = ' num2str(Tau_dl)  ', Delay_pv
                  = ' num2str(Delay_pv)])
text(xt,0.66*yt,['Delay_ah = ' num2str(Delay_ah)])
text(xt,0.46*yt,['Error  = ' num2str(norm(Error)) ', Last Error
                  = ' num2str(Lasterror)])
if Error  < Lasterror
  eval(['save err',string,' Error']);
  eval(['save Ans',string,' x']);
end,
return
% ------------------------------------------------------------------------
```

N.1.5 Displays Model Fit to Experimental Data

```
% ------------------------------------------------------------------------
% LIVER3 displays the model fit to the experimental data
%
%
% D.R. Fine 20-04-93

load liverbound
load Lret
load aorta
load Ansspleen
load iind
q      = x(1);
f      = x(2);
Tau_s  = 2/t_max;
Tau_p  = x(3)/t_max;
Tau_mp = x(4)/t_max;
len=length(aa)
```

```
keyboard
tt=tt(1:len);
aa=aa(1:len);
ll=ll(1:len);

load Ansliver
load Delay_ah
Tau_dl    = x(1);              %Liver Delay time in the sinusoids
Delay_pv  = x(2);              %Central Vein Delay
r         = x(3);              %0.76 Fraction to the Portal System
p         = x(4);              %0.2  Fraction to the Spleen
Tau_gi    = x(5);              %Mixing in the GIT
Tau_cv    = 0.04;              %Central Vein Mixing Constant
Tau_ha    = r*Tau_dl/(1-r);    %Residence time associated with
                               %the Hepatic Artery Flow

Tsample  = tt(2)-tt(1); % Sample Time

% ------------------------------Begin of Spleen--------------------------------
% Put Marginal Zone Plug Flow
[Am,Bm,Cm,Dm]=tf2ss(p*(1-q)*f,nconv([Tau_s/3 1],3));
[Am,Bm,Cm,Dm]=c2dt(Am,Bm,Cm,Tsample,Tau_mp+Tau_p+Delay_pv);

% Put Cental Artery in the system
[Ac,Bc,Cc,Dc]=tf2ss(p*q,nconv([Tau_s/3 1],3));
[Ac,Bc,Cc,Dc]=c2dt(Ac,Bc,Cc,Tsample,Delay_pv);

% Put Red Pulp
[Ar,Br,Cr,Dr]=tf2ss(p*(1-f)*(1-q),nconv([Tau_s/3 1],3));
[Ar,Br,Cr,Dr]=c2dt(Ar,Br,Cr,Tsample,Tau_p+Delay_pv);

% put the systems in parallel
[A1,B1,C1,D1]=parallel(Am,Bm,Cm,Dm,Ac,Bc,Cc,Dc,1,1,1,1);
[As,Bs,Cs,Ds]=parallel(A1,B1,C1,D1,Ar,Br,Cr,Dr,1,1,1,1);
% -------------------------------End of Spleen---------------------------------

% ------------------------------Begin of GIT-----------------------------------
% Put Marginal Zone Plug Flow
[Agi,Bgi,Cgi,Dgi]=tf2ss((1-p),nconv([Tau_gi 1],3));
[Agi,Bgi,Cgi,Dgi]=c2dt(Agi,Bgi,Cgi,Tsample,Delay_pv);
% -------------------------------End of GIT------------------------------------

% ------------------------------Begin of Portal--------------------------------
% Put Spleen and GIT in Parallel
[Apv,Bpv,Cpv,Dpv]=parallel(As,Bs,Cs,Ds,Agi,Bgi,Cgi,Dgi,1,1,1,1);
% -------------------------------End of Portal---------------------------------

% ------------------------------Begin of Liver---------------------------------
% Termi of formulation
[A11,B11,C11,D11]=tf2ss(1,[Tau_ha 1]);
[A11,B11,C11,D11]=c2dt(A11,B11,C11,Tsample,Delay_ah);

% Term 2 of formulation
[A12,B12,C12,D12]=tf2ss(-r,[Tau_ha 1]);
[A12,B12,C12,D12]=c2dt(A12,B12,C12,Tsample,Delay_ah +
                  Tau_ha*log(1/r));
```

```
% Sum Term1 and Term2
[A13,B13,C13,D13]=parallel(A11,B11,C11,D11,A12,B12,C12,D12,1,1,1,1);

% Term3 of formulation added to Terms 1 and 2
[A14,B14,C14,D14]=tf2ss(r,[1e-8 1]);
[A14,B14,C14,D14]=c2dt(A14,B14,C14,Tsample,Tau_ha*log(1/r));
[A14,B14,C14,D14]=series(A14,B14,C14,D14,Apv,Bpv,Cpv,Dpv,1,1);
[A14,B14,C14,D14]=parallel(A14,B14,C14,D14,A13,B13,C13,D13,1,1,1,1);

% Central Vein Mixing in series with the formulation
[A15,B15,C15,D15]=tf2ss(1,nconv([Tau_cv/2 1],2));
[A15,B15,C15,D15]=c2dt(A15,B15,C15,Tsample,0);
[AL,BL,CL,DL]=series(A15,B15,C15,D15,A14,B14,C14,D14,1,1);
% ----------------------------End of Liver-----------------------------
% Convert to Internal Age distribution equivalent using multiple
% input system equation

% 1/s in state space
[Aint,Bint,Cint,Dint]=tf2ss(1,[1 0]);
[Aint,Bint,Cint,Dint]=c2dt(Aint,Bint,Cint,Tsample,0);

[A1,B1,C1,D1]=series(0,0,0,r,Apv,Bpv,Cpv,Dpv,1,1);
[A2,B2,C2,D2]=tf2ss(1-r,[1e-8 1]);
[A2,B2,C2,D2]=c2dt(A2,B2,C2,Tsample,Delay_ah);
[A2,B2,C2,D2]=parallel(A2,B2,C2,D2,A1,B1,C1,D1,1,1,1,1);
[A3,B3,C3,D3]=parallel(A2,B2,C2,D2,AL,BL,-CL,-DL,1,1,1,1);
[A,B,C,D]=series(Aint,Bint,Cint,Dint,A3,B3,C3,D3,1,1);

y=dlsim(A,B,C,D,aa);
Iy=integ(y(iind:len),Tsample);
Ip=integ(ll(iind:len),Tsample);
K = Iy(len-iind)./Ip(len-iind);

% Generate RTD
E=dimpulse(AL,BL,CL,DL,1,len);
Int1=integ(E,Tsample);
E=E/Int1(len);

subplot(111)
plot(tt,E);
title('Liver E(t)');
xlabel('Time (s)');
ylabel('E(t)'),pause;
!del LE_t.met
meta LE_t

% Normalise the Non-Parametric deconvolved curves
fA = fft(aa);
fL = fft([zeros(11,1);ll(13)/2;ll(13:len)]);
HLfft2 = fill(real(ifft(fL./fA)),4);

% Eb(t)*I(t)
Et_It=dimpulse(A,B,C,D,1,len);
subplot(111)
plot(tt,Et_It,tt,HLfft2*K/2);
```

```
title('Liver effective I(t)');
xlabel('Time (s)');
ylabel('E(t)*I(t)'),pause;
!del Et_It.met
meta Et_It

plot(tt(1:len-1),y(1:len-1),'-',tt(1:len-1),ll(1:len-1)*K,'x');
title(['Spleen : Parametric Model']);
xlabel('Time (s)');
ylabel('Counts/px.s')
!del Liver.met
meta Liver
xt = max(tt)+30;
yt = max(I)/2;
chi_sq_data = sum(((y(13:len)/K - ll(13:len)).^2)./(y(13:len)/K));
chi_sq_actu = 20.71;
text(xt,1.0*yt,['q      = ' num2str(q)      ', f
                = ' num2str(f)])
text(xt,1.4*yt,['Tau_s  = ' num2str(Tau_s)  ',     Tau_p
                = ' num2str(Tau_p)])
text(xt,1.8*yt,['Tau_mp = ' num2str(Tau_mp) ', Aortafix
                = ' num2str(x(5))])
% ------------------------------------------------------------------------
```

Appendix O

O.1 Correlation Matrix Programs in Matlab-386^{TM}

O.1.1 Determination of the Sensitivity Matrix

```
% ------------------------------------------------------------------
% This matlab file finds the sensitivity matrix of a model at the
% minimum of the objective function of the liver.  The same program
% is used for the other organs except the model is changed.
%
%
% D.R. Fine 01-08-93

load splnbound
load liverbound
load anspleen
load iind
load aorta

len = length(aa)
keyboard;
Error = 1e6;
save errLiver Error
ll = ll(1:len);
aa = aa(1:len);
tt = tt(1:len);

clear Error
clear ss;

% Spleen Values
q      = x(1);
f      = x(2);
Tau_s  = 2/t_max;
Tau_p  = x(3)/t_max;
Tau_mp = x(4)/t_max;
xsp = [q f Tau_p Tau_mp Tau_s]; % initial guess

%Initial Guesses
```

```
]      \sliver
lo x Delay_ah
Tau_cv    = 2/t_max;          %Central Vein Mixing Constant
Tau_dl    = x(1);             %Liver Delay time in the sinusoids
Delay_pv  = x(2);             %Central Vein Delay.
r         = x(3);             %0.76 Fraction to the Portal System
y         = Tau_dl*r;
z         = Delay_pv*r;
p         = x(4);              %0.2  Fraction to the Spleen
Tau_gi    = x(5);              %Mixing in the GIT
Tau_cv    = 0.04;              %Central Vein Mixing Constant
x0 = [y Delay_pv r p Tau_gi]; %initial guess
string = 'Liver';
xold = x0;
X = [];

% Calculate the derivatives of the function with respect to the parameters
% at the minimum.  The model may be found using kidloop.m, livloop.m or
% splnloop.m with the appropriate parameter structure without determining
% the least squares estimate but just evaluating the function at the
% minimum.
for j = 1:length(x0)
    x0   = xold;
    x0(j)= xold(j)*0.99;
    low  = x0(j);
    Xlow = model(x0,tt,aa,ll,xsp,string,Delay_ah,iind,Tau_cv)/
           (len-length(x0));
    x0(j)= xold(j)*1.01;
    high = x0(j);
    Xhigh= model(x0,tt,aa,ll,xsp,string,Delay_ah,iind,Tau_cv)/
           (len-length(x0));
    d    = high - low;
    X    = [X (Xhigh - Xlow)/ d];
end
save sensitive X len
% ------------------------------------------------------------------------
```

O.1.2 Determination of the Correlation Matrix

```
% ------------------------------------------------------------------------
% Program to calculate the correlation matrix given the sensitivity
% and sum of squares values
%
%
% D.R. Fine 01-08-93

load sensitive
load liverbound
load summsq
omega = eye(len,len);
psi = omega*summsq;
Cov = inv(X'*inv(psi)*X);
save Covariance Cov
```

```
for i = 1:length(Cov(:,1))
  for j = 1:length(Cov(:,1))
    Correlation(i,j) = Cov(i,j)*(Cov(i,i)*Cov(j,j))^(-0.5);
  end
end

save Correlation Correlation
Eigen=eig(Correlation);
save Eigen Eigen
% ---------------------------------------------------------------------
```

Appendix P

P.1 Aorta Background Correction Programs in Matlab 386™

P.1.1 Global Aorta Background Program

```
% ------------------------------------------------------------------
% GETAORTA Dtermined the amount of aorta backgroung
%
% This file
% 1) Determines the aorta that minimizes the negative component in a
% deconvolution study.  This program has been used to determine the
% aorta for the sleen (and thus liver) but an analogous program has
% been used for the kidney.
%
% D.R. Fine 20-04-93

load splnbound  % Load non-parametric time data
len=length(aa)
keyboard
factor    = max(ss)/max(aa);
ss        = ss(1:len)/factor;
tt        = tt(1:len);
aa        = aa(1:len);
% Estimate the amount of background in t.   orta as 1/3
bgndasymp   = 0.6667*aa(len);
% Estimate the confidence time interval as 100s
Aortafix    = 100;
options(1)  = 0; % Do not print the results after each itteration
options(3)  = 1; % Termination criteria for minimised function
options(14) = 50; % Maximum iterations
x0=log([Aortafix,bgndasymp]);
HSfft2      = fill(real(ifft(fft(ss)./fft(aa))),5);
ind1        = min(find(HSfft2<0));
[minv ind2] = min((tt-2*tt(ind1)) ^2);

              % Levenberg-Marquard to minimize the negative component
x           = fminu('aortamin',x0,options,[],ss,aa,tt,[ind1 ind2]);
```

```
Aortafix    = exp(x(1));
bgndasymp   = exp(x(2));
save aortapara Aortafix bgndasymp
% ------------------------------------------------------------------
```

P.1.2 Objective Function for Aorta Background Minimisation

```
% ------------------------------------------------------------------
function Err = bgndasymp(x,ss,aa,tt,bound);
%function Err = bgndasymp(x,ss,aa,tt,bound);
% The file AORTAMIN determines size of the negative component in the
% deconvolved spleen curve.  See getaorta.m
%
% D.R. Fine 20-04-93

x=exp(x);

len=length(aa);
if (aa(len) - (1-exp(-tt(len)/x(1)))*x(2)) < mean(ss(len-20:len))*0.5
  Err = 1e6;
  return
end

% Remove the aorta background
aanew=aa-(1-exp(-tt'/x(1)))*x(2);
% Perform the Non-Parametric Deconvolution using the filtered FFT
% Method
fA      = fft(aanew);
fL      = fft(ss);
HSfft2  = fill(real(ifft(fL./fA)),5);
Err = min((mean(HSfft2(bound(1):bound(2))) - 0).^2);
plot(tt,HSfft2,tt,aanew*max(HSfft2)/max(aanew)), grid,
ylabel('Left'), xlabel('Seconds'), title('Filtered FFT'),
xt = max(tt)/3;
yt = max(HSfft2)/3;
text(xt,1.16*yt,['Aortafix =  ' num2str(x(1)) ', Bgndasymp = '
     num2str(x(2))]);
end
% ------------------------------------------------------------------
```

Appendix Q

Q.1 Renal Model Compared with Raw Renal Data

The raw data displayed in this appendix appears on a 1.44MB magnetic disk which may be found in Appendix S.1.

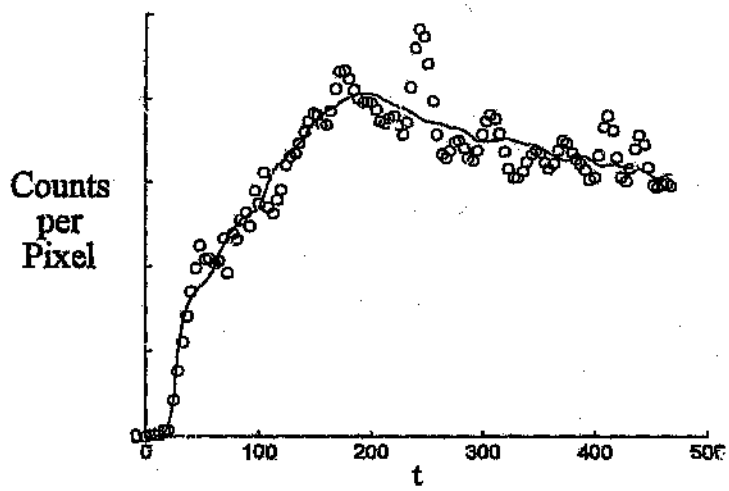

Figure Q.1: Typical fit of the renal model to the experimental renal activity/time curve. ——— Model, o Experimental data for kidney 1

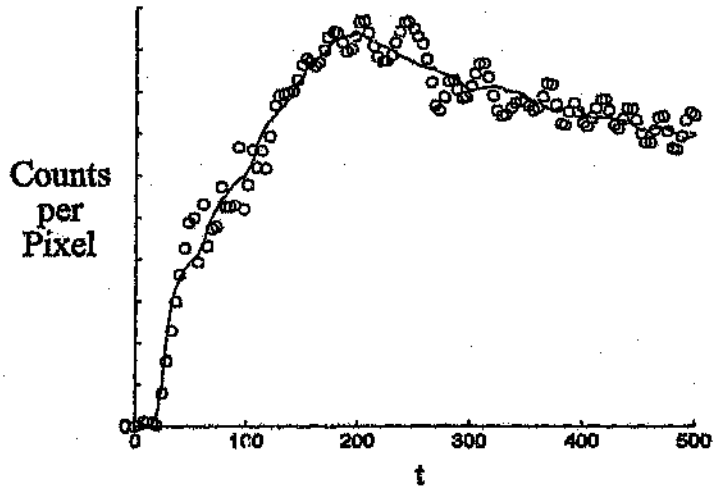

Figure Q.2: Typical fit of the renal model to the experimental renal activity/time curve. ——— Model, ○ Experimental data for kidney 2

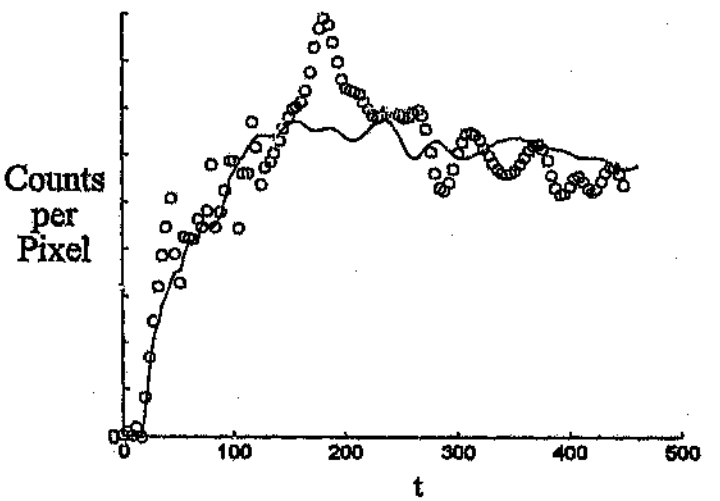

Figure Q.3: Typical fit of the renal model to the experimental renal activity/time curve. ——— Model, ○ Experimental data for kidney 3

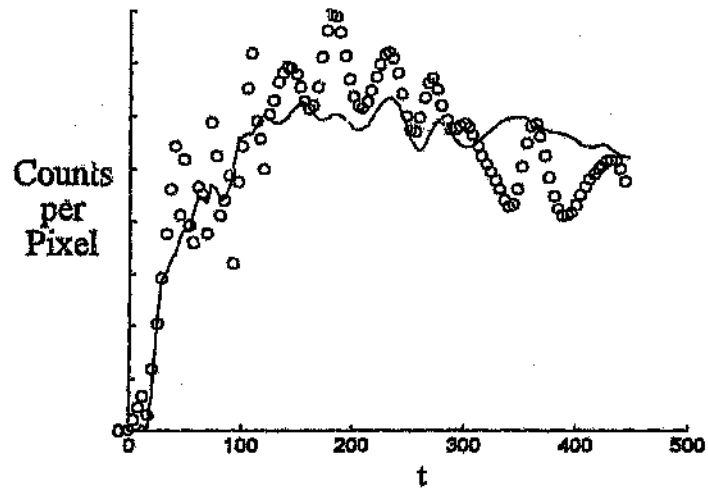

Figure Q.4: Typical fit of the renal model to the experimental renal activity/time curve. ——— Model, o Experimental data for kidney 4

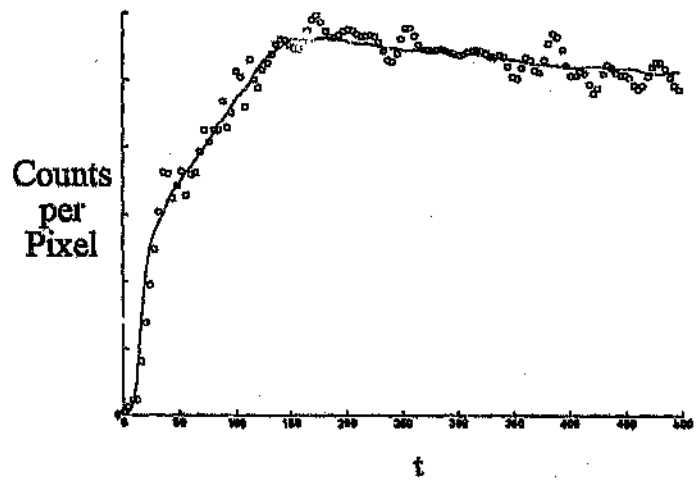

Figure Q.5: Typical fit of the renal model to the experimental renal activity/time curve. ——— Model, o Experimental data for kidney 5

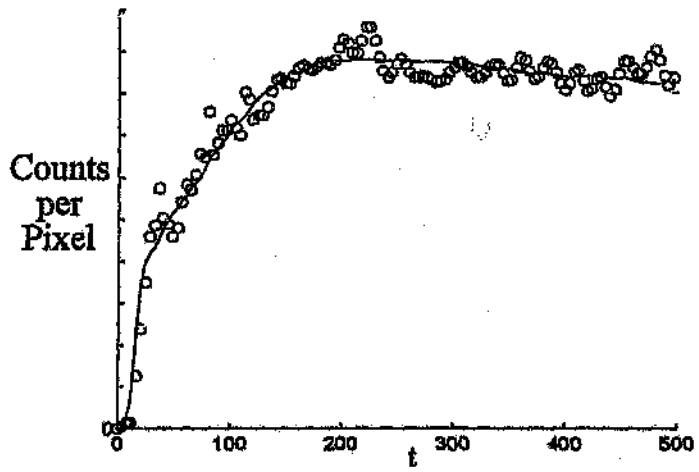

Figure Q.6: Typical fit of the renal model to the experimental renal activity/time curve. ——— Model, ○ Experimental data for kidney 6

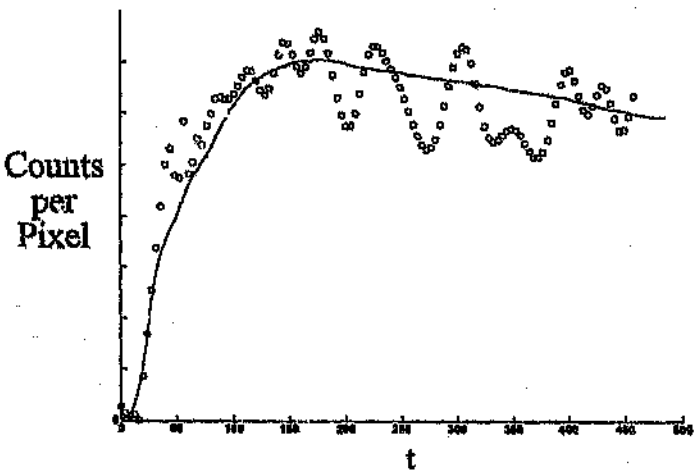

Figure Q.7: Typical fit of the renal model to the experimental renal activity/time curve. ——— Model, ○ Experimental data for kidney 7

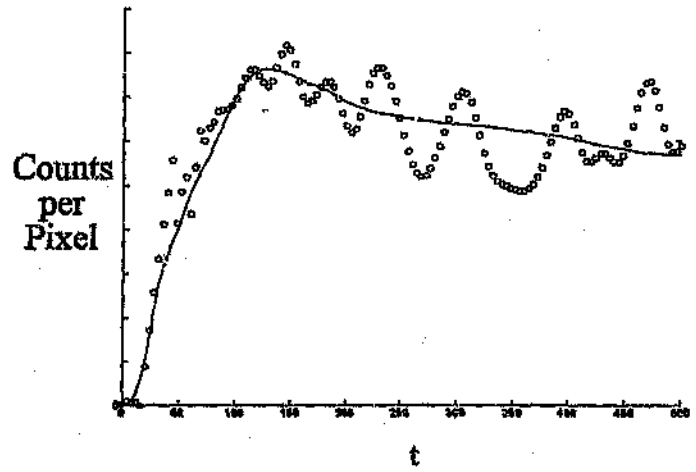

Figure Q.8: Typical fit of the renal model to the experimental renal activity/time curve. ——— Model, o Experimental data for kidney 8

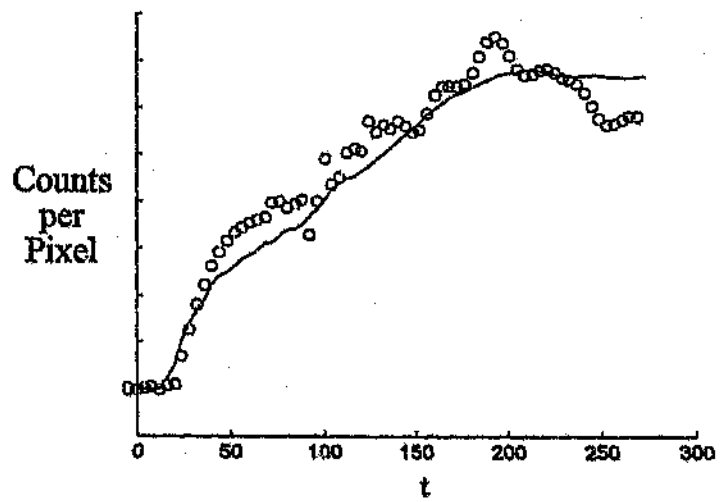

Figure Q.9: Typical fit of the renal model to the experimental renal activity/time curve. ——— Model, o Experimental data for kidney 9

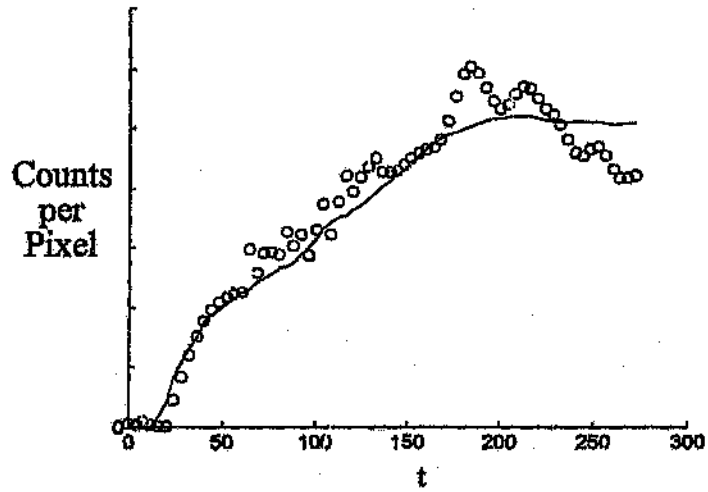

Figure Q.10: Typical fit of the renal model to the experimental renal activity/time curve. ——— Model, o Experimental data for kidney 10

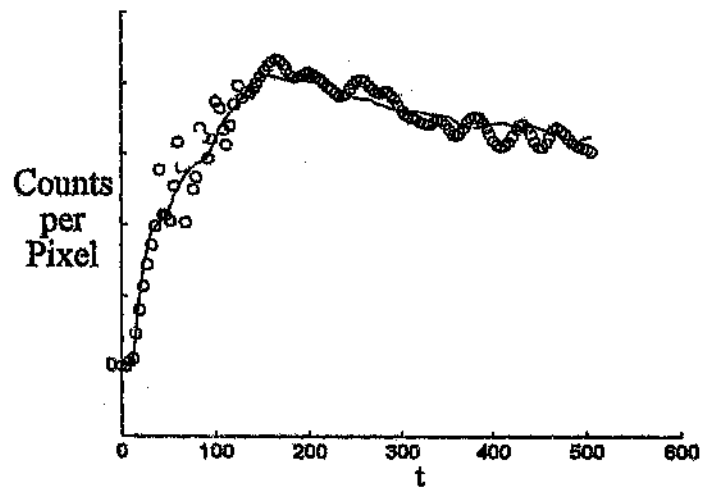

Figure Q.11: Typical fit of the renal model to the experimental renal activity/time curve. ——— Model, o Experimental data for kidney 11

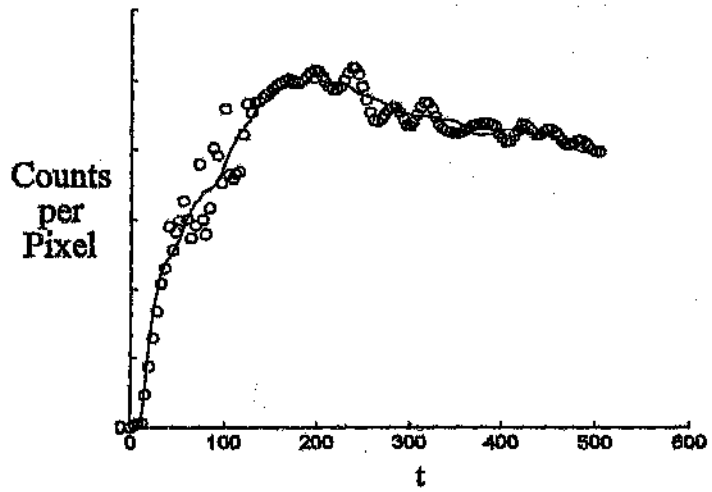

Figure Q.12: Typical fit of the renal model to the experimental renal activity/time curve. ——— Model, ○ Experimental data for kidney 12

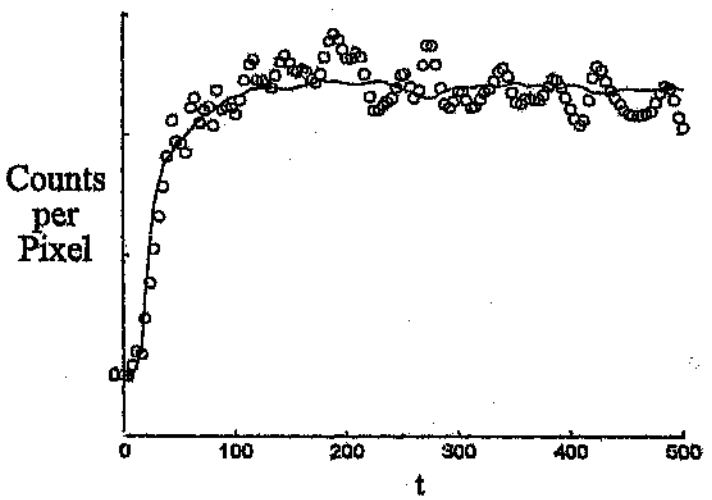

Figure Q.13: Typical fit of the renal model to the experimental renal activity/time curve. ——— Model, ○ Experimental data for the left kidney of renal pathology 1

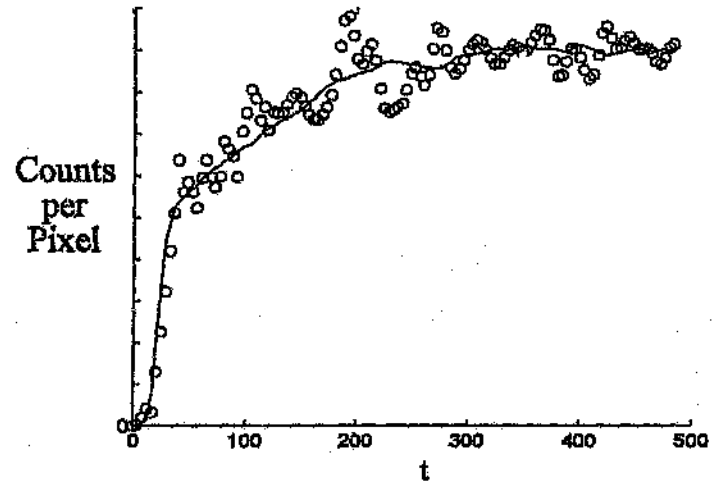

Figure Q.14: Typical fit of the renal model to the experimental renal activity/time curve. ——— Model, ○ Experimental data for the right kidney of renal pathology 1

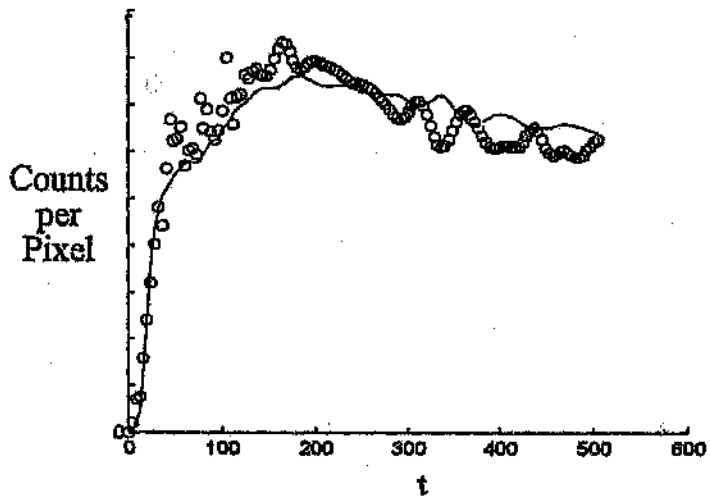

Figure Q.15: Typical fit of the renal model to the experimental renal activity/time curve. ——— Model, ○ Experimental data for the left kidney of renal pathology 2

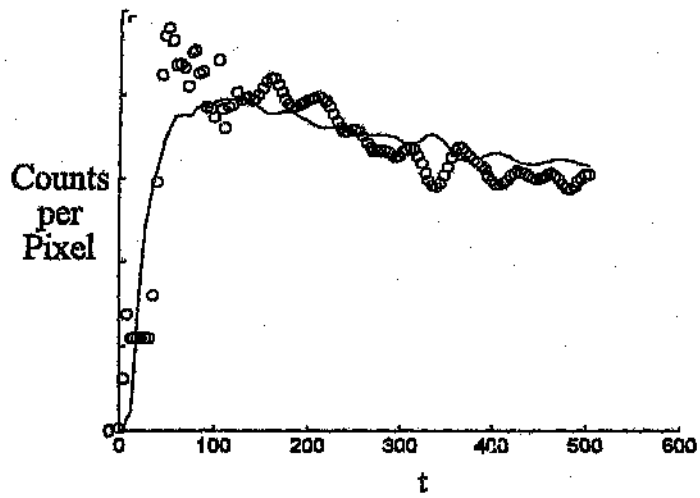

Figure Q.16: Typical fit of the renal model to the experimental renal activity/time curve. ——— Model, o Experimental data for the right kidney of renal pathology 2

Appendix R

R.1 Spleen and Liver Models Compared with Raw Liver and Spleen Data

The raw data displayed in this appendix appears on a 1.44MB magnetic disk which may be found in Appendix S.1.

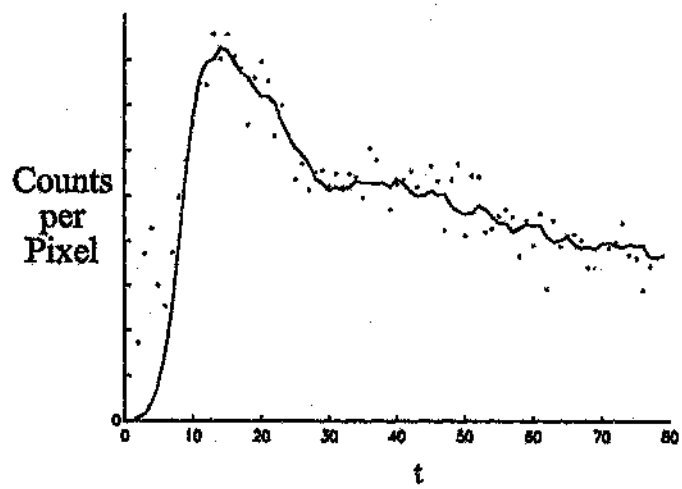

Figure R.1: Typical fit of the spleen model to the experimental spleen activity/time curve. —— Model, • Experimental data for spleen 1

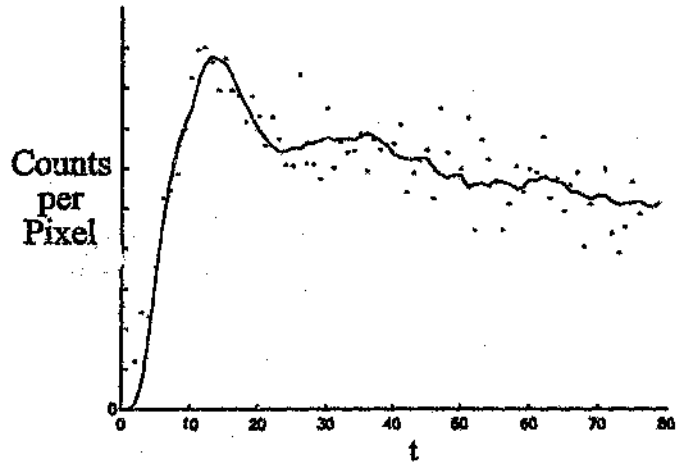

Figure R.2: Typical fit of the spleen model to the experimental spleen activity/time curve. ——— Model, • Experimental data for spleen 2

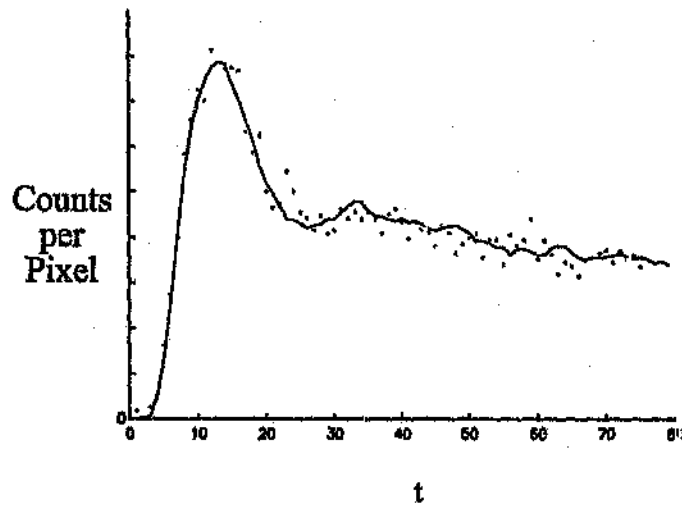

Figure R.3: Typical fit of the spleen model to the experimental spleen activity/time curve. ——— Model, • Experimental data for spleen 3

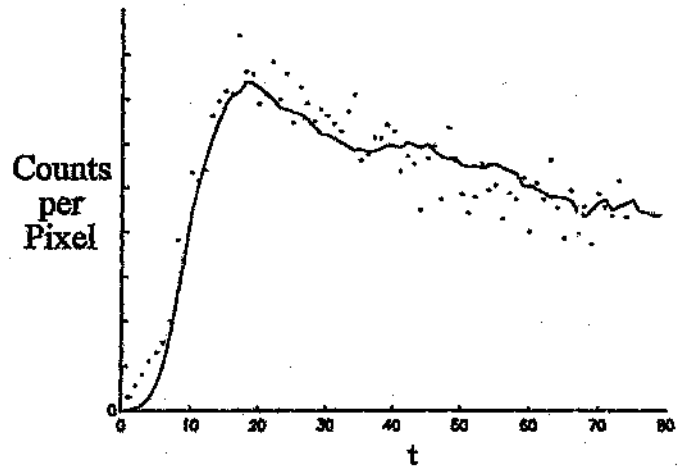

Figure R.4: Typical fit of the spleen model to the experimental spleen activity/time curve. ——— Model, • Experimental data for spleen 4

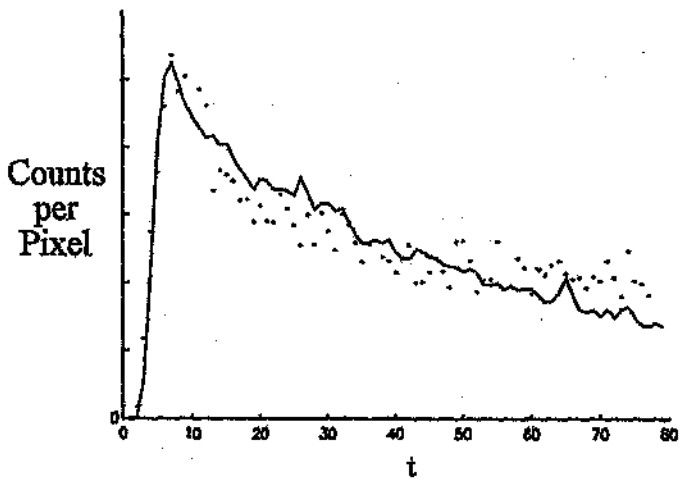

Figure R.5: Typical fit of the spleen model to the experimental spleen activity/time curve. ——— Model, • Experimental data for spleen 5

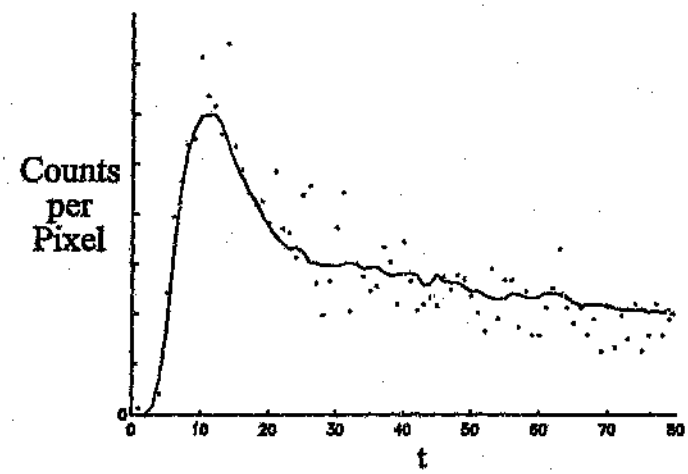

Figure R.6: Typical fit of the spleen model to the experimental spleen activity/time curve. ——— Model, • Experimental data for spleen 6

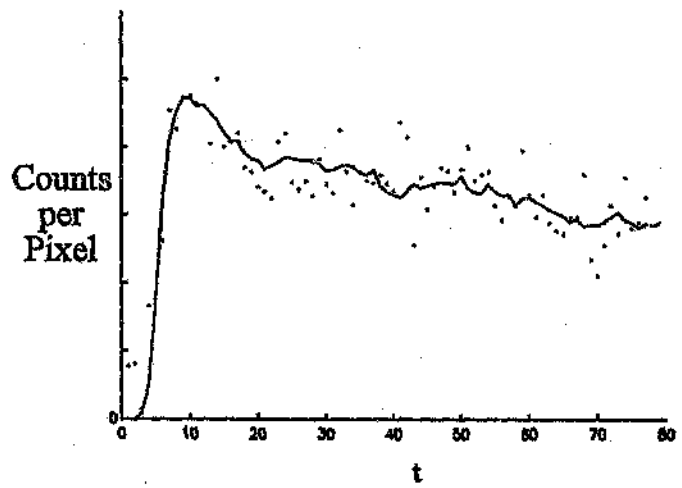

Figure R.7: Typical fit of the spleen model to the experimental spleen activity/time curve. ——— Model, • Experimental data for spleen 7

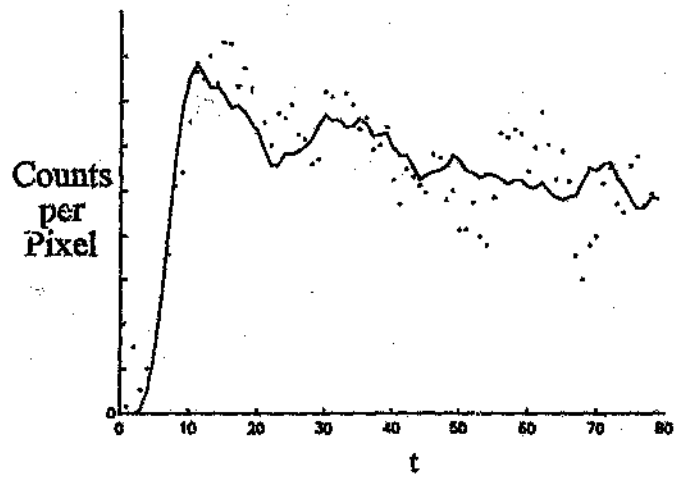

Figure R.8: Typical fit of the spleen model to the experimental spleen activity/time curve. ——— Model, • Experimental data for spleen 8

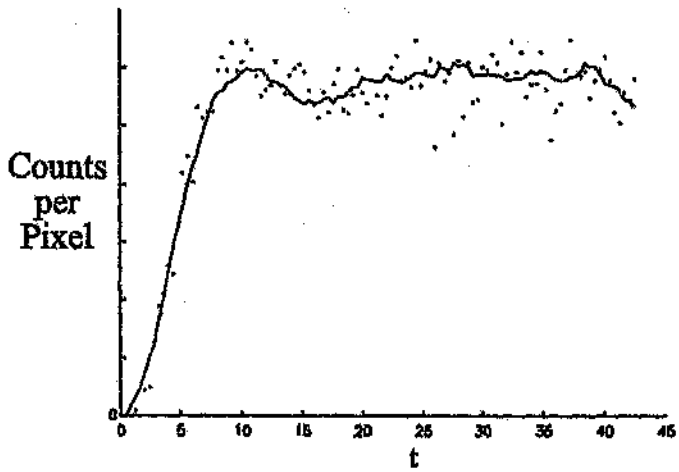

Figure R.9: Typical fit of the spleen model to the experimental spleen activity/time curve. ——— Model, • Experimental data for spleen pathology 1

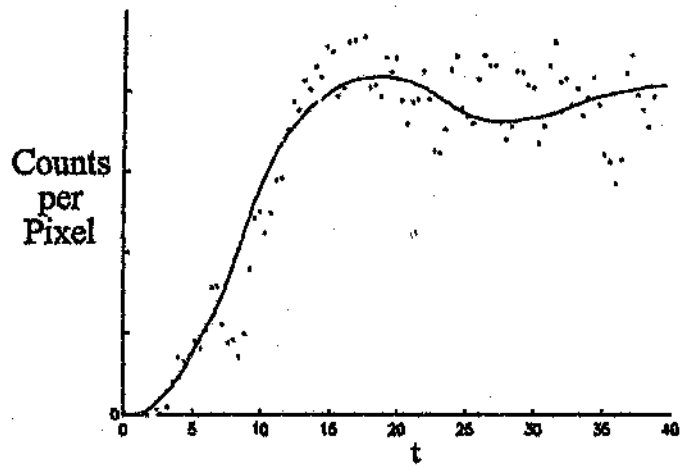

Figure R.10: Typical fit of the spleen model to the experimental spleen activity/time curve. ——— Model, • Experimental data for spleen pathology 2

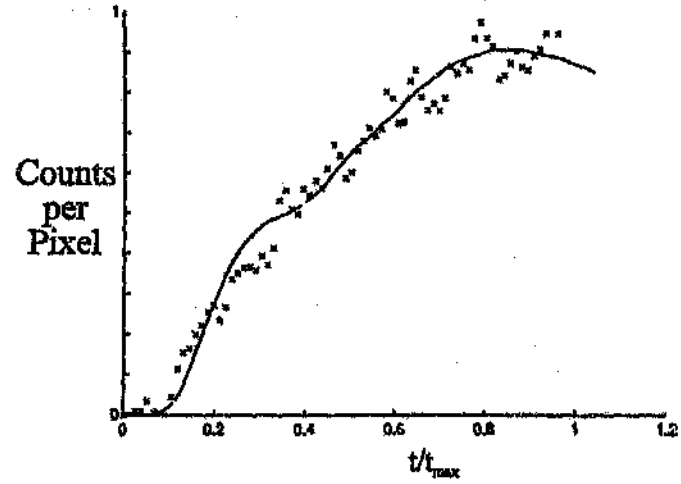

Figure R.11: Typical fit of the liver model to the experimental liver activity/time curve. ——— Model, x Experimental data for liver 1

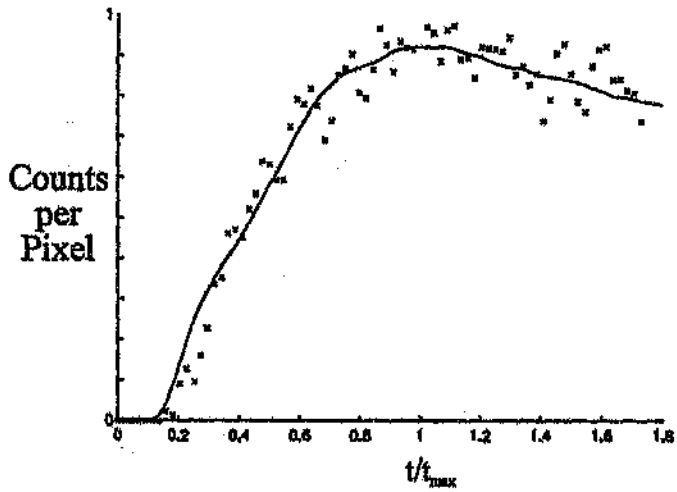

Figure R.12: Typical fit of the liver model to the experimental liver activity/time curve. ——— Model, x Experimental data for liver 2

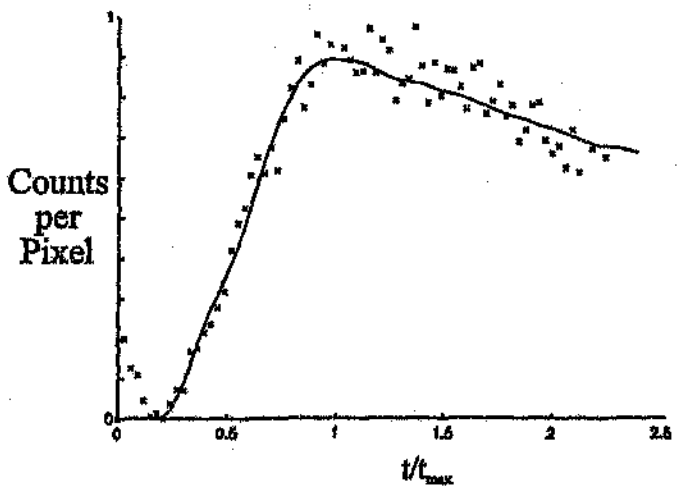

Figure R.13: Typical fit of the liver model to the experimental liver activity/time curve. ——— Model, × Experimental data for liver 3

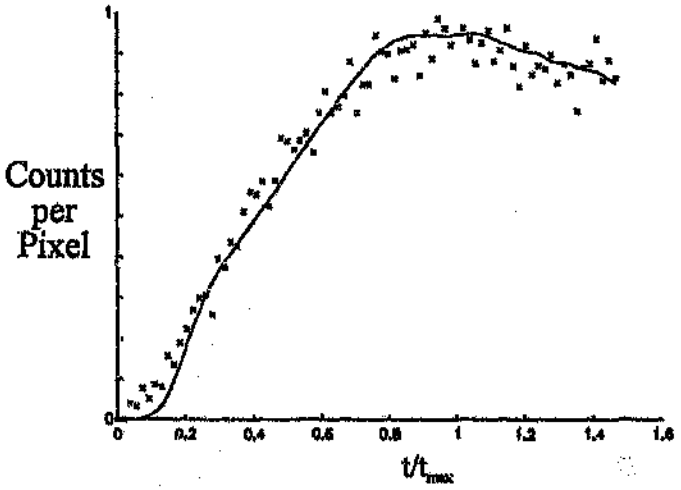

Figure R.14: Typical fit of the liver model to the experimental liver activity/time curve. ——— Model, × Experimental data for liver 4

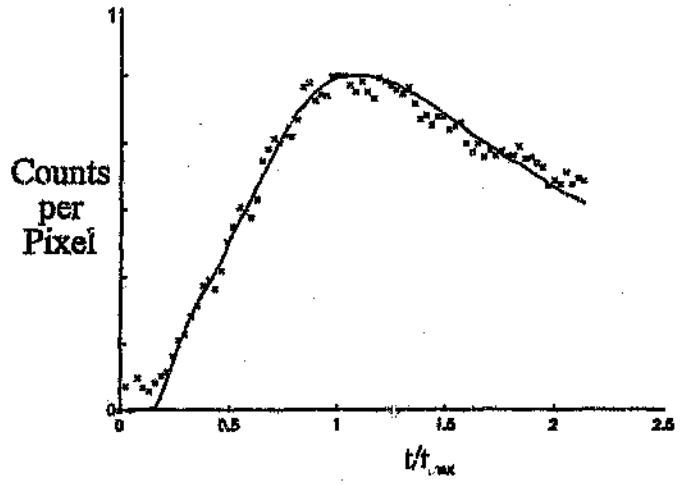

Figure R.15: Typical fit of the liver model to the experimental liver activity/time curve. ——— Model, × Experimental data for liver 5

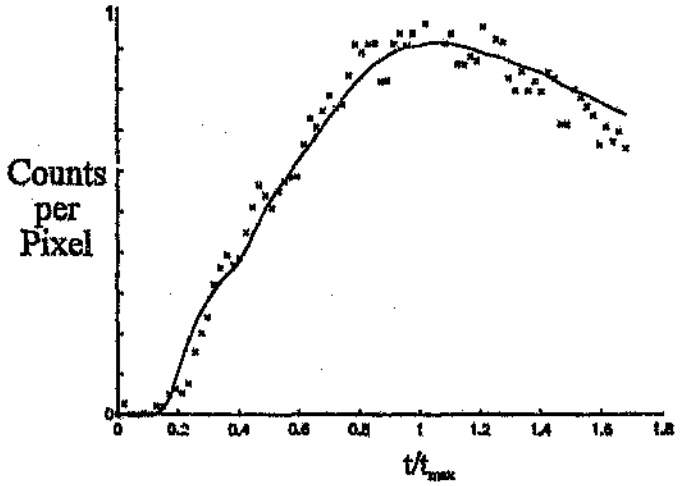

Figure R.16: Typical fit of the liver model to the experimental liver activity/time curve. ——— Model, × Experimental data for liver 6

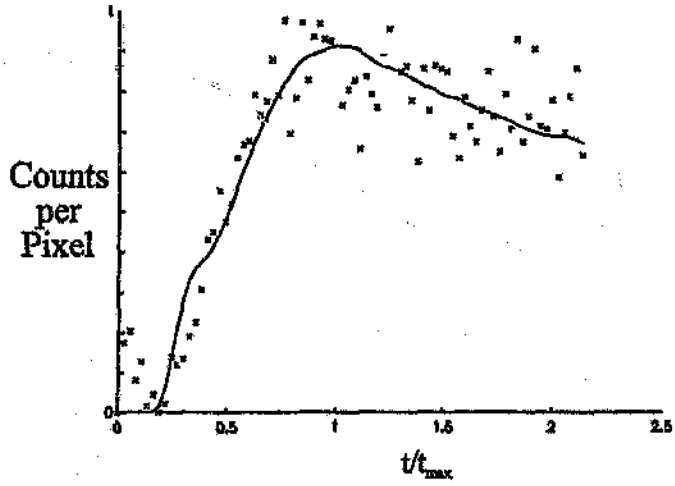

Figure R.17: Typical fit of the liver model to the experimental liver activity/time curve. ——— Model, × Experimental data for liver 7

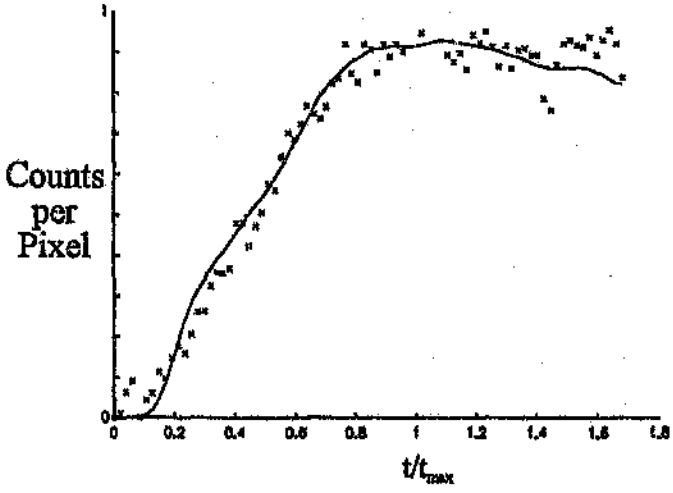

Figure R.18: Typical fit of the liver mouel to the experimental liver activity/time curve. ——— Model, × Experimental data for liver 8

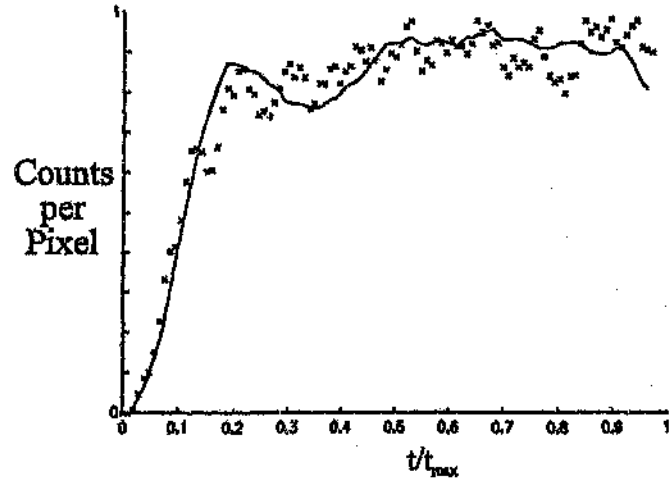

Figure R.19: Typical fit of the liver model to the experimental liver activity/time curve. —— Model, × Experimental data for liver pathology 1

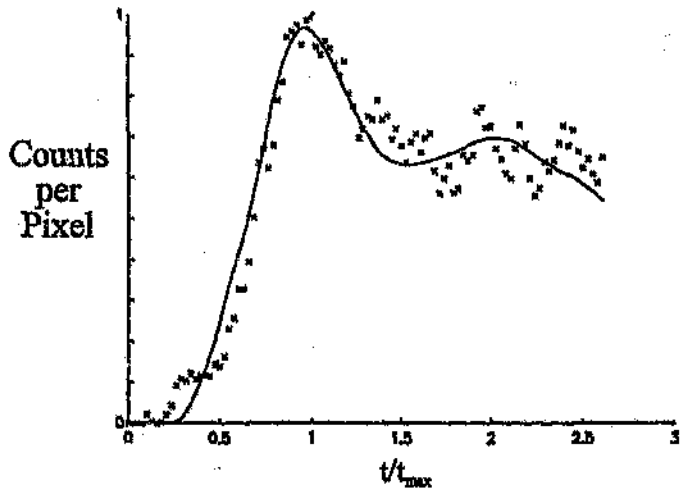

Figure R.20: Typical fit of the liver model to the experimental liver activity/time curve. —— Model, × Experimental data for liver pathology 2

Appendix S

S.1 Experimental Organ Activity/Time Data Files

The experimental data that is found on the magnetic disk may be accessed from any MS-DOS computer which can read 1.44MB disks. A "readme" file is located on this disk with further instructions.

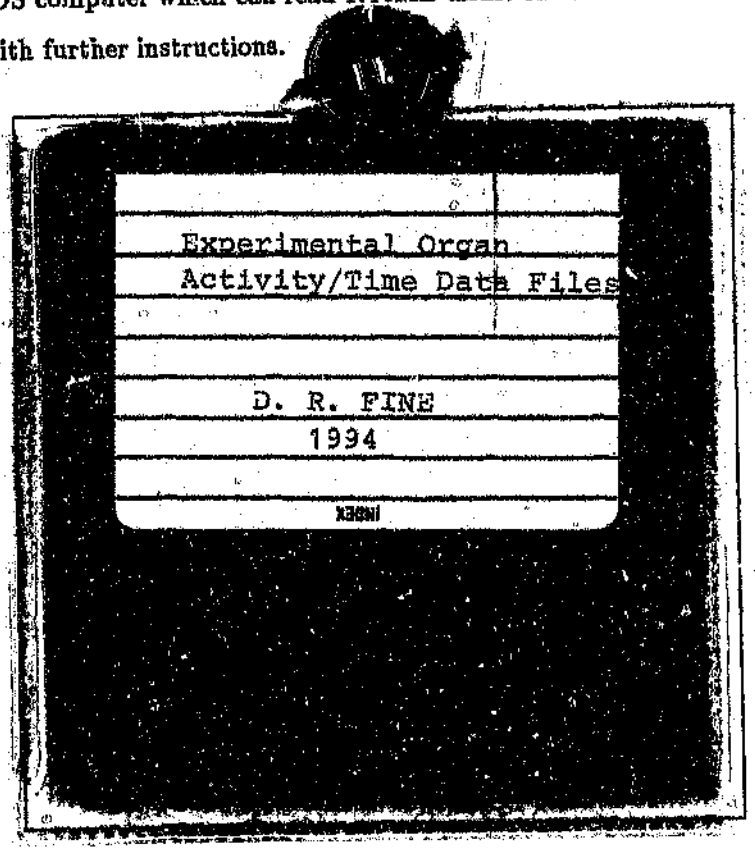

References

1. Ackroyd, F.W., Mito, M., McDermot, W.V., (1966), Autonomic vasomotor controls in hepatic blood flow, *American Journal of Surgery*, **112**, 356–362.

2. Ackroyd, N., Gill, R., Griffiths, K., Kossoff, G., Reeve, T., (1986), Duplex scanning of the portal vein and portasystemic shunts, *Surgery*, **99**, 591–597.

3. Bass, L., Roberts, M.S., Robinson, P.J., (1987), On the Relation Between Extended Forms of the Sinusoidal Perfusion and of the Convective-Dispersion Models of Hepatic Elimination, *Journal of Theoretical Biology*, **126**, 457–482.

4. Beck, J.V., Arnold, K.J, (1977), *Parameter Estimation in Engineering and Science*, John Wiley & Sons, New York, 346–489.

5. Biological Effects of Ionizing Radiation (BEIR), (1980), *The effects of populations of exposure to low levels of ionizing radiation*, BEIR Committee, Washington, DC, National Academy Press, 66–67.

6. Blaufox, M.D., (1989), Measurement of renal function with radioactive material. In *Evaluation of renal function and disease with radionuclides*. Blaufox, M.D. (Ed.), S. Karger, Basel, Switzerland, 23–24.

7. Britton, K.E., Nimmon, C.C., Whitfield, H.N., Hendry, W.F., Wickham, J.E.A., (1979), Obstructive Nephropathy: Successful Evaluation with Radionuclides, *The Lancet*, April 28, 905–907.

References

1. ACKROYD, F.W., MITO, M., MCDERMOT, W.V., (1966), Autonomic vasomotor controls in hepatic blood flow, *American Journal of Surgery*, **112**, 356–362.

2. ACKROYD, N., GILL, R., GRIFFITHS, K., KOSSOFF, G., REEVE, T., (1986), Duplex scanning of the portal vein and portasystemic shunts, *Surgery*, **99**, 591–597.

3. BASS, L., ROBERTS, M.S., ROBINSON, P.J., (1987), On the Relation Between Extended Forms of the Sinusoidal Perfusion and of the Convective-Dispersion Models of Hepatic Elimination, *Journal of Theoretical Biology*, **126**, 457–482.

4. Beck, J.V., Arnold, K.J, (1977), *Parameter Estimation in Engineering and Science*, John Wiley & Sons, New York, 346–489.

5. BIOLOGICAL EFFECTS OF IONIZING RADIATION (BEIR), (1980), *The effects of populations of exposure to low levels of ionizing radiation*, BEIR Committee, Washington, DC, National Academy Press, 66–67.

6. BLAUFOX, M.D., (1989), Measurement of renal function with radioactive material. In *Evaluation of renal function and disease with radionuclides*. BLAUFOX, M.D. (ED.), S. Karger, Basel, Switzerland, 23–24.

7. BRITTON, K.E., NIMMON, C.C., WHITFIELD, H.N., HENDRY, W.F., WICKHAM, J.E.A., (1979), Obstructive Nephropathy: Successful Evaluation with Radionuclides, *The Lancet*, April 28, 905–907.

8. Britton, K.E., Nawaz, M.K., Whitfield, C.C., Carroll, M.J., Granowska, M., Mlodkowska, E., (1987), Obstructive Nephropathy: Comparison between Parenchymal Transit Time Index and Frusemide Diuresis, *British Journal of Uropathy*, **59**, 127–132.

9. Britton, K.E., Nimmon, C.C., (1989), The measurement of renal transit times by deconvolution analysis. In *Evaluation of renal function and disease with radio-nuclides.* Blaufox, M. D. (Ed.), S. Karger, Basel, Switzerland, 108–116, 235–239, 280–287.

10. Burton, A. C., (1966), Role of geometry, of size and shape in the microcirculation, *Fed. Proc.*, **25**, 1753.

11. Carlisle, K.M., Halliwell, M., Read, A.E., Wells, P.N.T., (1992), Estimation of total hepatic blood flow by duplex ultrasound, *Gut*, **33**, 92–97.

12. Chatfield, C., (1978), *Statistics for technology.*, Chapman and Hall, New York, 124–125

13. Cosgriff, P.S., Lawson, R.S., Nimmon, C.C., (1992), Towards Standardisation in Gamma Camera Renography, *Nuclear Medicine Communications*, **13**, 580–585.

14. Diffy, B.L., Corfield,J.R., (1976), Data-bounding technique in discrete deconvolution, *Med. Biol. Eng.*, **14**, 478.

15. DeGrazia, J.A., Scheibe, P.O., Jackson, P.E., Lucas, Z.J., Fair, W.R., Vogel, J.M., Blumin, L.J., (1974), Clinical Application of a Kinetic Model of Hippurate Distribution and Renal Clearance, *Journal of Nuclear Medicine*, **15**, 102–114.

16. Doi, R., Kazutomo, I., Masafumi, K., Shoichiro, S., Kyoichi, T., Takashi, S., Takayoshi, T., (1988), Simultaneous measurement of hepatic arterial and portal venous flows by transit time ultrasonic volume flowmetry, *Surg., Gynecol. Obstet.*, **167**, 65–69.

17. Elias, H., Petty, D., (1953), Terminal distribution of the hepatic artery, *Anat. Rec.*, **116**, 9–18.

18. EVANS, R.L., (1959), Two comments on the estimation of blood flow and central volume from dye-dilution curves, *Journal of Applied Physiology*, 14, 457.

19. FLEMING, J.S., GODDARD, B.A., (1974), A Technique for the deconvolution of the Renogram, *Phys. Med. Biol.*, 19, 546–549.

20. FLEMING, J.S., ACKERY, D.M., WALMSLEY, B.H., KARRAN, S.J., (1983), Scintigraphic estimation of arterial and portal blood supplies to the liver, *J. Nucl. Med.*, 24, 1108–1113.

21. FLEMING, J. S. (1988), Functional radionuclide imaging of renal mean transit time and glomerular filtration rate. *Nucl. Med. Commun.*, 9, 85–96.

22. GAMBHIR, S.S., HAWKINS, R.A., HUANG, S., HALL, T.R., BUSUTTIL, R.W., PHELPS, M.E., (1989), Tracer kinetic modelling approaches for the quantification of hepatic function with technetium-99m DISIDA and scintigraphy, *J. Nucl. Med.*, 30, 1507–1519.

23. GATES, G.T., (1983) Split renal function testing using ^{99m}Tc-DTPA. A rapid technique for determining differential glomerular filtration, *Clin. Nucl. Med.*, 8, 400–407.

24. GIANPAOLO, M., MASSIMO, B., ENZO, S., CORRADO, M., (1989), Assessment of liver circulation by quantitative scintiangiography: evaluation of the relative contribution of hepatic arterial and portal venous blood flows to liver perfusion, *Eur. J. Nucl. Med.*, 12, 211–216.

25. GLASSER, D., JACKSON, R., (1984), A Generalised Residence Time Distribution Model for a Chemical Reactor, *I. Ch. E. Symposium Series*, 87, 535–542.

26. GODFREY, K., *Compartmental Models and their Application*, London, Academic Press, 1983.

27. GRIFFITH, R.C., JANNEY, C.G., (1990), Hematopoietic System: Bone Marrow and Blood, Spleen, and Lymph Nodes, *In Anderson's Pathology*, 9th ed., St Louis, The C.V. Mosby Company Chap. 28, 1415–1417.

28. GUYTON, A. C., (1986), *Textbook of Medical Physiology*, W. B. Saunders Co., Philadelphia, 336–346, 393–424.

29. HASE, T., BRIM, J., (1966), Observation on the microcirculatory architecture of the rat liver, *Anat. Rec.*, **156**, 157–173.

30. HEYNS, A. DU P., LÖTTER, M.G., BADENHORST, P.N., VAN REENEN, O.R., PIETERS, H., MINNAAR, P.C., (1980), Kinetics, Distribution and Sites of Destruction of ^{111}Indium-labelled Huma Platelets, *British Journal of Haematology*, 44, 269–280.

31. HORN, J.R., ZIERLER, B., BAUER, L.A., REISS, W., STRANDNESS, D.E., (1990), Estimation of hepatic blood flow in branches of the hepatic vessels utilizing a noninvasive, duplex doppler method, *J. Clin. Pharmacol.*, **30**, 922–929.

32. JACQUEZ, J.A., *Compartmental Analysis in Biology and Medicine*, Amsterdam, Elsevier, 1972.

33. JUNI, J.E., THRALL, J.H., FROELICH, J.W., WIGGINS, R.C., CAMPBELL, D.A., TUSCAN, M., (1988), The appended curve technique for deconvolution analysis - method and validation, *European Journal of Nuclear Medicine*, **14**, 403 – 407.

34. KREYSZIG, E., (1983), Advanced Engineering Mathematics, 5th ed., New York, John Wiley & Sons, 221.

35. LAMONT, J.T., ISSELBACHER, K.J., (1977), Cirrhosis, In. *Harrison's Principles of Internal Medicine*, Eds. Thorn, G.W., Adams, R.D., Braunwald, E., Isselbacher, K.J., Petersdorf, R.G., London, McGraw-Hill, 1604–1614.

36. LEE, C.Y.C., RUBINSKY, B., (1990), A Multidimensional Analysis of Momentum and Mass Transfer in the Liver, *International Journal of Heat and Mass Transfer*, **32**, 2421–2434.

37. LEVENSPIEL, O., *Chemical Reaction Engineering*, New York, John Wiley & Sons, 1972, 253–325.

38. LJUNG, L. (1987), *System Identification - Theory For the User*, Prentice-Hall, Englewood Cliffs, N.J.

39. MAISEY, M.M., GILDAY, D.L., (1992), *Clinical Nuclear Medicine*, 2nd Ed., Chapman and Hall Medical, London.

40. MCAFEE, J.G., GROSSMAN, Z.D., GAGNE, G., ZENS, A.L., SUBRAMANIAN, G., THOMAS, F.D., FERNANDEZ, P., ROSKOPF, M.L., (1981), Comparison of Renal Extraction Efficiencies for Radioactive Agents in the Normal Dog, *Journal of Nuclear Medicine*, **22**, 333–338.

41. MCCUSKEY, R.S., (1966), A Dynamic and Static Study of Hepatic Arterioles and Hepatic Sphincters, *Amer. J. Anat.*, **119**, 455–478.

42. MOLER, C., LITTLE, J., BANGERT, S. (1987), *PC-MATLAB for MS-DOS Personal Computers : User's Guide*, The MathWorks, Inc., Sherborn, M.A.

43. NAOR, P., SHINNAR, R., (1963), Representation and Evaluation of Residence Time Distributions, *Ind. Eng. Chem. Fundamentals*, **2**, 278–286.

44. NAOR, P., SHINNAR, R., KATZ, S., (1972), Indeterminacy in the estimation flowrate and transport functions from tracer experiments in closed circulation, *Int. J. Eng. Sci.*, **10**, 1153.

45. NIMMON, C.C., LEE, T.Y., BRITTON, K.E., GRANOWSKA, M., GRUENEWALDS, S., (1981), Practical Application of Deconvolution Techniques to Dynamic Studies. In *Medical Radionuclide Imaging*, International Atomic Energy Agency MacMillan and Co. Limited, Vienna, 367–381.

46. O'CONNOR, M.K., KROM, R.F., CARTON, E.G., SANCHEZ-URDAZPAL, L., JUNI, J.E., FERGUSON, D.M., WIESNER, R.F., (1992), Ratio of hepatic arterial-to-portal venous blood flow–Validation of radionuclide techniques in an animal model, *J. Nucl. Med.*, **33**, 239–245.

47. OPPENHEIM, B.E., APPLEDORN, C.R., (1978), An Anatomic-Physiological Renal Model, *Journal of Nuclear Medicine*, **19**, 739.

48. PAULSEN, A.W., KLINTMALM, G.B.G., (1992), Direct measurement of hepatic blood flow in native and transplanted organs, with accompanying systemic hemodynamics, *Hepatology*, **16**, 101–111.

49. PETERS, A.M., KLONIZAKIS, J.P., LAVENDER, J.P., LEWIS, S.M., (1980), Use of ^{111}Indium-labelled Platelets to measure Spleen Function, *British Journal of Haematology*, **46**, 587–593.

50. PIEPSZ, A., DOBBELEIR, A., ERBSMAN, F., (1977), Measurement of Separate Kidney Clearance by Means of Technetium-99m-DTPA Complex and Scintillation Camera, *Eur. J. Nucl. Med.*, **2**, 173–177.

51. PIEPSZ, A., DOBBELEIR, A., HAM, H.R., (1990) Effect of Background Correction on Separate Technetium-99m-DTPA Renal Clearance, *J. Nucl. Med.*, **31**, 430–435.

52. PRICE, J.B., BRITTON, R.C., PETERSON, L.M, REILLY, J.W., VOORHEES, A.B., (1965), The validity of chronic hepatic blood flow measurements obtained using electromagnetic flowmeter, *Journal of Surgical Research*, **5**, 313–317.

53. PROTHERO, J.W., BURTON, A.C., (1961), The physics of blood flow in capillaries-1-The nature of motion, *Biophys J*, **1**, 565–579.

54. RAPPAPORT, A.M., SCHNEIDERMAN, J.H., (1976), The function of the hepatic artery, *Rev. Physiol. Biochem. and Pharmacol.*, **76**, 129–175.

55. ROEDLER, H. D., (1981), Radiation dose to the patient, In IAEA-SM-246/206, *Proc. Int. Symp. Med. Radionuc. Imag.*, International atomic energy agency, 527–542.

56. ROSENTHALL, L., DAMTEW, B., KLOIBER R., (1981) Selection of renal background for quantitative 131-I-hippurate renal function studies, *Diag. Imag.*, **50**, 159–164.

57. SARPER, R., FAJMAN, W.A., RYPINS, E.B., HENDERSON, J.M., TARCAN, V.A., GALAMBOS, J.T., WARREN, W.D., (1981), A Non-invasive Method for Measuring Portal Venous/Total Hepatic Blood Flow by Hepatosplenic Radionuclide Angiography, *Radiology*, **141**, 179–184.

58. SWEETLOVE, M.A., (1990), The Mechanisms by which Funcional and Sequestrated Blood Platelets are Distributed in the Human Body as Determined by

Computed Assisted Compartmental Modelling, *MSc. Thesis at the University of the Orange Free State*, Bloemfontein.

59. THIBODEAU, G.A., (1987) *Anatomy and Physiology*, Times Mirror/Mosby College Publishing, St. Louis, 626.

60. THOMPSON, H.K., STARMER, F., WHALEN, R.E., MCINTOSH, H.D., (1964), Indicator Transit Time Considered as a Gamma Variate, *Circulation Research*, 14, 502–515.

61. VAN HUFFEL, S., VANDEWALLE, J., DE ROO, M. CH., WILLEMS, J.L., (1987), Reliable and efficient deconvolution technique based on total linear least squares for calculating the renal retention function, *Med. & Biol. Eng. & Comput.*, 25, 26–33.

62. VAN HUFFEL, S., (1992), *Private Communications (See Appendix K.1)*

63. VAN STEKELENBURG, L.H.M., (1978), Hippuran Transit Times in the Kidney: A New Approach, *Phys. Med. Biol.*, 23, 291–301.

64. WARNER, H.R., (1962), Analysis of the Role of Indicator Technics in Quantitation of Valvular Regurgitation, *Circulation Research*, 10, 519.

65. WILLIAMS, P.L., WARWICK, R., DYSON, M., BANNISTER, L.H., Eds., (1989), *Gray's Anatomy*, 37 ed., London, Churchill Livingstone, 1390–1391.

66. WRAIGHT, E.P., BARBER, R.W., RITSON, A., (1982), Relative Hepatic Arterial and Portal Flow in Liver Scintigraphy, *Nuclear Medicine Communications*, 3, 273–279.

67. WRENN, M. E., MCDONALD, E., MAYS, C. W., (1982), Ionizing Radiation, In Rom, W. N. ed., *Environmental and Occupational Medicine*, Boston, 667–696.

68. YALLOW, R. S., (1981), Reappraisal of potential risks associated with low-level radiation, *Com. Mol. Cell. Biophys*, vol. 1, p.149–157.

69. ZWIETERING, T. N., (1959), The degree of mixing in continuous flow systems, *Chemical Engineering Science*, 11, 1–15.